Two-dimensional MXenes for electrochemical capacitor applications: Progress, challenges and perspectives

Qizhen Zhu, Jiapeng Li, Patrice Simon, Bin Xu

Two-dimensional MXenes for electrochemical capacitor applications: Progress, challenges and perspectives

Qizhen Zhu [a], Jiapeng Li [a], Patrice Simon [b,c,*], Bin Xu [a,*]

[a] State Key Laboratory of Organic-Inorganic Composites, Beijing Key Laboratory of Electrochemical Process and Technology for Materials, Beijing University of Chemical Technology, Beijing 100029, China
[b] Université Paul Sabatier Toulouse III, CIRIMAT UMR CNRS 5085, 118 route de Narbonne, Toulouse 31062, France
[c] Réseau sur le Stockage Electrochimique de l'Energie (RS2E), FR CNRS no. 3459, Amiens, France

ARTICLE INFO

Keywords:
MXene
Electrochemical capacitor
Electrode materials
MXene-based composites
Devices

ABSTRACT

MXenes, a family of 2D transition metal carbides/nitrides with a general formula of $M_{n+1}X_nT_x$ (n=1~3), show promising potential for energy storage applications owing to their 2D lamellar structure, impressive density, metallic-like conductivity, tunable terminations and intercalation pseudocapacitance charge storage mechanism. Various combinations of transition metals, C and/or N, as well as different n layers result in a broad range of MXenes, but only about a small number have been prepared and used for capacitive energy storage applications (supercapacitors) so far, with $Ti_3C_2T_x$ being the most studied one. This review summarizes the recent advances, achievements and challenges of MXenes for supercapacitors. The preparation methods, composition versatility, material and electrode architectures, chemical modification and hybridization with other active materials of MXenes are presented. Moreover, the electrochemical characterizations and energy storage mechanisms of MXenes in aqueous and non-aqueous electrolytes are discussed, as well as the preparation of flexible and printable MXene-based electrodes and devices. Finally, perspective is also given, providing guidance for the future development of MXenes with advanced performances for designing the next generation of supercapacitors.

1. Introduction

The decrease of fossil fuel stocks and the global warming concern are highlighting the urgent need to use alternative, clean energy sources. In a future sustainable world, the electricity, generated from renewable energy sources like solar, wind and hydro sources, should be stored and then used on demand. Also, electric engines are targeted to replace thermal for mobility applications. Electrochemical energy storage devices such as rechargeable batteries and electrochemical capacitors (ECs, herein denoted as supercapacitors) are then key technologies to promote this sustainable development. Rechargeable batteries, due to their high energy density, are promising for consumer electronics and electric vehicles applications, but suffer from the limited power density because of the sluggish ion intercalation/de intercalation processes in electrode materials [1–4]. Supercapacitors with high power density and excellent cycle stability can be a supplement or even an alternative to rechargeable batteries in some applications where high power output, fast charge discharge and ultra long cycle life are needed [5,6]. According to charge storage mechanism, supercapacitors can be classified into two types: electrical double layer capacitors (EDLCs) and pseudocapacitors [7]. Charge storage in EDLCs is electrostatic by nature, via the charge separation at the electrode/electrolyte interface [8–10]. Pseudocapacitive materials store the charge using fast, surface confined non diffusion limited redox reactions, resulting in so called pseudocapacitance or redox capacitance mechanism [11,12]. Recently, hybrid supercapacitors combining a capacitive electrode with a battery type electrode attracted much interest, since they could potentially offer high power and high energy [13–15].

Electrode materials play a crucial role in supercapacitors, which determine the capacitance as well as cycle and rate performances of the devices. Conventional electrode materials used in supercapacitors include porous carbons for EDLCs, as well as transition metal oxides and conducting polymers for pseudocapacitors. Porous carbons generally store charge by reversible physical adsorption/desorption of electrolyte ions at the interface between carbon electrode and electrolyte. Porous carbons exhibit high specific surface area, tunable pore size and good chemical stability, resulting in excellent rate performance and exceptional cycle life, besides being abundant and low cost materials [16–20]. Nevertheless, most of the EDLCs cannot store a large amount of charge because of the electrostatic storage mechanism, and the low electrode density results in low volumetric capacitance. Metal oxides can typi

* Corresponding authors.
E-mail addresses: simon@chimie.ups-tlse.fr (P. Simon), xubin@mail.buct.edu.cn (B. Xu).

https://doi.org/10.1016/j.ensm.2020.11.035

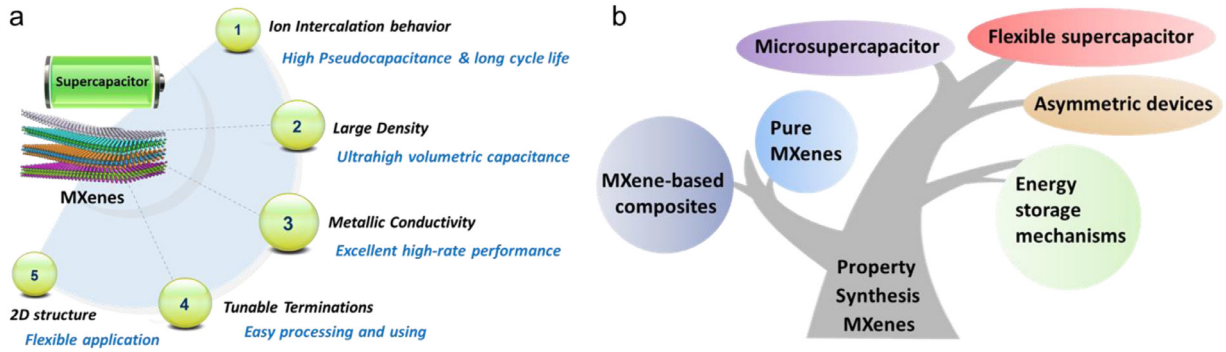

Fig. 1. (a) Advantages of MXenes for supercapacitor applications. (b) Schematic of the review content.

cally store much charge through pseudocapacitive processes, based on reversible, surface confined redox reactions [11]. They can deliver high capacity, but their use is currently restricted by limited electronic con ductivity and electrochemical stability, leading to unsatisfactory rate ca pability and cycle life. A promising and effective strategy is to develop electrode materials with intercalation pseudocapacitance behavior [21]. This charge storage, based on ion intercalation and rapid ion transport inside the host material, pushes the energy performance closer to batter ies while maintaining power performance close to that of ECs. Interca lation pseudocapacitive materials, such as T Nb_2O_5, $VOPO_4$, MoS_2 and α MoO_3 can achieve high capacitance even under heavy current [22 25]. However, most of these intercalation pseudocapacitive materials suffer from low electronic conductivity.

2D transition metal carbides/nitrides, known as “MXenes”, were firstly reported by Barsoum and Gogotsi in 2011 [26]. They have a gen eral formula of $M_{n+1}X_nT_x$ (M=Ti, Zr, V, Nb, Cr, Mo, etc.; X=C, N; T_x= F, OH, O, Cl, etc.; n=1~3) and are typically synthesized by extract ing the “A” layers from the layered carbides or carbonitrides ($M_{n+1}AX_n$ phase, A= Al, Ga, Si, Ge, etc.) [27 30]. MXenes have many special and tunable properties, like 2D structure with atomic thickness, hydrophilic surface and high mechanical performance, that make them suitable for various applications including sensors [31,32], medicine [33], photo and electrocatalysis [34 36], etc. Especially, MXenes are very promising candidates as electrode materials for electrochemical energy storage ap plications, due to their key features of intercalation pseudocapacitance mechanism, large density, metallic like conductivity, variable surface terminations and 2D lamellar structure [37 39] (Fig. 1a). Numerous studies have been dedicated to MXenes as high rate electrode materi als [40,41] or conductive framework to support active materials [42 44] for energy storage. MXenes can achieve high capacitance (especially volumetric capacitance) together with metallic like conductivity, which make them promising active materials for desiging supercapacitors with both high energy and high power densities, bridging the gap between batteries and conventional electrical double layer supercapacitors. Their 2D structure makes them also suitable for desiging flexible devices. Also, they can be used in combination with active materials with limited con ductivity, such as metal compounds and conducting polymers. As a re sult, many works have been reported recently on MXenes for designing high power energy storage devices. With these efforts, the huge poten tial of MXenes and their applications in supercapacitors are gradually developed. As shown in Fig. 1b, this review article intends to give a state of the art of MXenes for supercapacitor applications, including ma terials, energy storage mechanisms and electrochemical performances as well as their application in hybrid and flexible supercapacitors. To be consistent with the literature, we will describe the electrochemical performance of MXene using capacitance values (F), although capacity (C or mAh) should be alternatively used for pseudocapacitve materi als. Finally, the challenges with regard to the practical applications of MXenes in supercapacitors and perspectives for future development are highlighted.

2. Synthesis and key properties of MXenes

2.1. Preparation strategies

Since the discovery of $Ti_3C_2T_x$ MXene in 2011, about 30 compo sitions of MXenes have been synthesized by various strategies, such as wet etching [45 47], molten salt etching [30,48,49], chemical va por deposition [50,51], and electrochemical etching [52]. Generally, MXene flakes are prepared from their ternary MAX precursors. The metal like M A bond makes the delamination of MAX precursors diffi cult through physical exfoliation, e.g., ball milling and ultrasonication. However, the chemical reactivity of M A bond, higher than that of M X bond, makes it possible to selectively remove the A layers from the MAX phases through etching methods [53]. Therefore, etching becomes the mainstream preparation strategy for MXenes. When MAX phase pre cursors are treated with specific etching agents such as HF containing electrolytes, the A atoms are selectively removed and substituted with surface terminations, leading to the $M_{n+1}X_nT_x$ composition (where T_x stands, for example, for OH, O, or F groups) [27]. Delamination can be further obtained by further intercalation with various molecules or ions, e.g., dimethyl sulfoxide (DMSO) [54], tetrabutylammonium hy droxide (TBAOH) [55], and alkali metal ions [26,56], followed by son ication, to prepare 2D single or few layer MXene flakes. Most of the etching methods are based on immersion of the MAX precursor into HF or HF containing electrolyte, and fluoride free etching routes have just been recently reported (Fig. 2).

The first MXene (i.e., $Ti_3C_2T_x$) was prepared in 2011 by immersing a Ti_3AlC_2 powder in 50% concentrated HF for 2 h (Fig. 2a), resulting in an accordion like multilayered structure with abundant surface termi nations, such as O, OH, and F [27]. From then, a large variety of MX enes, such as Ti_2CT_x, Ta_4C_3, TiNbC, $(V_{0.5},Cr_{0.5})_3C_2$ and Ti_3CN_x, were obtained by HF etching using different HF concentration and etching time [28]. The etching synthesis reactions can be described as follows:

$$M_{n+1}AlX_n+3HF = AlF_3+3/2H_2+M_{n+1}X_n \quad (1)$$

$$M_{n+1}X_n+2H_2O = M_{n+1}X_n(OH)_2+H_2 \quad (2)$$

$$M_{n+1}X_n+2HF = M_{n+1}X_nF_2+H_2 \quad (3)$$

The delamination of exfoliated MXene into single or few layer flakes was further achieved by intercalating as prepared $Ti_3C_2T_x$ with DMSO molecules followed by ultrasonication, which leads to an enlarged in terlayer spacing and weak interlayer interaction [54]. In 2013, one of the first application of MXenes as supercapacitor electrode material was reported by exploring the capacitive performances of an exfoliated $Ti_3C_2T_x$ powder prepared via HF etching of Ti_3AlC_2 (Fig. 2b) [26]. Fur thermore, the multilayer $Ti_3C_2T_x$ was delaminated by DMSO to pro duce few layer MXene flakes, which were then fabricated into a binder free paper electrode through filtration [26]. However, DMSO has only

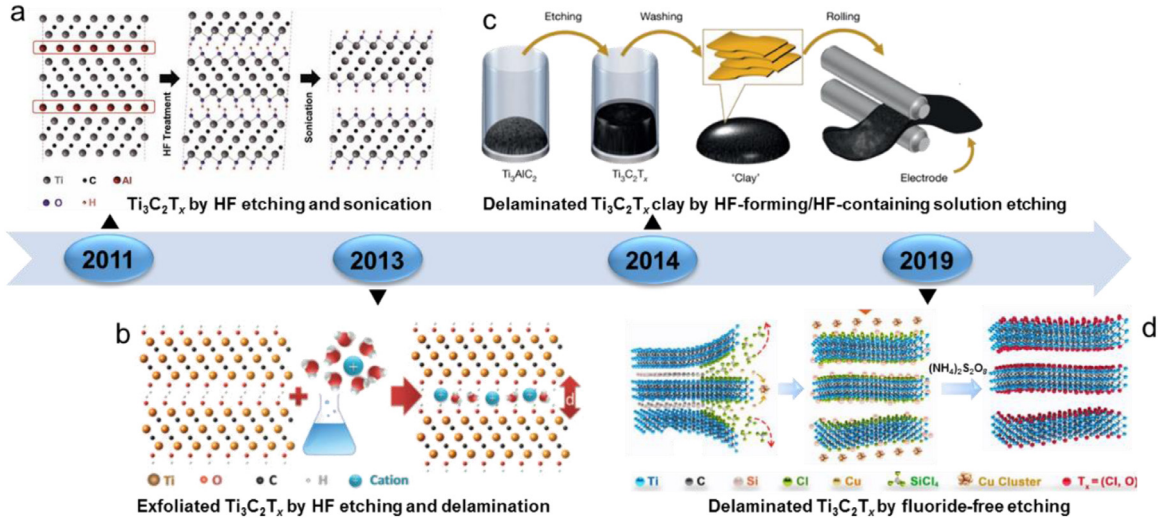

Fig. 2. Development of the preparation method of MXenes. (a) The first MXene material ever produced was prepared by HF etching Ti_3AlC_2 followed by sonication in 2011. Reproduced from Ref. [27] with copyright permission from Wiley-VCH. (b) The first report of MXenes for supercapacitors was made in 2013, and the reported multilayer exfoliated $Ti_3C_2T_x$ was prepared by HF etching Ti_3AlC_2, following further delamination. Reproduced from Ref. [26] with copyright permission from American Association for the Advancement of Science. (c) A breakthrough was made in 2014 when self-supported MXene 'clay' films were prepared from HF-forming/containing etching agents. Reproduced from Ref. [56] with copyright permission from Springer. (d) A fluoride-free etching method based on the use of molten salts was proposed for decreasing the hazardous issues from fluoride. Reproduced from Ref. [49] with copyright permission from Springer.

been confirmed as efficient intercalated agent for the delamination of $Ti_3C_2T_x$ [13] and $(Mo_{2/3}Ti_{1/3})_3C_2T_x$ [57]. Alternatively, other organic molecules like TBAOH can be used to prepared delaminated samples, like achieved for V_2CT_x and Ti_3CNT_x [55].

A breakthrough was obtained in 2014 by Gogotsi and Barsoum, when they reported the MXene synthesis without the direct use of HF etchant. This was achieved by adopting a mixed solution of LiF and HCl, which *in situ* produces HF and selectively etches the Al layers from Ti_3AlC_2, resulting in the formation of Ti_3C_2 "clay" (Fig. 2c) [56]. Compared with the direct HF etching method, this synthesis route combines the etching and delamination procedures in one step, and decreases the safety risk due to the use of concentrated HF. The cations (e.g. Li^+) intercalate between the MXene nanosheets at the same time during the etching process, leading to large interlayer spacing and weak interlayer interaction. As a result, the products could be directly delaminated into single layer flakes through only hand shaking or sonication. Combined with improved safety, employing LiF/HCl mixture as etchant has become the most widely studied approach in fabricating MXene monolayers. Additionally, although MXene monolayers are easily oxidized in moist air or aqueous solution, some methods have been proposed to mitigate the oxidation tendency, such as heating MXene in reducing gas [58], storing MXene at low temperatures under inert atmosphere [59] and adding additives [60,61]. With the development of these strategies, the oxidation tendency will no longer be a barrier for the application of MXenes.

Besides LiF/HCl, other fluoride salts (i.e., NaF, KF, NH_4F, FeF_3)/HCl mixtures or F containing ammonium salts (NH_4HF_2 and NH_4F) have also been used to obtain various MXenes, such as $Ti_3C_2T_x$, Ti_2CT_x, and V_2CT_x [62 66]. Because of the NH_4^+ intercalation between the MXene sheets during etching, the resultant MXenes have larger interlayer spacing than HF prepared, but cannot exfoliate single layer MXene flakes. Differently from the conventional etching in aqueous acidic solutions, Gogotsi et al. reported a novel non aqueous etching approach using a mixture of molten fluoride salts (LiF, NaF and KF) as the etchant in 2016. By this approach, the first 2D transition metal nitride, i.e., $Ti_4N_3T_x$, was successfully obtained, but the $Ti_4N_3T_x$ flakes still needed to be delaminated [48].

Etching processes based on HF or F containing solutions are effective, but the use of hazardous fluoride based etching agents causes considerable safety and environment issues [67]. In this regard, fluoride free etching agencies have been explored for sustainable development of MXenes. For instance, an alkali assisted hydrothermal method was proposed to prepare multilayer $Ti_3C_2T_x$. In this process, Al layers are selectively removed by immersion at 270 °C in highly concentrated NaOH (27.5 M) from Ti_3AlC_2, yielding in multilayer $Ti_3C_2T_x$ with no F terminations as well as 92 wt% purity [68]. Another reported fluoride free method for preparing $Ti_3C_2T_x$ MXene is to use electrochemical etching in a binary aqueous system of 1 M NH_4Cl and 0.2 M tetramethylammonium hydroxide (TMAOH) with pH > 9 [69]. Here, the presence of Cl^- ion helps in breaking the Ti Al bonds and etches Al atoms in an electrochemical anodic process, followed by the NH_4OH intercalation. This method provides the possibility of using a short etching time (5 h) under ambient conditions to produce single or bilayer $Ti_3C_2T_x$ nanosheets.

Recently, a general Lewis acidic molten salt etching route via a redox reaction mechanism was reported for preparing MXenes from various MAX phases with a wide chemical range of A elements such as Al, Zn, Si, Ga (e.g., Ti_2AlC, Ti_3ZnC_2, Ti_3AlCN, Ti_3SiC_2, Ta_2AlC, Ti_2GaC) [30,49]. For instance, $Ti_3C_2T_x$ with Cl terminations was prepared by immersing Ti_3SiC_2 in $CuCl_2$ molten salt (Fig. 2d) [49]. It is noteworthy that this etching strategy enables new MXenes to be produced, including some materials impossible to be prepared from conventional HF or F containing etching aqueous process. Moreover, the careful selection of molten salts provides important opportunities for tuning the surface chemistry and the properties of MXenes. The MXenes etched by this fluoride free approach present an accordion like multilayered structure with no F terminations, so the delamination process for these MXenes is still needed to be explored to meet the application requirements. Most recently, on basis of the Lewis acidic molten salt etching method, a post synthetic covalent surface modification strategy by exchange reaction was reported to install and remove surface groups [70]. By this strategy, bare MXenes without surface terminations was firstly synthesized, and MXenes with different terminations (NH, S, Cl, Se, Br, Te, etc.) were successfully produced, exhibiting unique structural and electronic properties, even including superconductivity. This work offers the diversity of MXene property and thus provides more chances for the application of MXenes.

2.2. Properties of MXenes for supercapacitors

From 2011, tens of stoichiometric MXene compositions and a lim itless number of solid solutions have been discovered, offering not only unique combinations of properties but also a way to tune them by varying the compositions and ratios of M or X elements and sur face chemistry. Their special and tunable properties, including metallic like electronic conductivity, good mechanical properties, hydrophilic, oxide/hydroxide like polar surfaces, dispersibility in water, large elec trochemically active surface, etc., make MXenes very promising candi dates for designing advanced supercapacitors with both high energy and power densities since:

(1) MXenes have high capacitance and long cycle life owing to the ion intercalation pseudocapacitive charge storage mecha-nism. Capacitance and cycle life are key parameters for supercapaci tors. The 2D lamellar structure of MXene provides fast ion intercala tion (e.g. H^+, Li^+, Na^+), which facilitates the accessibility of the large electrochemically accessible active surface of MXenes, resulting in fast pseudocapacitive charge storage behavior associated with high perfor mance in acid aqueous electrolyte and also (as recently shown) in non aqueous electrolyte. MXenes thus exhibit high capacitance (300~500 F g^{-1}), much higher than almost all the EDLC carbon materials in aque ous electrolytes. In addition, MXenes show excellent cycle life with tens of thousands of cycles with no or small capacitance decay, which is better than conventional pseudocapacitive materials (metal oxides and conducting polymers).

(2) MXenes have ultrahigh volumetric capacitance originated from high density and high gravimetric capacitance. For realistic applications, volumetric capacitance of the electrode material is of key significance for improving the energy and power density of the device. Thanks to their intrinsic properties, MXene electrodes show high density (about 3~4 g cm^{-3} for typical MXene films), offering great advantage to reach high volumetric capacitance [53,56]. For instance, vacuum filtered $Ti_3C_2T_x$ MXene film can deliver a volumetric capacitance of 900 F cm^{-3}, while an even larger volumetric capacitance of 1500 F cm^{-3} could be achieved when the MXene was fabricated into a hydrogel film [71]. The values outperform those of other electrode materials of super capacitors, e.g., the best activated graphene (200~350 F cm^{-3}) [72,73] or activated porous carbon (60~200 F cm^{-3}) [74 76] electrodes.

(3) MXenes have outstanding high-rate performance due to the metallic-like electronic conductivity. High power density and fast charge discharge are typical characteristics of supercapacitors, which require the electrodes with high conductivity. Depending on the com position of M, X, and surface terminations, MXenes may exhibit metallic, semiconducting or even insulating properties [77,78]. A recent study in dicates that the Nb_2C MXenes with surface terminations of Cl, S, Se, NH even show superconducting transitions in the low temperature re gions of below 6.3 K, 6.4 K, 4.5 K, 7.1 K, respectively [70]. So far, most of MXenes show outstanding conductivity values versus other 2D materi als, e.g., MoS_2 and graphene [79]. In general, MXenes with large laterals size and low defect concentrations have higher conductivities [53]. For example, a spin cast $Ti_3C_2T_x$ MXene film etched by the LiF/HCl solu tion can achieve an ultra high conductivity of 6500 S cm^{-1} [80], much higher than the highly defective cold pressed $Ti_3C_2T_x$ MXene film (1000 S cm^{-1}) [81]. MXene films prepared by blade coating can even achieve an ultrahigh conductivity of 15,000 S cm^{-1} due to the large lateral size and highly ordered alignment of MXene flakes [82]. The extremely high conductivity of MXenes not only is a key to achieve high power density, but also can eliminate the need for conductive agents during electrode fabrication or even current collector [56], improving the energy density of the whole device.

(4) MXene suspensions / dispersion in either aqueous or non-aqueous solutions can be prepared, making their processing easy. In practical application, the dispersibility of electrode materials in var ious solvents is the key for preparing the electrode ink to further pre pare the electrode or the composite electrode. Conventional synthesis routes lead to various surface terminations (O, OH, F, Cl, etc.), which allow for the preparation of stable MXene suspensions in aque ous solutions without the need for surfactants, making the processing and using of MXenes easy [83]. Moreover, surface termination groups mainly drive their electrochemical performance and O, OH groups contribute to hydrophilicity, in favor of the electrolyte infiltration [83]. In addition, good dispersibility of $Ti_3C_2T_x$ MXene can be also achieved in some organic solvents with polarity and dispersion interactions, e.g., DMF, NMP, PC, and ethanol [84], which could drive the advances of MX enes in various applications, including the fabrication of MXene based composites and films, inks for printable supercapacitors, and conductive binders for electrode fabrication.

(5) 2D-MXenes possess excellent mechanical flexibility, facilitating their use in flexible supercapacitor devices. There is grow ing demand for devices for portable and wearable microelectronic sys tems, such as flexible supercapacitors and micro supercapacitors. The 2D lamellar structure and excellent mechanical properties of MXenes facilitate their use in this field. For example, the effective Young's mod ulus of the $Ti_3C_2T_x$ monolayer was measured to be 0.33 ± 0.03 TPa us ing atomic force microscopy (AFM) indentation technique, outperform ing those of other solution processed 2D materials measured by nanoin dentation [85,86]. To date, most researches focus on the mechanical properties of MXene based films, as 2D MXene nanosheets can be eas ily assembled into film electrodes [87 89]. The assembled MXene films can support various mechanical deformations, such as bending, twisting, rolling, and folding. Besides, a 5 μm thick $Ti_3C_2T_x$ film rolled into a hol low cylinder can support about 4000 times its own weight, which even increased up to 15,000 times when integrating with 10 wt% polyvinyl alcohol (PVA) [87].

As a result, considerable research efforts on structure and morphol ogy control, chemical modification, composite construction, charge stor age mechanism, hybrid supercapacitor fabrication, flexible and micro supercapacitor assembly, etc., have been done, and important key ad vanced and valuable progress has been achieved recently.

3. MXenes as electrode materials for supercapacitors

As mentioned above, MXenes have fast ion intercalation behav ior, which results in large electrochemically accessible active surface and pseudocapacitive mechanism in acid aqueous electrolyte and non aqueous electrolyte. For example, $Ti_3C_2T_x$ undergoes reversible redox reactions between the oxygen containing terminations and H^+ protons associated with the change of the Ti oxidation state during charg ing/discharging in H_2SO_4 electrolyte. As a result, MXene performs high pseudocapacitance, good cycle stability and high rate capability, mak ing it a promising high performance electrode material for supercapac itors.

The first report of MXene as supercapacitor electrode materials was done in 2013 [26]. Multilayer $Ti_3C_2T_x$ was synthesized via HF etching Ti_3AlC_2 and cation delamination, which was then further delaminated by DMSO to produce few layer MXene flakes [26]. A $Ti_3C_2T_x$ binder free paper electrode prepared by filtration could achieve a high volumetric capacitance of 350 F cm^{-3} in KOH electrolyte [26], higher than those reported for conventional EDLC carbons (60~200 F cm^{-3}) [74 76] and comparable to those of the graphene based materials (200~350 F cm^{-3}) [72,73]. This result paved the way for developing MXene materials for supercapacitor operating in aqueous electrolytes.

In 2014, the use of LiF/HCl mixture as etching solution significantly improved the capacitive performance of MXene in H_2SO_4 electrolyte [56]. LiF/HCl etched Ti_3C_2 "clay" prepared as free standing and flexi ble films showed a high gravimetric capacitance of 245 F g^{-1} and an outstanding volumetric capacitance of up to 900 F cm^{-3} in the poten tial range of 0.35~0.2 V (vs. Ag/AgCl) at a scan rate of 2 mV s^{-1}. The cycling performance was also excellent with negligible capacitance loss after 10,000 cycles at 10 A g^{-1}. In addition, the Ti_3C_2 "clay" can be fab ricated into a 75 μm thick electrode with a capacitance of 350 F cm^{-3},

demonstrating the scalability of MXenes for supercapacitors. Further more, capacitance as high as 380 F g^{-1} or 1500 F cm^{-3} could be also ob tained using hydrogel $Ti_3C_2T_x$ MXene electrodes within a 1 V potential window (1.1~ 0.1 V vs Hg/Hg_2SO_4) in 3 M H_2SO_4 electrolyte, thanks to the use of glassy carbon current collectors [71]. Other F containing etching electrolytes like NH_4F aqueous and molten fluoride salts were used to prepare MXenes, but the energy storage performance of the ob tained MXenes still needs to be investigated.

The development of fluoride free etching synthesis routes not only makes the MXene preparation safer and environmentally sustainable, but also results in improved electrochemical performance due to the elimination of the F containing terminations of prepared MXenes [67]. Multilayer $Ti_3C_2T_x$ prepared by the alkali assisted hydrothermal method was fabricated into a film electrode with 52 μm in thickness and 1.63 g cm^{-3} in density, which showed a gravimetric capacitance of 314 F g^{-1} and a volumetric capacitance of 511 F cm^{-3} at 2 mV s^{-1} in H_2SO_4 electrolyte [68]. MXene film assembled with the sin gle or bilayer $Ti_3C_2T_x$ nanosheets, which were prepared with aqueous NH_4Cl/TMAOH solution, were used to assemble a symmetric superca pacitor and areal and volumetric capacitances of 220 mF cm^{-2} and 439 F cm^{-3} at 10 mV s^{-1} could be achieved, respectively [69].

However, while aqueous electrolyte offers great electrochemical per formance in terms of capacitance, the limited voltage window to about 1 V due to water electrolysis drastically limits the energy density of the cells. An important challenge then lies on designing MXene materials for non aqueous electrolytes. $Ti_3C_2T_x$ MXene with O and Cl termina tions prepared by a Lewis acidic molten salt etching route showed re markable pseudocapacitive like electrochemical signature together with a high capacity of 200 mAh g^{-1} in Li ion containing non aqueous elec trolytes, within a potential range of 2 V (from 0.2 V to 2.2 V vs Li^+/Li). Those results highlight the promising opportunities offered by MXenes for high rate devices such as hybrid capacitors or high power Li ion bat teries [30, 49].

Along with the development of the preparation method, MXenes ex hibit various structural and chemical features, resulting in different elec trochemical energy storage properties. For further improvement of the capacitive performance of MXenes, many strategies have been investi gated, such as more compositional versatility exploration, structure and morphology control, as well as chemical modification.

3.1. A broad range of composition to be explored

Besides $Ti_3C_2T_x$, the most studied MXene for energy storage applica tions [90, 91], other MXenes have also been identified as promising can didates as electrode materials for supercapacitors, see Table 1. For exam ple, Ti_2CT_x MXenes achieved impressive performance [92 96]. Nitride based MXenes can achieve higher conductivity than their carbide coun terparts [97]. A nanolayered Ti_2NT_x with accordion like structure and O/ OH terminations was prepared from Ti_2AlN MAX phase using an oxygen assisted molten salt reaction followed by HCl treatment, which showed a capacitance of 200 F g^{-1} at 2 mV s^{-1} and a potential window of 1.2 V at 50 mV s^{-1} in 1 M $MgSO_4$ electrolyte [98].

Vanadium based MXenes are expected to achieve high capacitance thanks to the multiple oxidation states available for vanadium [99, 100]. Delaminated HF etched V_2C film electrode could achieve a gravimetric capacitance of 487 F g^{-1} in H_2SO_4 electrolyte [101]. Next, considering MXenes' stability improvement with increasing n in $M_{n+1}X_nT_x$ [102], $V_4C_3T_x$ was explored. A multi layered $V_4C_3T_x$ prepared by HF etching exhibited large interlayer spacing (~0.466 nm) and good thermal stabil ity, but a practical capacitance of only ~209 F g^{-1} at 2 mV s^{-1} in H_2SO_4 electrolyte was reached, even lower than V_2C [103].

Moving to niobium carbides, a freestanding film of $Nb_4C_3T_x$ was pre pared by HF etching and TMAOH delamination, which showed a large interlayer spacing of 1.77 nm and a volumetric capacitance of 1075 F cm^{-3} at 5 mV s^{-1} in 1 M H_2SO_4 electrolyte [104]. However, those values were still lower than the predicted quantum capacitances by simulations [105].

Ta based [106] and Mo based [46] MXenes were also evaluated as electrodes for supercapacitor application. Mo_2CT_x MXene was prepared via selectively etching Ga from Mo_2Ga_2C by two different routes [46]. Etching with LiF/HCl solutions produced less defective flakes but with low reaction yield, while etching with HF followed by tetrabutylammo nium hydroxide (TBAOH) delamination resulted in smaller flakes and higher fraction of single layer flakes. A 2 µm thick Mo_2CT_x "paper" pre pared with the latter route delivered gravimetric and volumetric ca pacitances of 196 F g^{-1} and 700 F cm^{-3}, respectively, at 2 mV s^{-1} in 1 M H_2SO_4 electrolyte, still maintaining 120 F g^{-1} and 430 F cm^{-3} at 100 mV s^{-1}. Also, a high capacity retention of above 95% was obtained after 10,000 cycles at 10 A g^{-1}.

Besides combining single transition metal with C and/or N, using metal alloys on the M site broadens the MXene family to almost un limited numbers. MXenes combining alloys with C and/or N predicted from density functional theory (DFT) calculations have been prepared. One example is the stable, ordered, double M MXene $Mo_2TiC_2T_x$, which was synthesized by HF etching followed by DMSO delamination [57]. $Mo_2TiC_2T_x$ was isostructural with $Ti_3C_2T_x$, but its electrochemical be havior was quite different. $Mo_2TiC_2T_x$ has two voltage plateaus at 1.6 V and below 0.6 V during lithiation in Li^+ containing non aqueous elec trolyte, and more rectangular CV curves than $Ti_3C_2T_x$ with a working potential window of 0.1~0.4 V (vs. Ag/AgCl) in H_2SO_4 electrolyte [57]. These behaviors dominated by the surface Mo layers indicate that the properties of the MXenes with binary M elements were mainly decided by their surface atoms.

Based on various combinations of transition metals (such as Ti, Mo, V, Ta, Nb) and their alloys with C and/or N as well as surface termi nations, stoichiometric phases of more than 100 different MXenes and a limitless number of solid solutions have been predicted, out of which only about 30 different MXenes have been synthesized. Their properties, including atomic structure, conductivity, stability and electrochemical performance, strongly depend on the intrinsic nature of M and X ele ments, and the surface terminations also play an important role. On one hand, as their properties can be tuned by careful selection of the various M, X elements and control of the surface terminations, there are end less and extensive opportunities for producing new MXenes with favor able capacitive properties. As shown in the computational screening of the pseudocapacitive MXene in aqueous H_2SO_4 electrolyte [107], many candidates could theoretically offer improved capacitive performances compared to the well known $Ti_3C_2T_x$, especially considering nitrides (Zr_2N, Zr_3N_2, Zr_4N_3), although it has still to be verified in real exper iments. Therefore, with prospective potential in supercapacitors, more new MXenes with improved electrochemical performance are expected. On the other hand, every MAX precursor having unique atomic bonds, suitable synthesis route including etching and delamination procedures needs to be optimized to achieve desirable structures and performance. The exploration of new MXenes and preparation strategies needs signif icant amount of research efforts, which is an important and challenging task. Theoretical calculations have been used to predict structures and properties of MXenes with different compositions, which is expected to guide the experiments in the future.

3.2. Structure and morphology control

Although MXenes have been identified as promising candidates for supercapacitors, their practical capacitances are far from theo retical values. For example, the maximum theoretical capacity of $Ti_3C_2O_{0.85}(OH)_{0.06}F_{0.26}$ calculated by Faraday's law is up to about ~615 C g^{-1}, while only 245 F g^{-1} or ~135 C g^{-1} can be experimen tally achieved using MXene clay as electrodes in a voltage window of 0.55 V in 3 M H_2SO_4 electrolyte [56,75]. Furthermore, while 90 nm thick $Ti_3C_2T_x$ MXene film achieved a capacitance of 450 F g^{-1} through minimizing ion transport limitations, the capacitance decreased to 250

Table 1
Capacitive performances of various MXene versatilities as electrode materials for supercapacitors.

Versatility	Preparation method	Electrode assembly method	Electrolyte	Potential	Capacitance	Cycle stability	Ref.
$Ti_3C_2T_x$	HF etching Ti_3AlC_2 and DMSO delamination	Filtrating into film	1 M KOH	-0.4~0.95 V (vs. Ag/AgCl)	350 F cm^{-3} (2 mV s^{-1})	no degradation (10,000 cycles)	[26]
$Ti_3C_2T_x$	HCl/HF etching Ti_3AlC_2	Rolling	1 M H_2SO_4	-0.3~0.25 V (vs. Ag/AgCl)	900 F cm^{-3} or 245 F g^{-1} (2 mV s^{-1})	no degradation (10,000 cycles)	[56]
$Ti_3C_2T_x$	Lewis acidic molten salt etching Ti_3SiC_2	Rolling	1 M $LiPF_6$-EC/DMC	0.2~2.2 V (vs. Li^+/Li)	738 C g^{-1} or 205 mAh g^{-1} (C/1.5 rate)	90% (2400 cycles)	[49]
Ti_2CT_x	HF etching Ti_2AlC	Rolling	1 M KOH	-0.3~-1.0 V (vs. Ag/AgCl)	517 F cm^{-3} (2 mV s^{-1})	no degradation (3000 cycles)	[92]
Ti_2NT_x	Oxygen-assisted molten salt etching Ti_2AlN_2 and HCl treatment	Coating	1 M $MgSO_4$	-0.3~-1.5 V (vs. Ag/AgCl)	201 F g^{-1} (2 mV s^{-1})	140% (1000 cycles)	[98]
V_2C	HF etching V_2AlC and TMAOH delamination	Rolling	1 M H_2SO_4	-0.3~-1.1 V (vs. $Hg/HgSO_4$)	487 F g^{-1} (2 mV s^{-1})	83% (10,000 cycles)	[101]
$V_4C_3T_x$	HF etching V_4AlC_3	Coating	1 M H_2SO_4	-0.35~0.15 V (vs. Ag/AgCl)	~209 F g^{-1} (2 mV s^{-1})	97.23% (10,000 cycles)	[103]
$Nb_4C_3T_x$	HF etching Nb_4AlC_3 and TMAOH delamination	Rolling	1 M H_2SO_4	-0.9~0.1 V (vs. Ag)	1075 F cm^{-3} (5 mV s^{-1})	76% (5000 cycles)	[104]
Ta_4C_3	HF etching Ta_4AlC_3	Coating	0.1 M H_2SO_4	-0.2~1.0 V (vs. Ag/AgCl)	481 F g^{-1} (5 mV s^{-1})	89% (2000 cycles)	[106]
Mo_2CT_x	HF etching Mo_2Ga_2C and TBAOH delamination	Filtrating into film	1 M H_2SO_4	-0.3~0.3 V (vs. Ag/AgCl)	700 F cm^{-3} (2 mV s^{-1})	no degradation (10,000 cycles)	[46]
$Mo_2TiC_2T_x$	HF etching and DMSO delamination Mo_2TiAlC_2	Rolling	1 M H_2SO_4	-0.1~0.4 V (vs. Ag/AgCl)	413 F cm^{-3} (2 mV s^{-1})	no degradation (10,000 cycles)	[57]

F g^{-1} as the film thickness increased to 5 μm. This points out the importance of using decent electrode weight loadings (> 1 mg cm^{-2}) to reach significant and practical areal capacitance (mAh cm^{-2} or F cm^{-2}) for reporting electrochemical performance. The main reason for the large discrepancy between theoretical and experimental values is the horizontal aggregation and restacking of MXene nanosheets due to the strong van der Waals interaction between adjacent layers, which limits the accessibility to electrolyte ions and the utilization of the whole 2D MXene surface [108]. Designing open structure and tailoring the morphology of MXene nanosheets are of key importance to increase the electrochemically accessible surface area of MXenes and improve the ion transport rate to active redox sites. Various strategies have been proposed, such as controlling flake size, expanding interlayer spacing, designing three dimensional (3D) porous structures, or vertical alignments, etc. to achieve high capacitance and power performance.

3.2.1. *Controlling flake size*

Etching conditions have important impact on the morphology and structure of MXenes. For instance, while an accordion like $Ti_3C_2T_x$ MXene is obtained by HF etching of Ti_3AlC_2, a prolonging etching time results in more opened structure. The Ti_3C_2 with an etching time of 216 h exhibited the destructed octahedral structure for Ti loss and more exposed C on the surfaces, endowing with much enhanced capacitive performance compared with the Ti_3C_2 with a short etching time of 24 h [108].

$Ti_3C_2T_x$ MXene prepared by LiF/HCl etching and sonication usually have delaminated flakes with wide size distribution (Fig. 3a and b). Sonication and centrifugation can be used to control and sort the flake size of the MXenes (Fig. 3c): the sonication conditions affect the lateral sizes, and the density gradient centrifugation allows a selection of MXene flakes with controlled lateral sizes [109].

It is noteworthy that although the smaller MXene flakes provide more accessible ion diffusion paths and higher ionic conductivity, they suffer from decreased electrical conductivities due to more interfacial contact resistance. Kayali et al. studied the change of the MXenes electrochemical properties with their lateral sizes as shown in Fig. 3d [110]. As large $Ti_3C_2T_x$ MXene flakes offer high electrical conductivity and small flakes enhance ion accessibility, a 1:1 mixture delivers a capacitance of 195 F g^{-1} at 1000 mV s^{-1} in 3 M H_2SO_4 electrolyte (Fig. 3e). This value is higher than those of MXenes with average flake sizes, thus evidencing the high electronic and ionic conductivity of the mixture. Furthermore, when the mixture was assembled into a hydrogel structure, it achieved very high gravimetric and volumetric capacitances of 435 F g^{-1} and 1513 F cm^{-3} at 2 mV s^{-1}, which remained 86 F g^{-1} and 299 F cm^{-3} at an ultrahigh scan rate of 10 V s^{-1}, respectively, in 3 M H_2SO_4 electrolyte (Fig. 3f). Therefore, a rational combination of various flake sizes is suggested for optimum capacitive properties of MXenes.

3.2.2. *Adding spacer between MXene interlayer*

In general, MXenes prepared by HF etching have accordion like structures, which need to be opened up for facilitating ion transport. Carbon spacers, already widely introduced into graphene structures to prevent aggregation [111 113], can also be used to increase the interlayer spacing between the MXene layers [114,115]. For instance, a simple mixing of Ti_2CT_x powder with carbon nanospheres (CNS) results in improved capacitance [114]. Another strategy to open the MXene interlayer spacing is to create “pillars” between the layers by using molecules or ions [67,116,117]. For example, by immersing a wet $Ti_3C_2T_x$ powder in hydrazine, the hydrazine molecules intercalate between $Ti_3C_2T_x$ layers, increasing the interlayer spacing [67]. This opened structure leads to improved ion accessibility to reactive sites, resulting in increased capacitance up to 250 F g^{-1} for 75 µm thick electrodes in H_2SO_4 electrolyte. Another pillared Ti_3C_2 MXene structure with enlarged interlayer spacing was achieved by using a cationic surfactant cetyltrimethylammonium bromide (CTAB) intercalated by electrostatic interaction, while further Sn^{4+} intercalation was made by ion exchange interaction [117]. The Sn^{4+} cations between MXene interlayers undergo large volume expansion during alloying with lithium in non aqueous electrolyte, keeping MXene interlayers open to provide extra capacity. When used as anode in lithium ion capacitors, the CTAB Sn (IV)@Ti_3C_2 electrode performs remarkable capacity (765 mAh g^{-1} after 100 cycles at 0.1 A g^{-1}) with high capacity retention at different current densities in organic electrolyte.

Delaminated MXene nanosheets can be obtained by solvent intercalation into the accordion like MXenes under ultrasonication [118]. Moreover and as early mentioned, the LiF/HCl etching synthesis route, which combines etching and delamination processes, is a simple way to collect colloidal solution of delaminated single or few layer MXene flakes. Although the distance between different MXene flakes can be considered as very large in MXene suspensions, these nanoflakes suffer

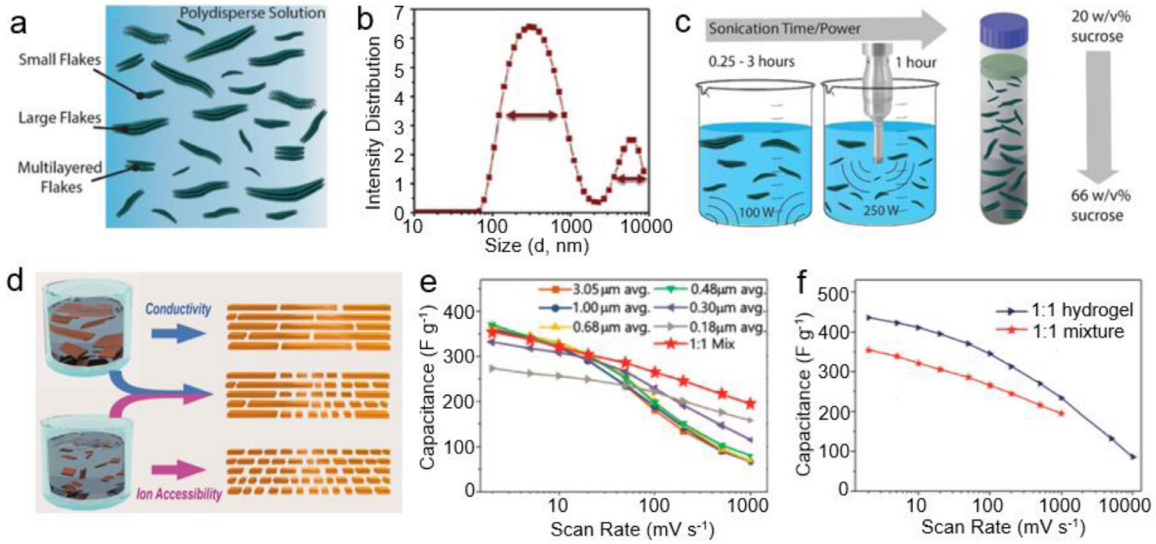

Fig. 3. Effect of sheet size on structure and capacitive performance of MXenes. (a) Schematic representation of a colloidal dispersion of MXene which is polydisperse in flake size. (b) Dynamic light scattering intensity distribution showing the wide distribution of particle sizes in a MXene solution with no centrifugation. (c) Schematic showing sonication time and power to affect the lateral size of MXene flakes, and density gradient centrifugation to separate MXene flakes with controlled lateral sizes. Reproduced from Ref. [109] with copyright permission from American Chemical Society. (d) Schematic showing the superiority of rational combination of various MXene flake sizes and (e and f) the capacitances in 3 M H_2SO_4 of the MXene mixture. Reproduced from Ref. [110] with copyright permission from American Chemical Society.

from dense restacking during conventional drying treatments. Adding a spacer is a very effective method to prevent nanoflakes restacking and keep the interlayer space open for accessible ion storage and transport. There are several methods to introduce spacers into the delaminated MXenes.

Mixing 2D MXene suspensions with spacer dispersions, followed by co filtration results in randomly mixed structures of MXene nanosheets and spacers [93,119 124]. One dimensional carbon nanotubes (CNTs) were used as interlayer spacers for delaminated Ti_2CT_x MXenes to pre vent restacking [93], providing rapid charge transport and enhanced electrochemical performances. Simon et al. further illustrated the im provement of MXenes' performances by introducing CNTs as spacers in organic electrolyte [119]. With organic electrolyte of 1 M 1 ethyl 3 methylimidazolium bis(trifluoromethylsulfonyl)imide (EMITFSI) in ace tonitrile, CNTs spacers resulted in the preparation of a $Ti_3C_2T_x$ electrode with a capacitance of 245 F cm^{-3} at 2 mV s^{-1}, that is 3 fold increase compared to the meant $Ti_3C_2T_x$ capacitance. Also in organic electrolyte (1 M $LiPF_6$ EC/DEC), a flexible Nb_2CT_x/CNT paper electrode delivered a volumetric capacitance of 325 F cm^{-3} for Li ion capacitor [124]. 2D graphene or reduced graphene oxide (rGO) nanosheets can also be ef fectively intercalated between delaminated MXene layers by this route. As shown in Fig. 4a, a holey graphene intercalated $Ti_3C_2T_x$ MXene was prepared by filtration of alkalized MXene and holey graphene oxide dis persions and the subsequent annealing. Here, the holey graphene effec tively prevents MXene from restacking and forms a porous network for boosting the ion transport [120]. Such holey graphene modified MXene film delivered an ultrahigh volumetric capacitance of 1445 F cm^{-3} at 2 mV s^{-1}, together with superior rate capability and high mass loading. Interestingly, MXene nanoparticles (prepared by HF etching) can also act as interlayer spacers to prevent the MXene nanosheets (prepared by HCl/LiF etching) from restacking, significantly improving the electro chemical performance [121].

Alternative filtration of MXene suspensions and spacer dispersions is a useful method to build sandwich like composite architectures [125,126]. Using this approach (Fig. 4b), a flexible MXene/CNTs film with only 5 wt% CNTs content showed significantly improved volu metric capacitance (280 F cm^{-3} at 200 mV s^{-1}) in 1 M $MgSO_4$ elec trolyte compared to that of pure MXene film (162 F cm^{-3}), or randomly mixed MXene/CNT paper (236 F cm^{-3}). The incorporation of CNTs ef fectively increased spacing between the $Ti_3C_2T_x$ nanosheets and pro vided improved ion accessible surface area [125]. Besides, sandwich like $Ti_3C_2T_x$/onion like carbon and $Ti_3C_2T_x$/rGO, produced by similar technique, also exhibited impressive electrochemical performances as supercapacitor electrodes.

Since MXene nanosheets are usually negatively charged, inserting positively charged spacers, like CTAB grafted CNTs [127,128] or PDDA modified rGO, [129] between MXene layers through electrostatic self assembly is an effective way to prevent MXene restacking. As shown in Fig. 4c, after modification with polydiallyldimethylammonium chloride (PDDA), positively charged rGO nanosheets were mixed with MXene for electrostatic self assembly. Then, the PDDA modified rGO was in tercalated between MXene nanosheets, preventing their restacking and increasing the interlayer spacing [129]. A flexible MXene film electrode prepared with only 5wt% graphene revealed volumetric capacitances as high as 1040 and 634 F cm^{-3} at 2 mV s^{-1} and 1 V s^{-1}, respectively, in 3 M H_2SO_4 electrolyte. It is noteworthy that cations also have pos itive charge and can play a pillaring role as spacers between MXene nanosheets [130,131]. A highly ordered V_2CT_x film was fabricated via electrostatic interaction of alkali metal cations and V_2CT_x flakes. The intercalated cations enlarged the MXene interlayer spacing and thus im proved the electrochemical properties, endowing the MXene with volu metric capacitances in excess of 1300 F cm^{-3} [94]. Moreover, the cation driven electrostatic assembly converted the chemically (and electro chemically) unstable V_2CT_x flakes to highly stable V_2CT_x films.

Ion exchange strategies have been employed to replace the interlay ered molecules or ions with larger spacers. By immersing $Ti_3C_2T_x$ hydro gel, which contained huge amounts of water and acetone, into 1 ethyl 3 methylimidazolium bis (trifluoromethylsulfonyl) imide (EMITFSI), an ionogel was formed with EMITFSI between $Ti_3C_2T_x$ flakes. Due to the pillaring effect of the ionic liquid, MXenes with increased interlayer spacing were prepared, that could operate in ionic liquid electrolyte with improved electrochemical performance compared with the non intercalated MXenes [132]. Another example is the use of hexade cylamine hydrochloride (HEXCl) for ion exchange reactions with the TMAOH delaminated MXene (Fig. 4d). The TMA^+ cations intercalated in the $Ti_3C_2T_x$ interlayers were replaced with HEX^+. Subsequently,

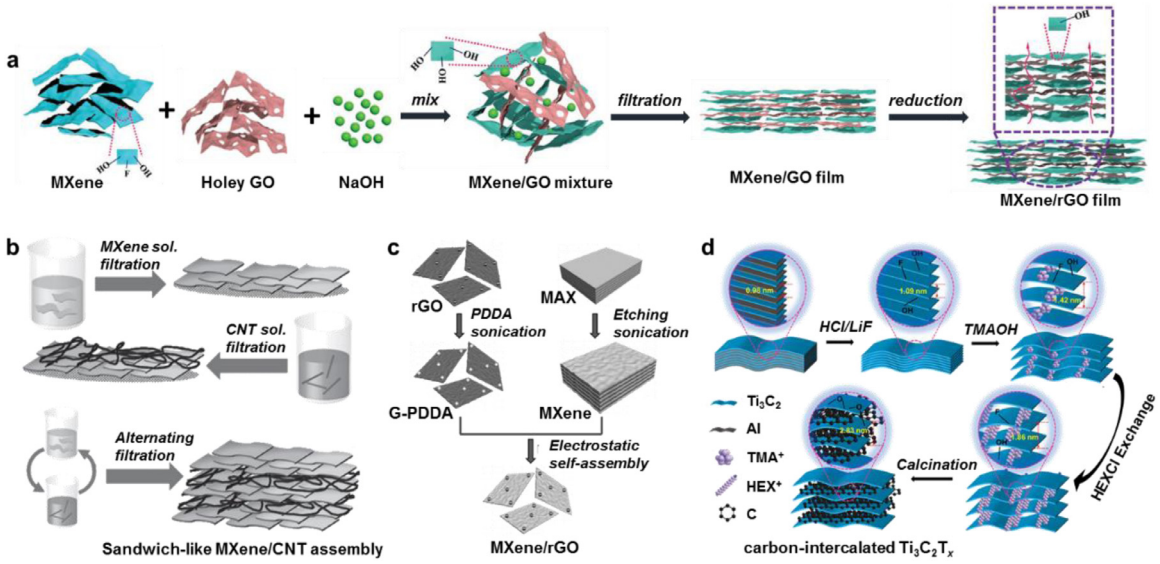

Fig. 4. Adding interlayer spacers to prevent the MXene nanoflakes from restacking. (a) Simple mixing and filtration of MXene and holey GO dispersions followed by thermal reduction. Reproduced from Ref. [120] with copyright permission from Wiley-VCH. (b) Alternative filtration of MXene suspensions and CNT dispersions to construct sandwich-like composite MXene/CNTs film. Reproduced from Ref. [125] with copyright permission from Wiley-VCH. (c) Electrostatic self-assembly of negatively charged MXene nanosheets and positively charged PDDA-modified rGO. Reproduced from Ref. [129] with copyright permission from Wiley-VCH. (d) Ion-exchange reactions by HEXCl to replace the TMA^+ cations in the TMAOH-delaminated MXene interlayers, followed by *in situ* carbonization, producing the carbon-intercalated $Ti_3C_2T_x$. Reproduced from Ref. [133] with copyright permission from Royal Society of Chemistry.

through *in situ* carbonization by annealing, the carbon intercalated $Ti_3C_2T_x$ MXenes were prepared, which exhibited enlarged interlayer spacing, enhanced electrical conductivity and improved electrochemical performances [133].

Other methods have also been developed to add spacers into the delaminated MXene materials by using electrophoretic deposition [134] or plasma exfoliation [135]. For instance, via electrophoretic deposition of a uniform mixed suspension of delaminated $Ti_3C_2T_x$ MXene and CNTs, CNTs were incorporated between MXene layers, building a robust structure, preventing MXene restacking, thus leading to the enhanced electrochemical performance [134].

3.2.3. Designing 3D/porous structure

Reducing flake size and enlarging interlayer spacing are beneficial to enhance the ion transport and ion accessibility to active sites, thus improving the performance of MXenes. However, designing 3D/porous electrode structure, with large ion accessible active surface area and interconnected pores for ion transport channels, can more efficiently improve the MXenes high rate capability.

Creating porous MXene architecture can offer paths for electrolyte impregnation and ion transport, shortening the diffusion distance and decreasing the resistance, so offering suitable porous architecture promises improved rate performance of MXenes. Several approaches, like chemical etching [136], template methods [137 140], hydrazine induced foaming [141], electrophoretic deposition [142], have been employed for building porous MXene electrodes. As an example, using poly(methyl methacrylate) (PMMA) spheres as hard templates, an open $Ti_3C_2T_x$ MXene architecture with 1~2 μm diameter macropores and submicrometer wall thicknesses was prepared (Fig. 5a) [71]. Owing to the greatly reduced ion transport lengths, macroporous 13 μm thick film with 0.43 mg cm^{-2} loading revealed a gravimetric capacitance of 310 F g^{-1} (0.14 F cm^{-2}) at an ultrahigh power performance, with 200 F g^{-1} (0.09 F cm^{-2}) still delivered at 10 V s^{-1} in 3 M H_2SO_4 electrolyte (Fig. 5b). EIS spectra of thicker films (3.7 mg cm^{-2} loading, Fig. 5c) further confirmed the small ion transport resistance in the macroporous architecture; those films could achieve specific capacitances beyond 2 F cm^{-2}. Nanoporous MXene film can also be prepared via template methods. A nanoporous MXene film was prepared using $Fe(OH)_3$ nanoparticles with diameters of 3~5 nm as templates [143]. The film maintained a typical layer structure (Fig. 5d) with the presence of a nanoporous network for ion transport, which was evidenced by an enhanced specific surface area (Fig. 5e). Remarkably, using an optimized porosity (56 m^2 g^{-1}, 0.1 cm^3 g^{-1}), a nanoporous MXene film could achieve an ultrahigh density of 3.3 g cm^{-3}, together with high volumetric capacitance of 1142 F cm^{-3} and 828 F cm^{-3} at 0.5 A g^{-1} and 20 A g^{-1}, respectively, in 3 M H_2SO_4 electrolyte (Fig. 5f). Recently, small ice grains were used as self sacrificial templates to fabricate free standing and flexible MXene/CNTs film with both macropores and nanopores. By freeze drying the wet MXene based film, a large amount of residual water molecules in MXene interlayer were *in situ* transformed into ice templates. Thanks to the controlled porous structure with improved ion accessibility, capacitance as high as 375 and 251 F g^{-1} could be reached at 5 and 1000 mV s^{-1}, respectively [144]. Besides, foaming by vapor [145], crumpling [146] and carbon assisted assembly [147,148] have been reported to be effective to build porous MXene frameworks.

Assembling 2D MXene sheets into 3D electrode architecture is also favorable to improve the performance of MXene materials for energy storage applications. 3D MXene aerogels can be obtained in combination with graphene [149 151]. As illustrated in Fig. 6a, during freeze drying of a mixed solution of GO and MXene, both GO and MXene nanosheets were forced to gradually align along the ice crystal boundary and finally cross linked by the π π interaction to form a 3D porous network. Interestingly, this 3D structure was maintained after the reduction reaction from GO to rGO [150]. Moreover, 3D MXene aerogels can be prepared by removing water via freeze drying from the MXene hydrogels [152,153]. Shang et al. reported a 3D macroscopic MXene hydrogel assembled with GO and ethylenediamine (EDA) [151]. The EDA reductant initiated ring opening of epoxy groups on GO surface to form oxygen dangling bonds, which then reacted with MXene flakes to form a hydrogel of MXene together with partially reduced GO under van der Waals forces and π π stacking interactions (Fig. 6b). The hydrogel with 3D porous structure exhibited high electron transfer rate and fast ion transport to active redox sites, and delivered an exceptionally high capacitance of 165 F g^{-1} even at 1000 A g^{-1} in H_2SO_4 electrolyte. Furthermore, through tuning the drying process, these MXene hydrogels could

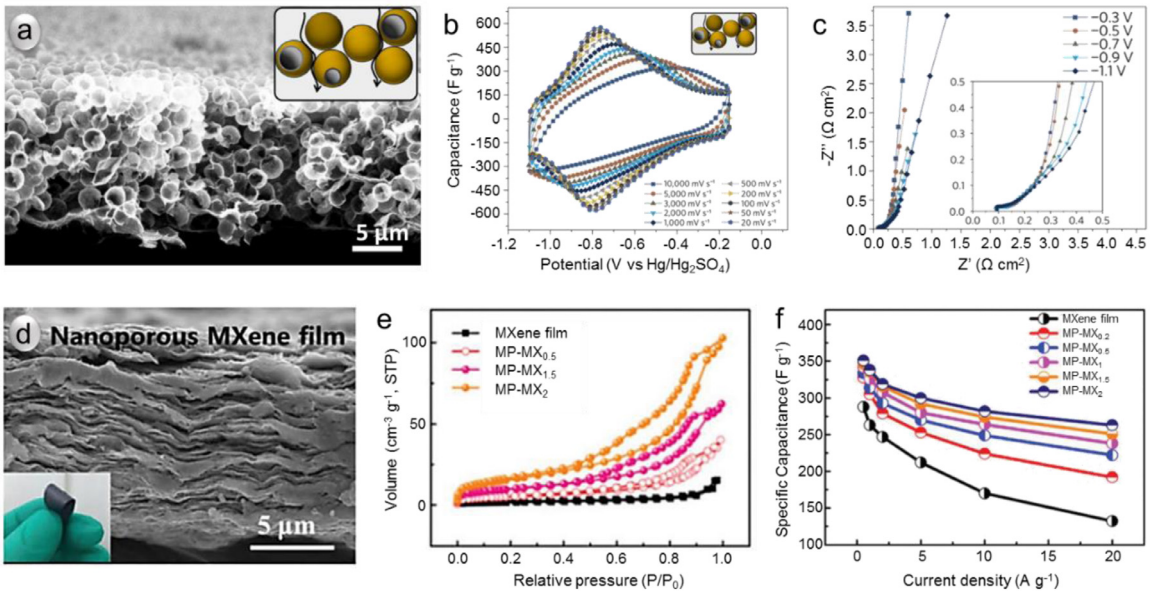

Fig. 5. Porous MXenes as electrode materials for supercapacitors. (a) Cross-sectional SEM image of the macroporous $Ti_3C_2T_x$ film prepared with PMMA template (inset: schematically macroporous architecture and ionic current pathways in it). (b) CVs of a macroporous 13-μm-thick film with 0.43 mg cm^{-2} loading in 3 M H_2SO_4 electrolyte at scan rates ranging from 20 to 10,000 mV s^{-1}. (c) Electrochemical impedance spectroscopy (EIS) at various potentials for a macroporous film with 3.7 mg cm^{-2} loading. Reproduced from Ref. [71] with copyright permission from Springer. (d) Cross-sectional SEM image of the nanoporous $Ti_3C_2T_x$ film prepared with $Fe(OH)_3$ nanotemplate. (e) N_2 adsorption–desorption isotherms of the nanoporous MXene films. (f) Capacitances of various nanoporous films. Reproduced from Ref. [143] with copyright permission from Royal Society of Chemistry.

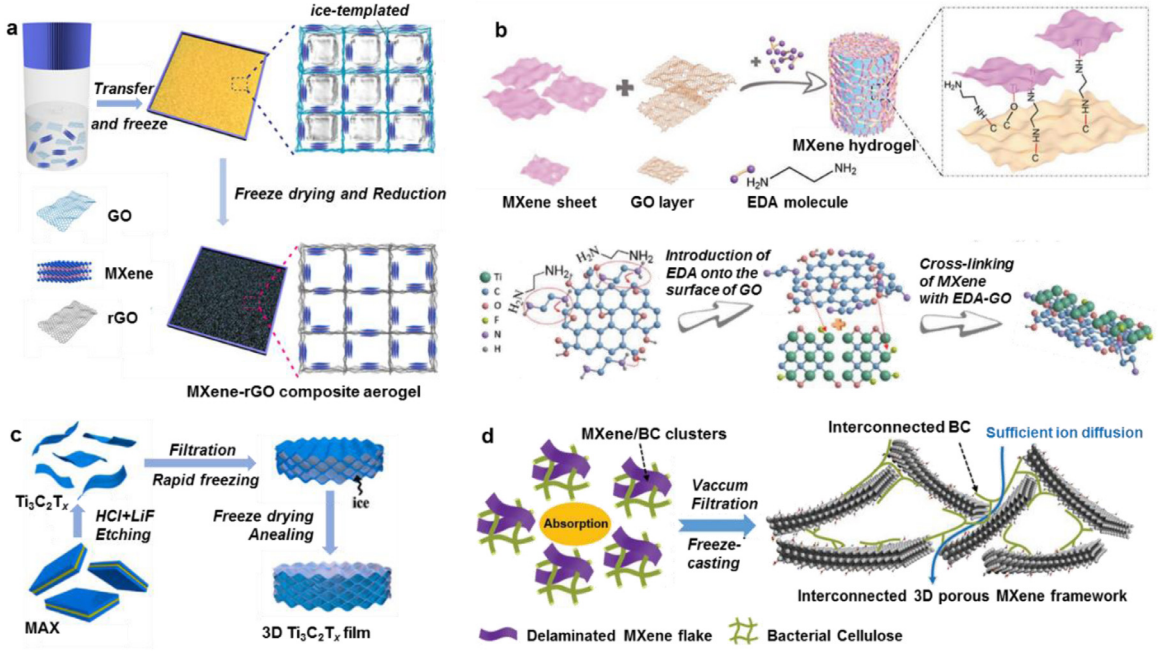

Fig. 6. Designs for 3D MXene architectures. (a) MXene-rGO composite aerogel constructed by freeze-drying of the mixture of GO and MXene and the subsequent mild chemical reduction. Reproduced from Ref. [150] with copyright permission from American Chemical Society. (b) 3D macroscopic MXene hydrogel assembled with the assistance of GO and ethylenediamine (EDA). Reproduced from Ref. [151] with copyright permission from Wiley-VCH. (c) 3D macroporous MXene prepared by a rapid freezing with liquid nitrogen and then freezing drying. Reproduced from Ref. [154] with copyright permission from Elsevier. (d) 3D porous MXene/bacterial cellulose (BC) composite film self-assembled with BC as interconnected substrate. Reproduced from Ref. [155] with copyright permission from Wiley-VCH.

be transformed into different structures ranging from a loosely porous aerogel to a dense solid, applicable for different fields.

In addition to aerogels/hydrogels, 3D macroporous MXenes could be fabricated via a simple and environmental friendly rapid freezing method with liquid nitrogen. As shown in Fig. 6c, when the $Ti_3C_2T_x$ film, prepared by vacuum filtration, was immersed into liquid nitrogen, water remained in the film was rapidly solidified into ice crystals and MXene nanosheets formed a continuous network along the ice crystal boundaries [154]. After subsequent freeze drying, a 3D macroporous MXene architecture was obtained. This 3D macroporous MXenes not only possessed much more active sites than the dense $Ti_3C_2T_x$ film, but also exhibited larger volumetric capacitance in H_2SO_4 electrolyte, higher

strength, lower cost and higher production efficiency than the $Ti_3C_2T_x$ aerogel. Another method to assemble 3D porous MXene was reported by using bacterial cellulose (BC) fibers as substrate (Fig. 6d) [155]. The MXene and BC could absorb together spontaneously on basis of the in teraction between their oxygen containing groups. After vacuum filtra tion, freeze casting and drying, a bicontinuous 3D porous MXene/BC architecture was formed, which was beneficial for fast ion transport and improved accessibility to active sites. Additionally, the intercon nected BC network provided robust mechanical strength and the MXene framework offered high electronic conductivity, enabling the MXene/BC composite film to achieve a linear increase of the capacitance when the electrode mass loading was increased from 1.2 to 8 mg cm^{-2} at current densities less than 30 mA cm^{-2}.

Loading MXenes onto 3D matrix such as carbon cloth [156 158] and nickel foam [159 162] is also an important and simple method to de sign 3D MXene frameworks. 2D delaminated MXene nanosheets can be assembled onto a 3D nickel foam skeleton by electrostatic self assembly [159, 160], electrophoretic deposition [161], or dropping mild baking approach [162]. The obtained structure provides high electronic con ductivity, massive active redox sites, high ion transfer efficiency and short ion diffusion paths, leading to great improvement of electrochem ical performances of the MXenes. But one consideration is high dead weight and low volumetric capacitance of nickel foam. Besides, the decoration with metals on MXenes can also enhance their conductiv ity [163, 164], which is beneficial to further improving the rate perfor mance.

Compared with restacked MXene nanosheets, the 3D/porous MXene frameworks have provided significant improvements on rate capabil ity of MXenes through facilitating the ion transport, resulting in im proved electrochemical performance. Nevertheless, the existence of a large number of macroporous results in the decrease of the density and volumetric capacitance of the MXene frameworks. Therefore, the porous structure should be optimized to balance the volumetric capacitance and rate capability of MXenes. Also, the weight of the porous current collector (Ni foam for instance) may significantly decrease the gravi metric performance of the whole electrode (including the current col lector weight). One simple strategy is mechanically pressing the 3D MX ene aerogel to increase its packing density and conductivity and main tain sufficient ion accessible active sites at the same time. Through this method, a compact and nanoporous $Ti_3C_2T_x$ MXene film was obtained, which delivered a high volumetric capacitance of 616 F cm^{-3} with a high mass loading of 12.2 mg cm^{-2} [165]. Recently, a reduced repulsion freeze casting assembly concept was proposed for producing ordered 3D porous MXene architectures [166]. When KOH solution was added into a $Ti_3C_2T_x$ suspension, the interlayer electrostatic repulsion was weak ened. Via a freeze casting process, KOH treated MXene nanosheets could be assembled into a stable 3D porous framework with relatively com pact honeycomblike structure, which can be scaled to a mass loading of 16.18 mg cm^{-2} with insignificant capacitance attenuation.

3.2.4. Fabricating vertical alignments

Vertically aligned $Ti_3C_2T_x$ MXene flakes were developed to further shorten the ion transport paths. For example, a vertical alignment of 2D MXene flakes was prepared from a high order discotic lamellar liquid crystalline MXene [167]. Indeed, 2D MXene flakes dispersed in an aque ous solution could spontaneously produce discotic liquid crystal phases, but the formation of the high order phase in 2D MXene nanosheets with large polydispersity needs the presence of a surfactant. As shown in Fig. 7a, when hexaethylene glycol monododecyl ether ($C_{12}E_6$), used as surfactant, was introduced with MXenes, strong hydrogen bonds were formed between the OH groups of $C_{12}E_6$ and F or O terminations on MXenes, enhancing molecular interactions between the nanosheets. The resultant increasing packing symmetry resulted in the formation of high order discotic lamellar phase of 2D MXene nanosheets. Under an external mechanical shearing, coherent lamellar MXene flakes were aligned vertically to minimize the elastic distortion energy (Fig. 7b). The MXene lamellar liquid crystal aligned almost unidirectional and vertically under shear flow, which was confirmed by polarized optical microscope (Fig. 7c) and SEM observations (Fig. 7d). The vertical align ment provided monidirectional ion transport, resulting in excellent elec trochemical performances in H_2SO_4 electrolyte (Fig. 7e g). Indeed, the gravimetric capacitance (above 200 F g^{-1}) was nearly independent on the film thickness up to 200 μm at scan rates below 2000 mV s^{-1}, far ex ceeding the performance of 100 μm thick commercial carbon electrodes. Also, for the film with a mass loading of 2.80 mg cm^{-2}, the areal capac itance achieved above 0.6 F cm^{-2} at 1000 mV s^{-1}, making these thick, vertically aligned MXene electrodes very attractive for high rate energy storage applications. Afterwards, a MXene film electrode composed of “anti T shape” flakes was prepared for effective vertical ion transport [168]. The “anti T shape” $Ti_3C_2T_x$ film was obtained by vacuum fil trating a MXene solution through a entwined metal mesh as filtration membrane (Fig. 7h). Thanks to the improvement of ion transport, the “anti T shape” $Ti_3C_2T_x$ film electrodes showed a capacitance of 361 F g^{-1} at 2 A g^{-1} and a capacitance retention of 76% as the current density increased to 20 A g^{-1} in H_2SO_4 electrolyte.

In order to meet the requirements on capacitance and rate perfor mance, various architectures of MXenes have been prepared. As listed in Table 2, rational design of MXene and MXene based electrode struc tures is of high importance to achieve desirable performances of super capacitors. Designing hydrogel framework can push the capacitance of MXenes closer to its theoretical limit, while a porous MXene structure can achieve high rate performance at potential scan rate up to 10 V s^{-1}. Vertically aligned MXene flakes can exhibit high capacitive and power performance independent from film thickness up to 200 μm. These de signs and their combination offer new exciting opportunities for MXenes for supercapacitor applications.

These electrodes can achieve high performance in aqueous elec trolytes, which is within a limited voltage window (about 1 V), because of the limitation by water electrolysis and associated O_2 and H_2 gas evo lution. Improving the energy density will then need MXene electrodes to operate in non aqueous electrolytes, where the electrochemical perfor mances are known to be lower because of the limited cation accessibility to the redox sites of MXenes, as a consequence of the use of bigger ions vs. H^+ and the lower ion transport rate in non aqueous electrolytes. As a result, more effort will have to be directed towards the preparation of MXene architectures with balanced open ion transport channels to gether with higher density to improve the electrode gravimetric and volumetric capacity in non aqueous electrolytes. Moreover, the design of advanced structures will need to use simple processes for practical applications.

3.3. Chemical modification

Computational studies suggest that the chemical modification of MX enes can result in improved performance, which is a promising direction for its rational engineering. For example, designing specific surface ter minations on MXene surface can be used to control the bandgap, elec tronic conductivity, work functions, half metallicity and 2D ferromag netism [70]. Most recently, a post synthetic exchange reaction strat egy was used to tune surface groups on MXenes prepared by Lewis acidic molten salt etching method [70]. Through this strategy, MXenes with different surface terminations (NH, S, Cl, Se, Br, Te, etc.) and even bare MXenes without terminations were prepared, which per formed unique structural and electronic properties. Moreover, MXene doping with heteroatoms for instance can affect their lattice parameter, electronic property, bandgap, and density of states. For different appli cations, various heteroatoms and metal elements have been introduced into MXene lattice. For example, MXenes doping with metal elements (such as Pt, Co, Ru, Nb, etc.) were used to enhance the kinetics of cat alytic hydrogen evolution reaction [169 173]. Additionally, the intro duction of vacancies can influence the surface morphology and reactiv ity of MXenes [174]. Therefore, the chemical modification of MXenes

Table 2
Capacitive performances of the MXene electrodes with rational structural designs.

Electrode	Fabrication method	Electrolyte	Potential	Capacitance	Cycle stability	Ref.
Controlling flake size						
$Ti_3C_2T_x$ film	Mixing large & small flakes	3 M H_2SO_4	-0.7~0.2 V (vs Ag/AgCl)	435~86 F g^{-1} (2~10,000 mV s^{-1})	98% (10,000 cycles)	[110]
Adding spacer between MXene interlayer						
75 μm $Ti_3C_2T_x$ pillared by hydrazine	Suspending in hydrazine	1 M H_2SO_4	-0.3~0.2 V (vs Ag/AgCl)	250~210 F g^{-1} (2~100 mV s^{-1})	no decay (10,000 cycles)	[67]
$Ti_3C_2T_x$/graphene-3% film	Mixing and filtration	3 M H_2SO_4	-0.7~0.3 V (vs Ag/AgCl)	438~302 F g^{-1} (2~500 mV s^{-1})	93% (10,000 cycles)	[120]
Sandwiched $Ti_3C_2T_x$/CNT-5% film	Alternative filtration	1 M $MgSO_4$	-0.8~0.1 V (vs Ag/AgCl)	390~280 F cm^{-3} (2~200 mV s^{-1})	no decay (10,000 cycles)	[125]
$Ti_3C_2T_x$/rGO-5% film	Electrostatic self-assembly	3 M H_2SO_4	-0.7~0.3 V (vs Ag/AgCl)	1040~634 F cm^{-3} (2~10,000 mV s^{-1})	no decay (20,000 cycles)	[129]
V_2CT_x/alkali metal cations film	Cation-driven assembly	3 M H_2SO_4	-0.4~0.2 V (vs Ag/AgCl)	1315~>300 F cm^{-3} (5~10,000 mV s^{-1})	~77% (10^6 cycles)	[94]
$Ti_3C_2T_x$ ionogel film	Immersing into EMITFSI	EMITFSI	0~3 V (2-electrode)	70~52.5 F g^{-1} (20~500 mV s^{-1})	>80% (1000 cycles)	[132]
Carbon-intercalated $Ti_3C_2T_x$	*in situ* carbonization	1 M H_2SO_4	-0.1~0.5 V (vs Ag/AgCl)	364.3~193.3 F g^{-1} (1~20 A g^{-1})	>99% (10,000 cycles)	[133]
Ti_3C_2/CNTs film	Electrophoretic deposition	6 M KOH	-0.9~-0.4 V (vs Hg/HgO)	134~55 F g^{-1} (1~10 A g^{-1})	no decay (10,000 cycles)	[134]
$Ti_3C_2T_x$@rGO film	Plasma exfoliation	PVA/H_2SO_4	0~0.7 V (2-electrode)	54~35 mF cm^{-2} (0.1~10 mA cm^{-2})	~100% (1000 cycles)	[135]
Designing 3D/porous structure						
13 µm $Ti_3C_2T_x$ film	1~2 µm PMMA template	3 M H_2SO_4	-1.1~-0.15 V (vs Hg/Hg_2SO_4)	310~100 F g^{-1} (10~40,000 mV s^{-1})	–	[71]
Nanoporous $Ti_3C_2T_x$ film	3~5 nm $Fe(OH)_3$ template	3 M H_2SO_4	-0.5~0.3 V (vs Ag/AgCl)	1142~828 F cm^{-3} (0.5~20 A g^{-1})	90.5% (10,000 cycles)	[143]
MXene/CNTs film	Ice template	3 M H_2SO_4	-0.7~0.3 V (vs Ag/AgCl)	375~92 F g^{-1} (5~10,000 mV^{-1})	95.9% (10,000 cycles)	[144]
$Ti_3C_2T_x$-rGO aerogel	Freeze-drying	PVA/H_2SO_4	0~0.6 V (micro supercapacitor)	34.6~9.2 mF cm^{-2} (1~100 mV s^{-1})	91% (15,000 cycles)	[150]
Ti_3C_2 aerogel	EDA-assisted assembly and freeze-drying	1 M KOH	-1.0~0.4 V (vs Ag/AgCl)	87.1~66.7 F g^{-1} (2~100 mV s^{-1})	87.7% (10,000 cycles)	[152]
$Ti_3C_2T_x$ aerogel	Ammonia-assisted assembly and freeze-drying	3 M H_2SO_4	-0.6~0.2 V (vs Ag/AgCl)	438~173 F g^{-1} (10~20,000 mV s^{-1})	94% (20,000 cycles)	[153]
$Ti_3C_2T_x$ hydrogel	GO&EDA-assisted assembly and freeze-drying	H_2SO_4	-1.1~-0.15 V (vs Hg/Hg_2SO_4)	370~165 F g^{-1} (5~1000 A g^{-1})	98% (10,000 cycles)	[151]
3D macroporous $Ti_3C_2T_x$ film	Rapid freezing	3 M H_2SO_4	-0.3~0.2 V (vs Ag/AgCl)	1355~826.5 F cm^{-3} (1~20 A g^{-1})	97% (8000 cycles)	[154]
$Ti_3C_2T_x$/BC film	Filtration and freeze-casting	3 M H_2SO_4	-0.65~0.3 V (vs Ag/AgCl)	416~260 F g^{-1} (3~50 mA cm^{-2})	93% (10,000 cycles)	[155]
$Ti_3C_2T_x$/carbon cloth	Dipping, freeze-drying, KOH treatment	1 M H_2SO_4	-0.4~0.4 V (vs Ag/AgCl)	312~200 mF cm^{-2} (1~20 mA cm^{-2})	97% (8000 cycles)	[157]
Ti_3C_2/Ni foam	Electrostatic self-assembly	1 M Li_2SO_4	-0.9~-0.3 V (vs SCE)	370~117 F g^{-1} (2~10,000 mV s^{-1})	86.3% (10,000 cycles)	[160]
$Ti_3C_2T_x$/Ni foam	Electrophoretic deposition	1 M KOH	-0.75~-0.25 V (vs SCE)	140~110 F g^{-1} (5~50 mV s^{-1})	100% (10,000 cycles)	[161]
$Ti_3C_2T_x$/Ni foam	Dropping-mild baking	1 M H_2SO_4	0~0.4 V (2-electrode)	499~350 F g^{-1} (2~100 mV s^{-1})	~100% (10,000 cycles)	[162]
Compact and nanoporous $Ti_3C_2T_x$ film	Freeze-drying and mechanically pressing	3 M H_2SO_4	-0.5~0.3 V (vs Ag/AgCl)	932~462 F cm^{-3} (2~500 mV s^{-1})	88.4% (5000 cycles)	[165]
3D porous $Ti_3C_2T_x$ film	reduced-repulsion freeze-casting assembly	3 M H_2SO_4	-0.5~0.3 V (vs Ag/AgCl)	358.8~207.9 F g^{-1} (20~10,000 mV s^{-1})	93.8% (10,000 cycles)	[166]
Fabricating vertical alignments						
200 µm $Ti_3C_2T_x$ film	Mechanical shearing of a discotic lamellar liquid-crystal MXene	3 M H_2SO_4	-1.0~-0.1 V (vs Hg/Hg_2SO_4)	>200 F g^{-1} (10~2000 mV s^{-1})	~100% (20,000 cycles)	[167]
Anti-T $Ti_3C_2T_x$ film	Filtrating through a entwined metal mesh	1 M H_2SO_4	-0.5~0.3 V (vs Ag/AgCl)	361~275 F g^{-1} (2~20 A g^{-1})	70.3% (10,000 cycles)	[168]

Blue data in Cycle stability was tested in symmetric systems.

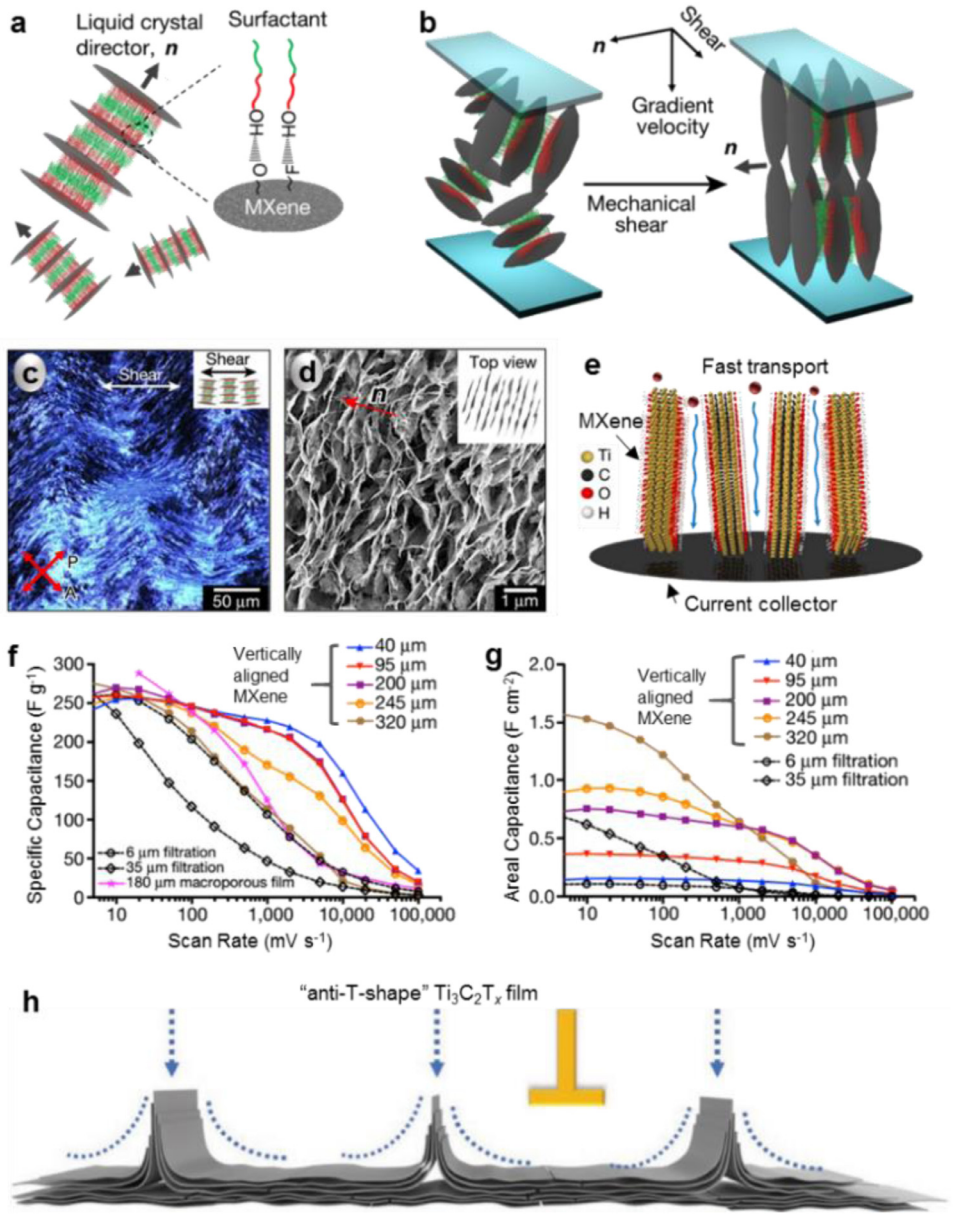

Fig. 7. Vertically aligned MXenes. (a) Illustration of the $C_{12}E_6$ surfactant created high-order discotic lamellar phase of MXene by the hydrogen bonding. (b) The alignment of the MXene flakes under mechanical shearing with the flow direction. (c) Optical microscope image with shear direction at 45° to the polarizer angle and (d) top-view SEM image of the MXene liquid crystal. (e) Fast ion transport in vertically aligned MXene. (f) Gravimetric and (g) areal capacitance of the vertically aligned MXene films at scan rates in range of 10~100,000 mV s^{-1}. Those of the vacuum-filtered MXene papers and a 180-μm thick macroporous MXene film [51] are listed for comparision. (a–g) Vertical alignment of MXene lamellar liquid crystal. Reproduced from Ref. [167] with copyright permission from Springer. (h) Schematic of "anti-T-shape" $Ti_3C_2T_x$ film. Reproduced from Ref. [168] with copyright permission from Wiley-VCH.

is an important direction to improve capacitive performance of MXenes by playing with electronic conductivity and surface reactivity with elec trolyte ions.

3.3.1. *Surface termination control*

MXenes, as being mainly prepared from MAX phases by etching process in F containing electrolytes, have abundant surface termina tions such as O, OH and F groups. These terminations greatly im pact on MXene interlayer spacing, electronic conductivity, ion adsorp tion and thus electrochemical performance [175]. Therefore, tuning the surface terminations is a way to improve electrochemical performances of MXenes [67,176]. It was demonstrated that the presence of oxygen containing terminations (O, OH) can endow MXenes with outstand ing hydrophilicity and induce bonding/debonding with ions from the electrolyte, resulting in pseudocapacitive behavior [177]; however, the presence of F terminations may block electrolyte ion transport [178], limit active redox sites [179], and decrease the electronic conductivity [175]. MXenes prepared by fluorine free etching routes exclude the F terminations [49,68,69]. However, the electrochemical performance of the obtained materials was somehow limited, possibly due to the poor quality of the etching without fluorine. Since most of the etching meth ods use HF or LiF/HCl as etching agents, F terminations are presented at MXene surface. Then, much efforts have been devoted to remove F terminations to improve the electrochemical performances of MXenes.

Annealing is a common method for termination modification. MXene annealed in N_2/H_2 atmosphere exhibited lower surface fluorine content, which improved the capacitive performance in KOH electrolyte by pro viding high ion accessibility [180]. Moreover, Simon et al. found that the F terminations on the MXene surface could be replaced with O terminations by treating in alkali solution as reagent, since Ti F bonds became unstable in basic solution [181]. After further annealing under Ar atmosphere, $Ti_3C_2T_x$ MXene electrodes with low termination con centration and high pseudocapacitance were obtained [182]. Fig. 8a summarizes the modifying procedures of this $Ti_3C_2T_x$ MXene. During treatment in KOH solution, K^+ ions spontaneously intercalate between the $Ti_3C_2T_x$ MXene nanosheets, leading to enlarged interlayer spacing. A further annealing under Ar atmosphere remove the terminated groups, leading to larger interlayer voids and lower termination concentration [182]. Thus, more active Ti atoms are exposed to the electrolyte, which significantly increase the capacitance up to 517 F g^{-1} at 1 A g^{-1} in

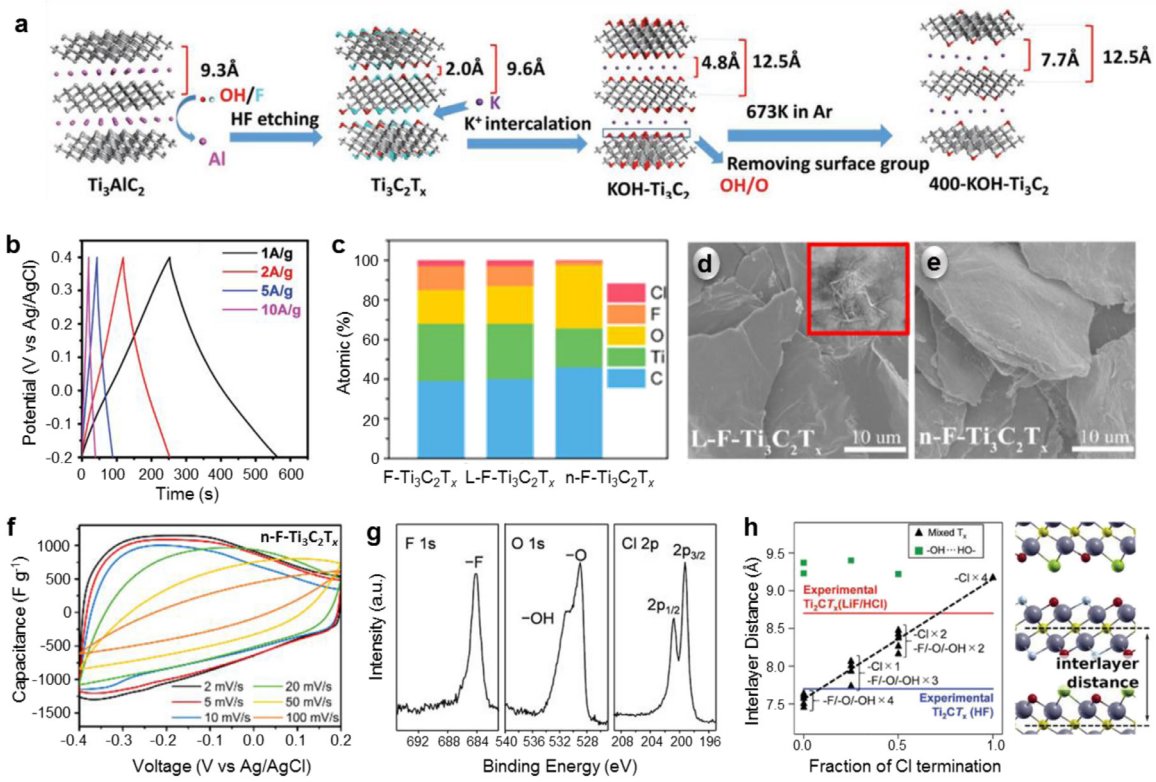

Fig. 8. Surface termination control of MXenes. (a) Schematic of modified $Ti_3C_2T_x$ MXenes by KOH treatment with further annealing under Ar. (b) Galvanostatic charge/discharge curves of the modified MXene at different current densities. Reproduced from Ref. [182] with copyright permission from Wiley-VCH. (c–f) Element distribution by XPS, SEM images and CV curves of the n-butyllithium modified MXenes (The few-layer $Ti_3C_2T_x$ (F-$Ti_3C_2T_x$) after modification by n-butyllithium and LiOH were denoted as n-F-Ti_3C_2T and L-F-Ti_3C_2T, respectively). Reproduced from Ref. [183] with copyright permission from American Chemical Society. (g and h) XPS spectra and optimized interlayer distance of Ti_2CT_x MXene prepared via LiF/HCl etching. Reproduced from Ref. [184] with copyright permission from Wiley-VCH.

H_2SO_4 electrolyte (Fig. 8b), that is about twice compared to the un treated one. However, the annealing treatment, even achieved under inert atmosphere, leads to partial oxidization of MXenes and the alkali treatment may also result in partial dissolution of the MXene structure. To better tune the oxygen and fluorine containing termination groups on MXenes, n butyllithium was employed as a strong nucleophilic and reducing reagent, which can transform OH and halogen groups into ether groups [183]. Compared with the alkali treated MXenes, the n butyllithium modified MXene showed more O groups and limited F terminations (Fig. 8c), as well as more stable structure (Fig. 8d and e). Therefore, outstanding electrochemical performance was achieved, with a high capacitance of 523 F g^{-1} at 2 mV s^{-1} (Fig. 8f) and 96% capaci tance retention after 10,000 cycles.

Other terminations might also be introduced onto MXene surface by etching or using delamination agents. A Ti_2CT_x MXene prepared from conventional LiF/HCl etching method showed the presence of Cl ter minations in addition to the O, OH, F groups (Fig. 8g) [184]. Dif ferently from F terminations, Cl terminations result in expanded in terlayer spacing, which was confirmed by the continuous increase of interlayer distance together with the Cl termination fraction (Fig. 8h). Furthermore, the lower electronegativity of Cl terminations than O, F terminations was demonstrated to be beneficial for enhancing the pseudocapacitance [185]. Besides, a sulfanilic diazonium salt was used as surface modifiers to functionalize the Ti_3C_2 MXene nanosheets with phenylsulfonic groups, causing improved dispersibility, larger specific surface area and enhanced capacitive performance [186].

It is noteworthy that the covalent surface modification strategy re cently reported provides large opportunities for tuning the surface ter minations on MXenes, leading to remarkable properties [70]. The effect of the new terminations, such as NH, Se, Br, Te, etc., on the capaci tive performance of MXenes and the mechanism are of great significance and needs to be further explored.

3.3.2. *Heteroatoms doping*

Heteroatoms doping can trim the electron donor capability of the material and modify the surface properties. Therefore, heteroatoms, es pecially nitrogen, have been introduced into MXenes to enhance their electrochemical performances. Taking N doped $Ti_3C_2T_x$ as an example, it is assumed that nitrogen atoms replace carbon atoms in the carbon lay ers, which can increase the MXene interlayer spacing, enhance the elec tronic conductivity, and create defects for additional active sites [187].

Heat treatment in ammonia atmosphere is one of the most commonly used ways for nitrogen doping. By annealing $Ti_3C_2T_x$ in ammonia, a N doped $Ti_3C_2T_x$ MXene was synthesized, in which the nitrogen mainly existed in types of Ti N, Ti O N (or Ti N O, O Ti N) and chemisorbed γ N_2 [187]. The nitrogen doping remarkably increases the d spacing from 0.96 nm (pristine $Ti_3C_2T_x$) to 1.23 nm and improves the electron con centrations, resulting in better ion accessibility and higher electronic conductivity. Therefore, N doped MXene exhibited enhanced capaci tance (192 F g^{-1} at 1 mV s^{-1} in H_2SO_4 electrolyte) than that of the un doped counterpart (34 F g^{-1}). It should be noted that these rela tively low capacitances were achieved in a 0.2~0.35 V (vs Ag/AgCl) potential window. A further widening of the potential window to 0.6~0.35 V (vs Ag/AgCl) may significantly increase the capacitance. Similarly, nitrogen doped $V_4C_3T_x$ MXene was prepared by annealing in ammonia and obtained a capacitance of 210 F g^{-1} at 10 mV s^{-1} in 1 M H_2SO_4 [188].

Doping from liquid phase is the most studied route for preparing N doped MXenes. With low cost industrial urea as nitrogen source, meth ods like hydrothermal treatment [189,190], solvothermal treatment

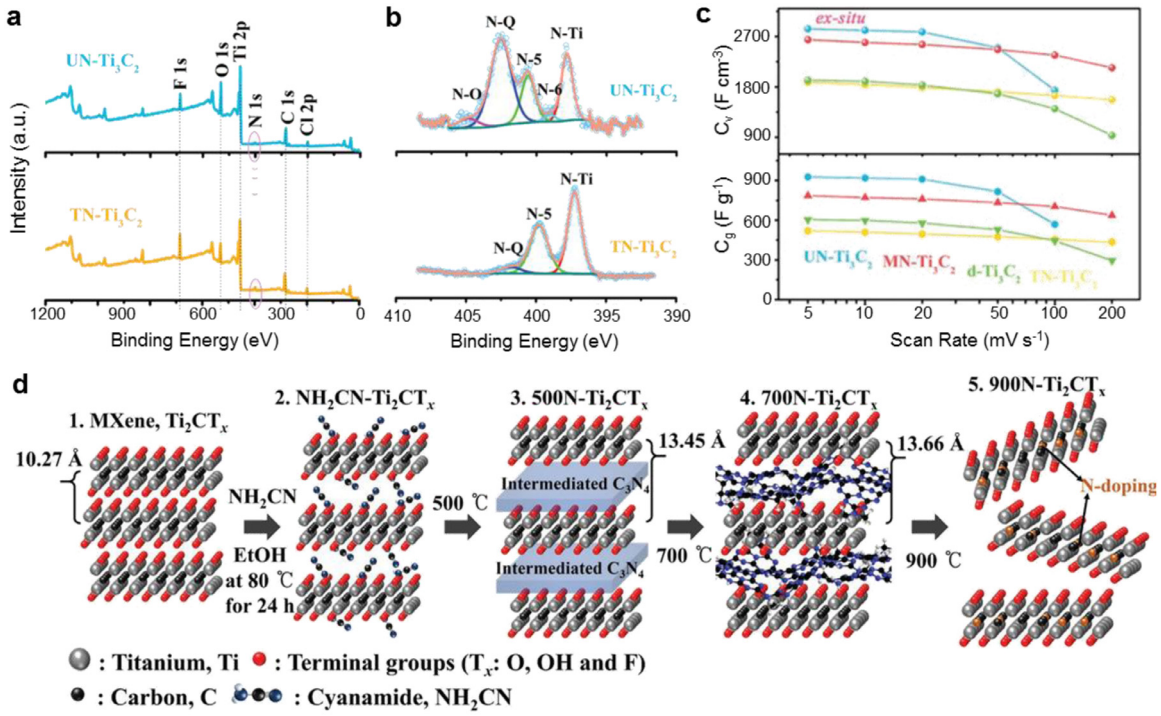

Fig. 9. N-doped MXenes. (a–c) XPS spectra and capacitances of the N-doped Ti_3C_2 prepared by *ex situ* solvothermal method (UN-Ti_3C_2: urea-assisted N-doped delaminated Ti_3C_2; MN-Ti_3C_2: MEA-assisted nitrogen-doped delaminated Ti_3C_2; TN-Ti_3C_2: delaminated $Ti_3C_{1.8}N_{0.2}$ solid solution films). Reproduced from Ref. [191] with copyright permission from Wiley-VCH. (d) Illustration for chemically doping a Ti_2CT_x with nitrogen from NH_2CN. Reproduced from Ref. [95] with copyright permission from Wiley-VCH.

[191], and liquid exfoliation [192] have been used for doping nitrogen into MXenes. For instance, a flexible, freestanding, and compact N doped delaminated Ti_3C_2 film was prepared with urea saturated alcohol solution as liquid nitrogen source through electrostatic adsorption and *ex situ* solvothermal treatment [191]. The film possessed a relatively high nitrogen concentration of 7.7 at% (Fig. 9a), enlarging the d spacing of MXene from 1.15 nm to 1.24 nm. Comparing with the delaminated $Ti_3C_{1.8}N_{0.2}$ solid solution film prepared by LiF/HCl etching of $Ti_3AlC_{1.8}N_{0.2}$ in Fig. 9b, the *ex situ* N doped film had extra pyridinic nitrogen (N 6) and oxynitride (N O) as well as much more quaternary nitrogen (N Q) [191]. N Q contributed to high capacitance, and the stable and high energy N 6 provided electron donor properties in the N doped MXene layers by rendering a pair of electrons for conjugation with the π conjugated rings. This is the possible reason for the ultrahigh volumetric capacitance achieved by the N doped Ti_3C_2 film, which delivered 927 F g^{-1} and 2836 F cm^{-3} at 5 mV s^{-1} in H_2SO_4 electrolyte (Fig. 9c). In addition, the NH_4F etching method for preparing MXene provides an interesting synthesis route for nitrogen doping. When Ti_3AlC_2 was selectively etched by HCl/NH_4F solution, $Ti_3C_2T_x$ flakes with NH_4^+ intercalated between layers were formed [193]. After annealing treatment, nitrogen atoms were incorporated into the in plane lattice of the $Ti_3C_2T_x$. The obtained N doped $Ti_3C_2T_x$ delivered a high capacitance of 586 F g^{-1} at 5 mV s^{-1} and a capacitance retention of 96.2% after 10,000 cycles at 5 A g^{-1} in H_2SO_4 electrolyte.

Besides, Ti_2CT_x MXene was chemically doped with nitrogen and simultaneously delaminated in liquid gas phase as shown in Fig. 9d [95]. Under inert atmosphere, the NH_2CN used as nitrogen source and intercalant was attached on the Ti_2CT_x nanosheets, which was further transformed into polymeric carbon nitride (p C_3N_4) by a condensation reaction during heat treatment. With increasing heating temperature, the p C_3N_4 decomposed and released nitrogen containing gasses, resulting in not only nitrogen doping, but also delaminated structures. The obtained N doped delaminated Ti_2CT_x with nitrogen content as high as 15.48 at% showed a capacitance of 327 F g^{-1} at 1 A g^{-1} and 96.2% capacitance retention after 5000 cycles at 5 A g^{-1} in 6 M KOH electrolyte.

Solid state doping was also achieved. By pyrolysis of thiourea, a nitrogen and sulfur co doped $Ti_3C_2T_x$ MXene was obtained which exhibited a capacitance of 175 F g^{-1} at 2 mV s^{-1} in Li_2SO_4 electrolyte [194].

To date, most of the studies of doping in MXenes focused on nitrogen. Other kinds of doping atoms, including heteroatoms and metal, also show potential for modifying MXenes. Calculation results indicate that B doping is beneficial for enhancing the elastic property of MXenes, which is suitable for applications in flexible devices [195]. Metal atoms, like V [196] and Nb [197], doping in MXenes can also enlarge the interlayer spacing, improve the conductivity and boost the capacitance of MXenes. As an example, via a hydrothermal method with NH_4VO_3 as the vanadium source, V doped $Ti_3C_2T_x$ MXene was prepared, where the V atoms help to tune the interaction between MXene and alkali metal adsorbates (e.g. Li^+, Na^+ and K^+) in the neutral electrolyte [196]. Thus, the V doped MXene performed a capacitance of 404.9 F g^{-1} in LiCl electrolyte, comparable to the performance under acidic conditions.

As demonstrated above, chemical modification can be successfully used to tune properties and enhance performances of MXenes. Introducing vacancy may be also an effective route to tune the MXene properties, as vacancy can create defects in the MXene matrix and thus influence the structure, surface property and activity of MXenes. Along with the deepening study on the strategies of chemical modification, more and more new kinds of terminations and doped atoms have been introduced into MXenes. Their effect on the capacitive performance of MXenes is a valuable researching task in the future.

4. MXene-based composite materials

Thanks to their special 2D lamellar structure and high electronic conductivity, MXenes have been considered as a promising material to prepare composite materials for energy storage applications. Various active materials, including metal oxides and conducting polymers, have

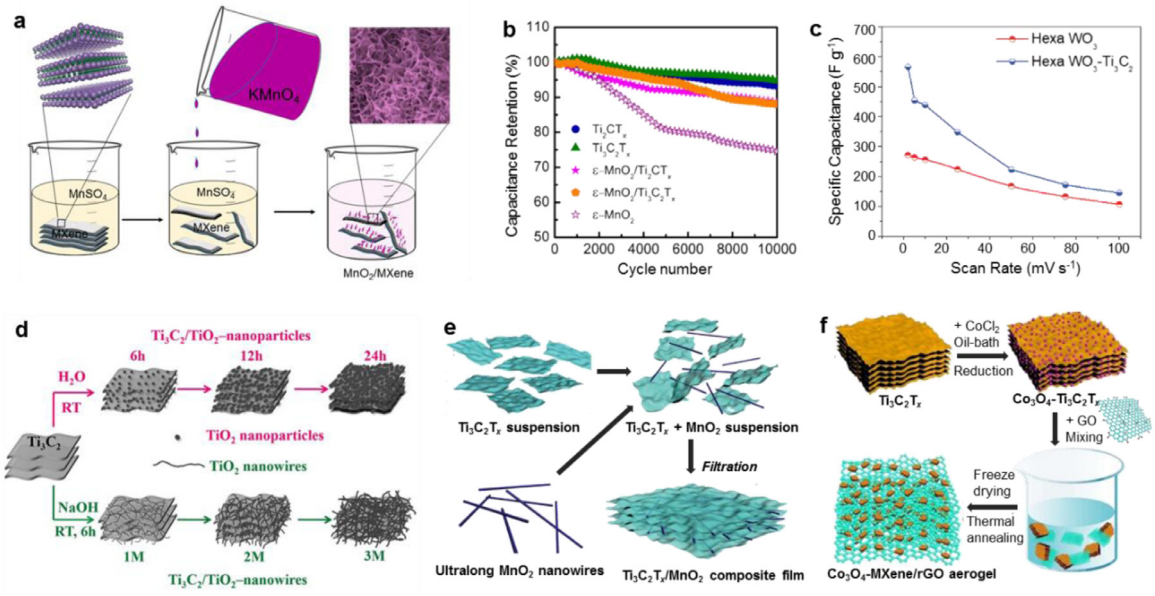

Fig. 10. MXene/metal oxide composites for supercapacitors. (a) Synthesis of MnO_2/MXene composite through the reaction of $MnSO_4$ and $KMnO_4$. (b) Cycling performance of symmetric two-electrode supercapacitors based on the MnO_2/MXene composite electrode at 5 A g^{-1} for 10,000 cycles. Reproduced from Ref. [201] with copyright permission from American Chemical Society. (c) Capacitances of hexagonal WO_3/Ti_3C_2 composite and pure hexagonal WO_3 electrodes. Reproduced from Ref. [212] with copyright permission from Wiley-VCH. (d) Preparation processes of two types of Ti_3C_2/TiO_2 composites. Reproduced from Ref. [210] with copyright permission from The Electrochemical Society. (e) *Ex situ* assembly of $Ti_3C_2T_x/MnO_2$ film via vacuum filtration of the mixed dispersion of MXene and MnO_2. Reproduced from Ref. [205] with copyright permission from Wiley-VCH. (f) Fabrication process of Co_3O_4-doped 3D MXene/rGO porous aerogel through a facile *in situ* reduction and thermal annealing. Reproduced from Ref. [216] with copyright permission from Wiley-VCH.

been used in combination with MXenes to achieve synergistic effects. In these composites, MXenes can provide high electronic conductivity to promote fast electron transfer, increase the accessible surface area, and stabilize the structure of the active materials. On the other hand, the active components can also serve as spacers to increase interlayer spacing and mitigate the restacking of MXenes, leading to fast ion transport and improved ion accessibility. As a result, MXene based composite materials often have enhanced electrochemical performances, which represents a significant and promising direction for MXenes in supercapacitor application. Moreover, 2D MXene nanosheets can be assembled into a freestanding and flexible framework which, after further loading to form the composite, can be directly used as electrodes for flexible devices.

4.1. MXene/metal compounds

Among a variety of pseudocapacitive materials investigated for supercapacitors, metal based compounds (transition metal oxides, chalcogenides, etc.) are promising for their high theoretical capacitances, but usually suffer from unsatisfactory electronic conductivity. Thanks to the metallic like conductivity of MXenes, MXene/metal compound composites have thus been investigated to tackle this issue.

4.1.1. MXene/metal oxides

Metal oxides, such as MnO_2 [198 205], MoO_3 [206], RuO_2 [207], SnO_2 [208], TiO_2 [209,210], NiO [211], WO_3 [212], and ZnO [213], have been widely used in combination with MXenes to reach superior capacitive performances. The routes for preparing the MXene/metal oxide composites can be divided into *in situ* preparation and *ex situ* assembly [203]. For *in situ* preparation, direct chemical growth of metal oxides on MXene nanosheets in liquid phase is a simple way to achieve strong interaction between the components [200 202]. As shown in Fig. 10a, through the reaction of $MnSO_4$ and $KMnO_4$ with MXene ($Ti_3C_2T_x$ or Ti_2CT_x) nanosheets in an aqueous solution, ε MnO_2 nanowhiskers were deposited on the MXene nanosheets [201]. ε MnO_2/MXene composites delivered a capacitance of 212 F g^{-1} at 1 A g^{-1} within a voltage window of 0~0.7 V in 30 wt% KOH electrolyte, and a capacitance retention of 87.7% after 10,000 cycles, superior to the pure ε MnO_2 based electrode (Fig. 10b). The improvement of the cycling performance is attributed to the MXene, which improves the conductivity and the stability of the MnO_2 in the composite material. Furthermore, several methods were employed in order to promote the growth of metal oxides such as thermal annealing [198,203,213]. For example, a free standing MnO_2/Ti_3C_2 film was developed by *in situ* growing of MnO_2 nanoparticles on delaminated Ti_3C_2 nanosheets through electrostatic interactions followed by thermal annealing. A high capacitance of 602 F cm^{-3} at 2 mV s^{-1} in 1 M Li_2SO_4 electrolyte could be achieved [203]. Hydrothermal method is another effective way to synthesize MXene/metal oxide composites, which can promote the growth of metal oxides on MXene nanosheets [199,206] and control the phase and morphology of the formed metal oxides [212]. Nanorods of monoclinic WO_3 and nanoparticles of hexagonal WO_3 were combined with Ti_3C_2 MXene using various hydrothermal conditions with HCl and HNO_3, respectively [212]. The capacitance of the hexagonal WO_3/Ti_3C_2 composites (566 F g^{-1}) was almost doubled from that of the pure hexagonal WO_3 in 0.5 M H_2SO_4 electrolyte within a 0.5 to 0 V vs. Ag/AgCl potential window (Fig. 10c). Besides, microwave treatment was also applied for combining metal oxides with MXene [208]. It is noteworthy that in basic electrolytes, the main role of MXenes in the composites is to allow for fast electron transfer and sometimes flexibility with limited capacitance contribution, while in the acidic electrolytes MXenes are also active materials as they can provide high pseudocapacitance based on redox reaction originated from the H^+ intercalation.

TiO_2 is a metal oxide which can be prepared from the transformation of Ti_3C_2 MXenes; as a result, TiO_2/Ti_3C_2 composites can be *in situ* prepared by either adding TiO_2 precursor or direct partial oxidation of Ti_3C_2. An *in situ* hydrolysis with tetrabutyltitanate as precursor followed by further heating treatment was employed to incorporate TiO_2 nanoparticles into Ti_3C_2 nanolayers, resulting in high specific surface area, large MXene interlayer spacing and opened ion diffusion

pathways [209]. Right after, a simpler one step oxidation method at room temperature was proposed to synthesize Ti_3C_2/TiO_2 nanocom posites. By controlling the reaction time and NaOH concentration in the reacting solution, two types of TiO_2 nanomaterials were introduced into Ti_3C_2 nanosheets. In a first route, the oxidation of Ti_3C_2 MXene in aqueous solution led to the formation of Ti_3C_2/TiO_2 nanoparticle com posite, while Ti_3C_2/TiO_2 nanowires were formed by addition of NaOH solution to the suspension of Ti_3C_2 nanosheets (Fig. 10d) [210]. The Ti_3C_2/TiO_2 nanoparticles showed slightly lower capacitance at a scan rate of 2 mV s^{-1} in KOH electrolyte than the Ti_3C_2/TiO_2 nanowires (128 F g^{-1} vs. 143 F g^{-1}), but better rate performance with a capaci tance retention of 87% from 2 to 100 mV s^{-1}. Similarly, a one step CO_2 oxidation of Nb_2CT_x MXene was used to prepare a hierarchical com posite material with T Nb_2O_5 nanoparticles uniformly supported on the surface of Nb_2CT_x sheets with disordered carbon [214]. A 50 μm thick Nb_2CT_x /T Nb_2O_5 composite electrode with a mass loading of 2.4 mg cm^{-2} could achieve high capacitance (275 F g^{-1} and 0.66 F cm^{-2}) at a charge discharge time of 4 min in a non aqueous electrolyte (1 M $LiClO_4$ EC/DMC). Such high performance resulted from the high intrin sic pseudocapacitive of T Nb_2O_5 coupled with the fast charge transfer pathways provided by the conductive Nb_2CT_x MXene and disordered carbon.

Ex situ assembly of MXene/metal oxide composites have been made by electrostatic reaction [204, 215], simple mixing [205], and freeze drying [211] methods. As shown in Fig. 10e, delaminated MXene nanosheets and ultralong MnO_2 nanowires were transformed into a $Ti_3C_2T_x$ /MnO_2 composite film via vacuum filtration of a mixed disper sion of MXene and MnO_2 [205]. The resultant freestanding film exhib ited remarkable capacitances of 1025 F cm^{-3} and 205 mF cm^{-2} in a symmetric cell using PVA/LiCl as electrolyte with a voltage range of 0~0.8 V.

In addition, 3D structural MXene/metal oxide composites could also be prepared in combination with graphene framework. A Co_3O_4 doped 3D MXene/rGO hybrid porous aerogel was prepared through a facile *in situ* reduction and thermal annealing process, in which 3D rGO frame work was electrically connected with the separated Co_3O_4–MXene com posite nanosheets (Fig. 10f) [216]. The obtained 3D Co_3O_4–MXene/rGO composite exhibited a superior capacitance of 345 F g^{-1} at 1 A g^{-1} in 6 M KOH electrolyte within a potential window of 0~0.6 V (vs Hg/HgO), much higher than that of pure $Ti_3C_2T_x$ MXene, rGO, and MXene/rGO electrodes.

4.1.2. MXene/metal sulfides

Metal sulfides with high theoretical capacitance, are also promising electrode materials for supercapacitors. Furthermore, compared with the metal oxides, metal sulfides usually have higher electronic conduc tivity. For further improving the conductivity and buffering the volume change during the redox process, various metal sulfides, such as CoS_2 [217], NiS [218, 219], Ni Co binary metal sulfides [220 223] and MoS_2 [224] have been combined with MXenes recently.

Similar to the MXene/metal oxides, strategies to prepare MX ene/metal sulfides also include *in situ* growth and *ex situ* assembly. Most metal sulfides are *in situ* grown on the MXene nanosheets via hydrother mal or solvothermal methods. For example, through a solvothermal treatment of $Ti_3C_2T_x$ MXene solution and cobalt source ($CoCl_2{\cdot}6H_2O$), CoS_2 was grown on MXene surface, resulting in the formation of MXene/CoS_2 composite [217]. As the formed CoS_2 can inhibit MXene restacking and the MXene can buffer volume change of CoS_2 and im prove the conductivity, the MXene/CoS_2 composite showed a capaci tance of 1320 F g^{-1} at 1 A g^{-1} and a capacitance retention of 78.4% after 3000 cycles at 10 A g^{-1} in KOH electrolyte. As an example of *ex situ* as sembly, a MXene/$NiCo_2S_4$ composite was prepared by simple mixing of MXene and $NiCo_2S_4$, which had a sandwich architecture with $NiCo_2S_4$ particles between MXene layers and exhibited a capacitance of 1266 F g^{-1} at 0.5 A g^{-1} with a retention of 95.21% after 10,000 cycles in KOH electrolyte [221].

4.1.3. Other MXene/metal compounds

Composites of MXenes and other metal compounds have also been explored. Polyoxometalates, with high theoretical capacitance, thermal stability, highly soluble property and fast electron transfer, are interesting pseudocapacitive candidates for supercapacitors [225]. A MXene/polyoxometalate nanohybrid composite was prepared us ing a cationic poly(ionic liquid) as linker and stabilizer, where the polyoxometalate nanoparticles were uniformly distributed on MX ene nanosheets [226]. The MXene poly(ionic liquid) polyoxometalate nanohybrid architecture displayed a specific capacitance of 384.6 F g^{-1} at 1 A g^{-1} in 0.5 M H_2SO_4 electrolyte, within a potential win dow of 0.1~0.4 V (vs SCE electrode). 2D metal porphyrin framework nanosheets (MPFs) were also hybridized with MXenes. Via vacuum co filtration, a MXene/MPFs with 3D interconnected “MPFs to MXene to MPFs” conductive framework was prepared with hydrogen bonded al ternatively stacked MXene and MPFs [227]. With enlarged interlayer spacing, more active sites and rapid charge transport, the MXene/MPFs film electrode delivered a capacitance of 326.1 F g^{-1} at 0.1 A g^{-1}, 1.64 F cm^{-2} at 1 mA cm^{-2} and 694.2 F cm^{-3} at 1 mA cm^{-3} in a potential range of 0.3~0.3 V vs Ag/AgCl in 0.5 M H_2SO_4 electrolyte.

The synergistic effects of the MXene/metal based compounds with high capacitance and conductivity provide important opportunities for achieving outstanding electrochemical performances, such as already re ported in many works. However, most of these works were studied with basic electrolytes. As MXenes have higher capacitances in acidic elec trolyte, metal compounds electrochemically active in acidic electrolyte, such as WO_3 and RuO_2, might be a better choice to combine with MX ene, which can further highlight the superiority of the MXene/metal compound composites. Furthermore, taking the cell operating voltage into consideration, the MXene/metal oxide composites that can achieve excellent electrochemical performances in non aqueous electrolytes are expected for high energy density supercapacitors.

4.2. MXene/conducting polymers

Compared with other pseudocapacitive materials, conducting poly mers show additional advantages for wearable supercapacitors, be cause of their intrinsic flexibility and conductivity. Many conducting polymers can achieve high capacitance in acidic electrolytes, so do the MXene/conducting polymer composites. Nowadays, many kinds of conducting polymers, such as polyaniline (PANI) [228], poly(3,4 ethylenedioxythiophene) (PEDOT) [229,230], polypyrrole (PPy) [231], polymeric dopamine (PDA) [232] and polyfluorene derivatives (PFDs) [233], have been combined with MXenes to yield hybrids with excellent electrochemical performances.

PANI with high conductivity is a popular conducting polymer to integrate with MXene [96,228,234,235]. As shown in Fig. 11a, a $Ti_3C_2T_x$/PANI film electrode was synthesized by *in situ* and oxidant free polymerization of aniline monomers on the surface of single layer $Ti_3C_2T_x$ sheets [228]. Owing to the high conductivity of MXene and increased interlayer spacing by PANI, such $Ti_3C_2T_x$/PANI films with thicknesses of 4 μm and 13 μm showed similar pseudocapacitive signa tures and could achieve high capacitance of about 383 F g^{-1} at 20 mV s^{-1} in 3 M H_2SO_4 electrolyte (Fig. 11b). Even with a high thicknesses of 90 μm and a mass loading of 23.82 mg cm^{-2}, the $Ti_3C_2T_x$/PANI film still delivered a capacitance of 336 F g^{-1} (888 F cm^{-3}) as shown in Fig. 11c.

PEDOT, thanks to its excellent chemical and electrochemical stabil ity, remarkable conductivity and fast redox reactions, is one of the most widely studied conducting polymer for supercapacitors. It is most of the time used together with poly(styrenesulfonic acid) (PSS) as a surfactant and dopant to promote its suspension in aqueous solutions. Through vacuum co filtration of a hybrid solution of $Mo_{1.33}C$ MXene and PE DOT:PSS followed by post treatment with concentrated H_2SO_4, a flex ible aligned $Mo_{1.33}C$ MXene/PEDOT:PSS composite film was obtained [229]. The concentrated H_2SO_4 significantly removed the uncoupled PSS and changed the PEDOT networks into crystalline nanofibers. Due to

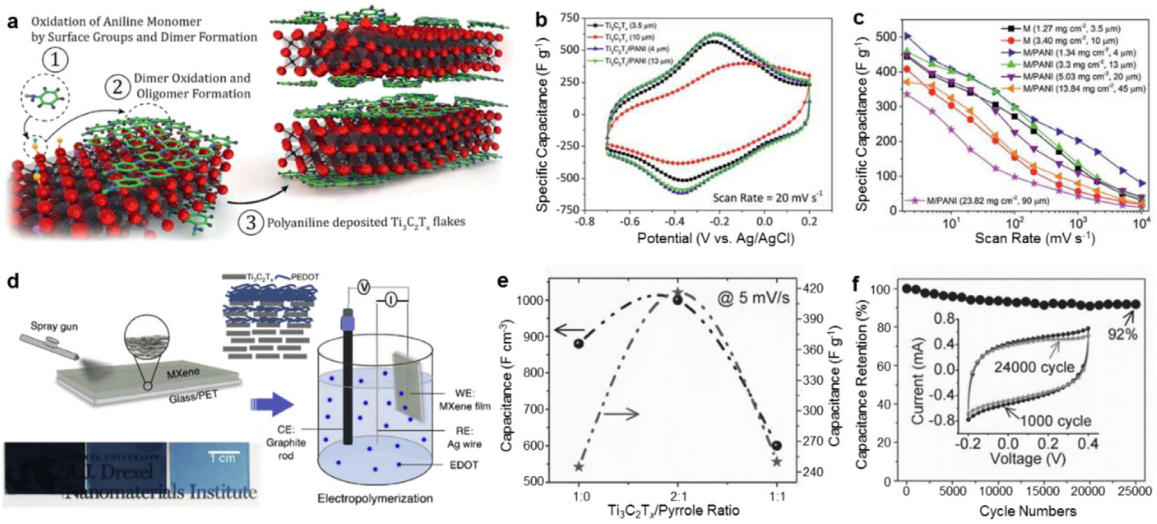

Fig. 11. MXene/conducting polymer composites for supercapacitors. (a) Suggested mechanism for the polymerization of aniline on the surface of $Ti_3C_2T_x$ MXene. (b) CV profiles of the $Ti_3C_2T_x$/PANI electrodes and the pristine $Ti_3C_2T_x$ electrodes. (c) Capacitance of electrodes with different thicknesses and mass-loadings (M: pristine $Ti_3C_2T_x$ electrodes; M/PANI: $Ti_3C_2T_x$/PANI electrodes). Reproduced from Ref. [228] with copyright permission from Royal Society of Chemistry. (d) Formation process of $Ti_3C_2T_x$/PEDOT film by spray coating MXene and electrochemical polymerization of PEDOT on MXene films, with photo and schematic illustrating of the $Ti_3C_2T_x$/PEDOT hybrid films. Reproduced from Ref. [236] with copyright permission from Elsevier. (e) Effect of pyrrole loading on capacitance of PPy/$Ti_3C_2T_x$ hybrid film at 5 mV s^{-1}. (f) Cycling performance of the PPy/$Ti_3C_2T_x$ (1:2) film for 25,000 cycles at 100 mV s^{-1}. Reproduced from Ref. [239] with copyright permission from Wiley-VCH.

the surface redox processes from the two components and the increased MXene interlayer spacing by the PEDOT insertion, the resultant flexible film exhibited a high capacitance of 1310 F cm^{-3} in 1 M H_2SO_4 electrolyte. In another example, PEDOT was electrochemically deposited and polymerized on the $Ti_3C_2T_x$ film to prepare a $Ti_3C_2T_x$/PEDOT heterostructure with an intimately coupled interface (Fig. 11d) [236]. Interestingly, this heterostructure not only offered excellent electrochemical performances, but also can be used in electrochromic energy storage devices with a high rate color switch between a deep blue and colorless state. Moreover, a strongly interacting, porous MXene/PEDOT hybrid fabricated by spray coating was designed for a symmetric supercapacitor with two identical electrodes deposited on Au patterned PET film [237]. The extremely rapid charge transport owing to its porous structure and high conductivity led to both high capacitance and high frequency response that makes this system interesting for signal filtering applications.

PPy as a redox active polymer has also been combined with MXenes [231,238 241]. For instance, through a facile *in situ* polymerization of pyrrole confined between $Ti_3C_2T_x$ layers, a PPy/$Ti_3C_2T_x$ composite film with layered architecture was self assembled [239]. It delivered high conductivity, fast reversible redox reactions and rapid ion transport owing to the increased interlayer spacing by PPy. When tested in 1 M H_2SO_4 electrolyte within 0.2~0.35 V vs Ag/AgCl, a PPy/$Ti_3C_2T_x$ (1:2) composite film yielded a high capacitance of 416 F g^{-1} at 5 mV s^{-1} (Fig. 11e). Although the density of the PPy/$Ti_3C_2T_x$ film (2.4 g cm^{-3}) is lower than that of the pristine $Ti_3C_2T_x$ film (3.6 g cm^{-3}) due to the polymer intercalation, a volumetric capacitance of 1000 F cm^{-3} and good cycling performance (Fig. 11f) were still achieved. Another $Ti_3C_2T_x$/PPy hybrid film was prepared by intercalating PPy into layered Ti_3C_2 via electrochemical polymerization, which showed capacitances of 203 mF cm^{-2} and 406 F cm^{-3}, and almost 100% capacitance retention after 20,000 cycles in 0.5 M H_2SO_4 electrolyte [240]. Additionally, for 3D structure fabrication, a $Ti_3C_2T_x$@PPy composite was *in situ* formed by a 3D tangled PPy nanowires network tightly caging the $Ti_3C_2T_x$ MXene within, which exhibited interconnected porous structure and high conductivity [241].

Based on the advantages of MXenes in metallic like electronic conductivity and 2D structure, combining with various active materials for fabricating MXene based composites is a facile strategy with great potential to obtain materials with desirable electrochemical and/or mechanical performances. There is a growing interest in the synthesis of MXene based composites with various active materials, and the diversity of the integrated components produces numerous feasibility for satisfactory properties in different directions. However, as electrically conducting polymers are usually unstable in non aqueous electrolytes upon cycling, most of these MXene/polymer composites operate today in aqueous electrolyte (H_2SO_4 solutions for instance). As a result, the narrow voltage window achieved in aqueous electrolyte (about 1 V) limits the interest of these electrodes because of the limited energy density that can be achieved. This is why MXene based composites with high electrochemical performance in non aqueous electrolytes have to be developed to increase the cell voltage, including for high rate performance electrodes in Li/Na/K ion battery electrolytes.

5. Capacitive mechanisms of MXenes in various electrolytes

The understanding of the energy storage mechanisms of MXenes is not only important to explain their excellent capacitive performances but also conducive to develop improved or new strategies to prepare MXene electrodes for energy storage applications. The electrochemical signature of MXene in acidic electrolyte shows broad redox peaks on top of rectangular like CV shape even at large scan rates, which is characteristic of a redox pseudocapacitance. The localization of the reaction sites, between the layers of MXenes for H^+ insertion in acidic electrolytes without any phase change defines the storage mechanism as an intercalation pseudocapacitance [242]. Together with long cycle life (beyond 10,000 cycles), this feature differs from the slow ion intercalation in the battery type layered electrode materials, e.g. graphite. Despite remaining unclear in details, great attention has been paid on the fundamental understanding of the electrochemical behavior and the charge storage mechanisms of MXene materials for energy storage applications. In this section, research advances related to capacitive characteristics and charge storage mechanisms of MXenes in different electrolytes are reviewed and discussed.

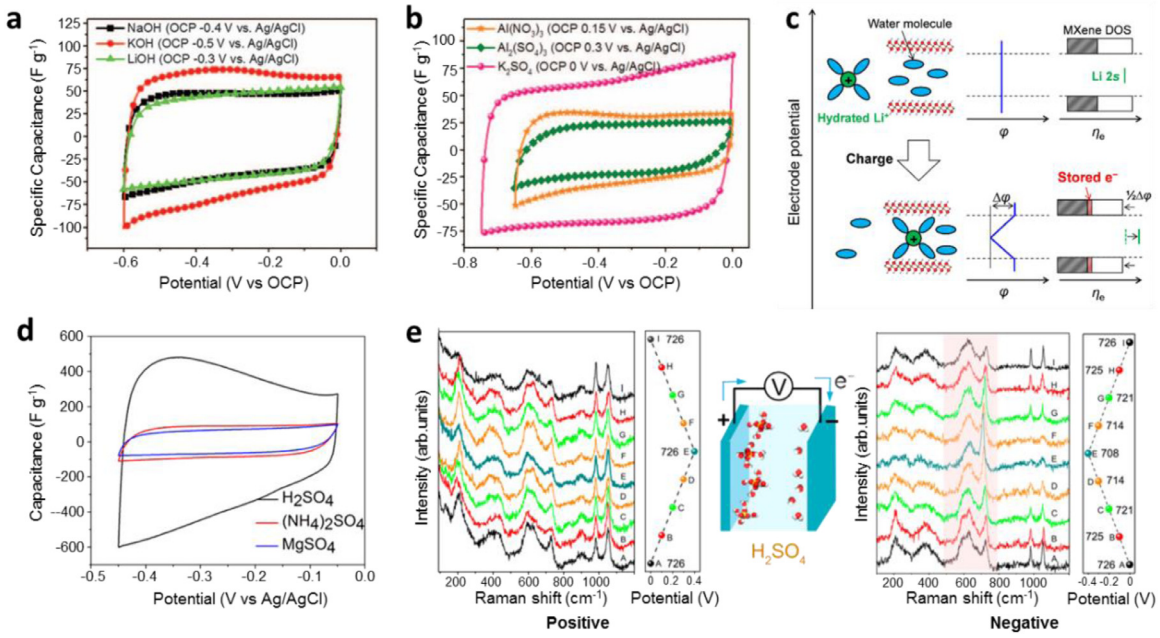

Fig. 12. Electrochemical characteristics of MXenes in aqueous electrolytes. (a and b) CV profiles of $Ti_3C_2T_x$-based supercapacitors in basic electrolytes (NaOH-, KOH-, and LiOH-containing solutions) and neutral electrolytes (K_2SO_4, $Al_2(SO_4)_3$, and $Al(NO_3)_3$ solutions) at 20 mV s^{-1}. Reproduced from Ref. [26] with copyright permission from American Association for the Advancement of Science. (c) Schematic illustration of structural changes and the electronic structure changes of MXene in aqueous electrolytes. Reproduced from Ref. [185] with copyright permission from American Chemical Society. (d) CV curves of $Ti_3C_2T_x$ films in H_2SO_4, $(NH_4)_2SO_4$, and $MgSO_4$ solutions at 20 mV s^{-1}. (e) *In situ* Raman spectra of $Ti_3C_2T_x$ MXene recorded on positive electrode and negative electrode in H_2SO_4 electrolyte. Reproduced from Ref. [246] with copyright permission from American Chemical Society.

5.1. *In aqueous electrolytes*

5.1.1. *In basic and neutral electrolytes*

The electrochemical behavior of MXenes in basic and neutral elec trolytes was investigated from the first report on MXenes (etched by HF) for supercapacitor applications [26]. Various cations (e.g. Li^+, Na^+, K^+, NH^{4+}, Mg^{2+} and Al^{3+}) can be spontaneously or electrochemically in tercalated into 2D MXene layers [26]. Either in basic (e.g. NaOH, KOH and LiOH) or in neutral (e.g. K_2SO_4, $Al_2(SO_4)_3$, $Al(NO_3)_3$) solutions, the $Ti_3C_2T_x$ MXene exhibited rectangular like capacitive CV profiles with out apparent redox peaks (Fig. 12a and b) [26], such as reported by Conway for MnO_2 electrode as a surface redox process [243]. Further more, the electrochemical responses such as capacitance and potential window depended on the selected cations, not the anions, in the elec trolytes to some degree.

In situ XRD study of a $Ti_3C_2T_x$ electrode under polarization in ba sic and neutral solutions evidenced the change of *c* lattice parameters during charge discharge processes, indicating the intercalation and de intercalation of cations between the delaminated MXene layers dur ing electrochemical reaction. Electrochemical quartz crystal admittance (EQCA) was used to characterize the mechanical deformations of MX enes at various states of charge with different cations (such as Li^+, Na^+, K^+, Mg^{2+} and Ca^{2+}) during cycling. It showed that both the ion adsorp tion at solid liquid interfaces and the ion intercalation/de intercalation, evidenced by the rapid deformation (expansion/contraction) of the MX ene particles, were involved during the electrochemical polarization of 2D MXenes in basic or neutral electrolytes [244].

The presence of water molecules between MXene layers play an im portant role in achieving high capacitances. They not only facilitate the ion adsorption [244], but also assist the electric double layer (EDL) formation in the MXene interlayer spacing after the ion intercalation [185,245]. As shown in Fig. 12c, the water molecules surround the cations (e.g. Li^+), forming hydrated cations, which are then interca lated between the MXene layers without dehydration. As the hydration shell isolates atomic orbitals of the cation and the MXene, no orbital hybridization occurs, and positive and negative charges are separated. Thus, a potential difference within the interlayer spacing appears, re sulting in an inner EDL formation [185]. However, in the narrow poten tial range accessible to aqueous electrolytes because of water hydrolysis, only small amount of electrons and ions could be stored (e.g. 0.05 e^- and 0.05 Li^+ per Ti atom for Ti_2CT_x in 1 M Li_2SO_4 aqueous electrolyte), re sulting in negligible pseudocapacitance. Therefore, in basic and neutral aqueous electrolytes, MXenes mainly show a typical EDLC characteris tics with almost constant capacitances within the potential window of the aqueous electrolytes, although hydrated cations intercalation in the interlayer spacing. Based on this mechanism, the MXenes, although after structural design or chemical modification, yielded gravimetric capac itances of only 60~150 F g^{-1} in basic and neutral electrolytes, despite high volumetric capacitances of about 450 F cm^{-3} could be reached due to the large density of MXenes.

5.1.2. *In acidic electrolytes*

MXene electrodes show the highest capacitance in H_2SO_4 electrolyte, together with excellent rate performances, as a result of a different charge storage mechanism from that of basic and neutral electrolytes. The comparison of CV profiles of $Ti_3C_2T_x$ film electrodes in acidic and neutral electrolytes is presented in Fig. 12d [246]. In H_2SO_4 electrolyte, CV plots show distorted rectangular shape signature with broad redox bumps at 0.4~ 0.3 V (vs. Ag/AgCl), indicating the presence of pseudo capacitive behavior. As a result, much higher capacitance was obtained in H_2SO_4 electrolyte than those in its neutral counterparts ($(NH_4)_2SO_4$ and $MgSO_4$) [246].

In situ X ray absorption spectroscopy (XAS) measurements have ev idenced a change of oxidation state of Ti during the electrochemical charge discharge processes of $Ti_3C_2T_x$ MXene in H_2SO_4 electrolyte, confirming the pseudocapacitive behavior based on redox intercalation reactions [179]. Fig. 12e shows *in situ* electrochemical Raman spec troscopy used to characterize the charge discharge processes of $Ti_3C_2T_x$ film electrodes in H_2SO_4 electrolyte. The observed reversible voltage dependent change indicated an electrochemical reaction upon discharg

ing according to [246]:

$$(M=O_x)+1/2xH^+ +1/2xe^- \rightarrow M-O_{(1/2)x}(OH)_{(1/2)x} \quad (4)$$

The bonding/debonding between the hydroniums ions (H_3O^+) and the oxygen containing terminations on the MXene surface are responsible for the change of the Ti oxidation state, accounting for the reversible redox reactions and the high pseudocapacitance in H_2SO_4 electrolyte. Therefore, two factors, the H^+ protons from H_2SO_4 electrolyte and the surface chemistry, play critical roles for the pseudocapacitive behavior of the H^+ involving redox reaction in MXenes. A density functional theory (DFT) calculation based on an implicit solvation model and the analysis of Gibbs free energy under constant potential was employed to theoretically describe the surface redox process of $Ti_3C_2T_x$ (T*x*=O, OH) in H_2SO_4, and confirmed this mechanism [247]. Furthermore, the H^+ intercalation mechanism in H_2SO_4 electrolyte was demonstrated by the change of the *c* lattice parameter of $Ti_3C_2T_x$ MXene during electrochemical reactions, which showed a fluctuating expansion/shrinkage phenomenon, shrinking 0.1 Å from 0 to −0.6 V and then expanding 0.5 Å from −0.6 to −0.9 V (vs Ag wire) [248]. The H_2O molecules confined between $Ti_3C_2T_x$ MXene layers greatly contribute to the fast H^+ transport via Grotthuss mechanism by forming a hydrogen bond network [177,249]. As they are essential to trigger the redox activity of Ti and enable the fast charge compensation through high H^+ diffusion rate, the intercalated H_2O molecules play a critical role in the pseudocapacitive charge storage mechanism of $Ti_3C_2T_x$ MXene [249]. On the other hand, the great effect of surface chemistry on the capacitive response in H_2SO_4 was also verified. The presence of −OH terminations on MXene surface can facilitate the intercalation of H_2O molecules, but a large amount of −OH is assumed to limit the proton transport and thus decrease the power performance [249]. The detrimental effect of −F terminations is confirmed by the significantly increased capacitance after replacing the −F terminations with the oxygen containing terminations on MXene surface [181].

Compared with basic and neutral electrolytes, acidic electrolytes provide pseudocapacitive behavior with redox reaction, resulting in higher capacitance and fast kinetics due to fast proton transport, for instance still delivering 500 F cm^{-3} at a potential scan rate of 1000 mV s^{-1} [71]. Similar good compatibility between acidic electrolytes and electrode materials with fast faradic reaction (like metal oxides) has been widely reported [250]. MXenes superiority in capacitance (above 1500 F cm^{-3}) can be brought into full play in the acidic electrolytes. However, despite MXenes can achieve high capacitance and high rate performance in acidic aqueous electrolytes based on the intercalation pseudocapacitive mechanism, the narrow operating voltage range (about 1 V) limits the practical interest of such devices. Enlarging the voltage range is of great importance for supercapacitors to achieve high energy density, as the energy density (W) was determined according to the equation of $W=CV^2/2$ (where C is the capacitance and V is the cell voltage).

5.2. *In non aqueous electrolytes*

Non aqueous electrolytes show wider potential window than aqueous electrolytes, which make them attractive to increase the energy density of the devices. Most of the reported organic electrolytes used in MXene based supercapacitors consist of organic solvents and metal ion salts, such as Li+ and Na+ ion. As shown in Fig. 13a, Ti_2CT_x MXene electrode showed CV profiles with redox peaks (ca. 2.0 V vs Li/Li^+) in 1.0 M $LiPF_6$ EC/DMC electrolyte. A reversible change of interlayer distance between 9.4 and 9.8 Å was observed during charge discharge processes (Fig. 13b), indicating reversible Li^+ deintercalation/intercalation in the MXene interlayer spacing [184,185]. Furthermore, Li^+ intercalation was associated with the reduction of Ti (Fig. 13c) [185].

Compared with the hydration in aqueous electrolytes, the solvation energy is much weaker in non aqueous electrolytes, causing partial desolvation at the MXene electrolyte interface during cation intercalation (Fig. 13d) [185]. Consequently, atomic orbitals of the cations were hybridized with those of the surface terminations on MXenes, resulting in a donor band for charge transfer and significantly screening the electric field between the electron and cation. Moreover, the large potential window of organic electrolytes ensured large quantities of charge storage. Therefore, the capacitance of MXenes mainly originated from fast redox reactions.

Interestingly, the electrolyte solvents also drastically influence the ion transport and intercalation in the interlayer spacing of MXenes [251]. Taking Ti_3C_2 as an example, 1 M LiTFSI in PC electrolyte offered higher charge storage capability (195 F g^{-1} and 410 F cm^{-3} at 2 mV s^{-1}) and wider potential window (2.4 V) than those of LiTFSI DMSO (130 F g^{-1}) and LiTFSI ACN (110 F g^{-1}) electrolytes (Fig. 13e). The attractive performance in the PC based system is assumed to originate from the full desolvation of Li^+ during charging, which is evidenced by the constant *d* spacing of the Ti_3C_2 (10.7 Å) during cycling in PC based electrolyte (Fig. 13f). This points out the importance of optimizing electrolyte solvent for maximizing capacitance of MXenes.

The electrolytes based on ionic liquid provide an alternative to organic systems, which have excellent stability as well as safety and promise wider voltage range. The charge storage mechanism of MXenes in ionic liquid electrolytes was also revealed as the ion intercalation behavior by *in situ* XRD and molecular dynamic simulation [252,253]. The volume change of MXenes during charge discharge cycling is explained by large cations intercalated at negative potentials while cations and anions swapping at positive potentials. As a result of the large ion size, only low capacitances (80~100 F g^{-1}) can be achieved in ionic liquid electrolytes.

The understanding on energy storage mechanisms of MXenes in supercapacitors is still at an early stage. Generally, the hydrated ion intercalation in basic and neutral aqueous electrolytes is considered to contribute to the EDLC capacitance, while in H_2SO_4 electrolyte, pseudocapacitive behavior comes from H^+ intercalation, leading to much higher capacitance. However, the aqueous electrolytes still suffer from narrow potential window. In non aqueous electrolytes, wide potential window can be achieved but the capacitance currently achieved is not yet satisfactory. It is then needed to push further our basic understanding of the MXene/electrolyte interface, and more specifically the role of the surface groups at MXene surface on the electrochemical performance and the charge storage mechanism in these non aqueous electrolytes. Recent results from Li et al. [49] and Kamysbayev et al. [70] may bring a beginning of answer. A series of MXenes, including Ti_3C_2, were prepared from a molten salt route in $CuCl_2$ at 750 °C, with a surface free from any −F and −OH groups, but rich in −Cl [49]. The CVs of the prepared Ti_3C_2 electrode in 1 M $LiPF_6$ EC/DMC electrolyte showed a unique pseudocapacitive like signature, together with a high capacity of 200 mAh g^{-1} (corresponding to about 300 F g^{-1}). The electrode was still able to deliver 75 mAh g^{-1} for a time less than 30 s (128 C rate). Furthermore, based on the MXenes prepared by molten salt route, an exchange reaction strategy was used to tune the surface groups, and MXenes with different surface terminations (−NH, −S, −Cl, −Se, −Br, −Te, etc.) have been prepared [70]. These results show that MXenes with tailored surface chemistry offer opportunities as high rate negative electrode material for electrochemical energy storage applications and further work will be needed to exploit this effect.

6. MXenes in hybrid supercapacitors

Based on the high capacitance and excellent rate capability, MXene based electrode materials can be assembled into symmetric supercapacitors [120,129,142,168,190,201]. However, MXene based symmetric supercapacitors suffer from low operating voltage (≤1 V) and low energy density because of the oxidation of MXenes at high anodic potential in aqueous solutions and the limitation by proton reduction at low potential. For example, $Ti_3C_2T_x$/graphene // $Ti_3C_2T_x$/graphene film symmetric supercapacitor showed a voltage of 1 V and an energy density of 11 Wh kg^{-1} at a power density of 62.4 W kg^{-1} based on the mass

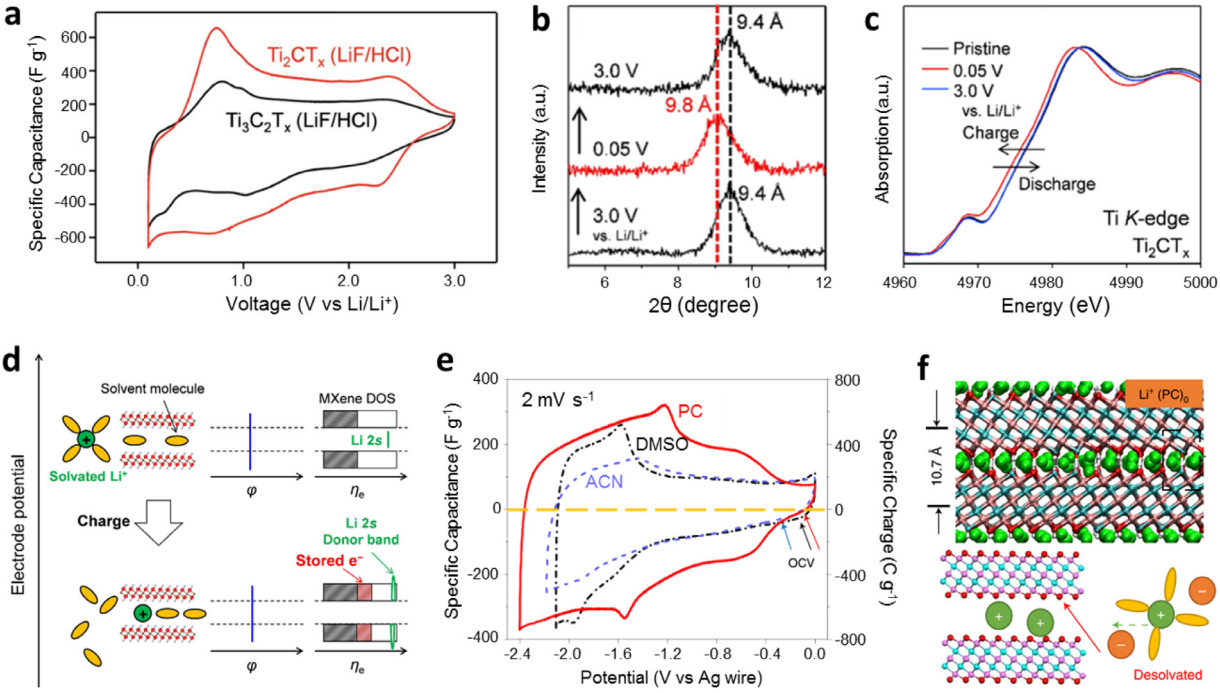

Fig. 13. Electrochemical characteristics of MXenes in non-aqueous electrolytes. (a) CV profiles of Ti_2CT_x and $Ti_3C_2T_x$ (LiF/HCl etching) in 1 M $LiPF_6$/EC-DMC at 0.1 mV s^{-1}. Reproduced from Ref. [184] with copyright permission from Wiley-VCH. (b and c) *Ex situ* XRD patterns and Ti K-edge X-ray absorption spectra of Ti_2CT_x in 1 M $LiPF_6$/EC-DMC. (d) Schematic illustration of structural changes and the electronic structure changes of MXene in non-aqueous Li^+ electrolytes. Reproduced from Ref. [185] with copyright permission from American Chemical Society. (e) CV curves of macroporous Ti_3C_2 electrode with 1 M LiTFSI in DMSO, ACN and PC organic electrolytes. (f) Schematic of MXene as negative electrode in the PC-based system with fully desolvated states. Reproduced from Ref. [251] with copyright permission from Springer.

of the electrodes [109]. Combining MXene based anodes with another electrochemically stable active materials as cathodes to assemble hybrid capacitors with high operating voltage is a more reliable design choice.

6.1. *Hybrid supercapacitors operating in aqueous electrolytes*

Combining electrode materials with high operating potential and large pseudocapacitances at positive potentials in H_2SO_4 electrolyte, such as conducting polymers [155,254,255] or RuO_2 [256], with MXene based electrodes is attractive to increase the energy density of the device. Three conducting polymers, PANI, PPy and PEDOT, de posited on rGO sheets were used as cathodes for preparing hybrid super capacitors with $Ti_3C_2T_x$ anode, respectively. The PANI@rGO//MXene device achieved the largest voltage window up to 1.45 V and highest en ergy density of ~17 Wh kg^{-1}, calculated based on the total mass of the active materials (Fig. 14a) [254]. A RuO_2//$Ti_3C_2T_x$ device could deliver an energy density of 29 Wh kg^{-1} (based on the mass of active material) at a power density of 3.8 kW kg^{-1} in 1.5 V in H_2SO_4 electrolyte, oper ating at a scan rate of 1000 mV s^{-1} (Fig. 14b and c) [256].

Carbon electrodes, like graphene, were also exploited as cathodes to match the MXene based electrodes. Assembling $Ti_3C_2T_x$ MXene an ode with a potential range of 0.7~0.25 V (vs. Ag/AgCl) and rGO cath ode in 0.2~1.1 V (vs. Ag/AgCl), a working voltage of 1.8 V for the hybrid supercapacitor was achieved, much higher than that of the rGO//rGO and $Ti_3C_2T_x$//$Ti_3C_2T_x$ symmetrical supercapacitors [257]. Furthermore, redox active additives are used in H_2SO_4 electrolyte for boosting the capacitances of the carbon//MXene systems, in which MX ene anode performs energy storage based on H^+ involving redox in H_2SO_4 electrolyte, while the redox active additive contributes to pseu docapacitance besides the EDLC of carbon cathode. For instance, when the anionic Br^-/Br_3^- redox reaction with Br^- adsorption/desorption behavior was introduced to the rGO//$Ti_3C_2T_x$ hybrid supercapacitor (50 mM LiBr in 3 M H_2SO_4 electrolyte), a pair of redox peaks at ap proximately 1.2 V were observed, and a high energy density of 34.4 Wh kg^{-1} was obtained based on the mass of total electrodes (Fig. 14d and e) [257]. Hydroquinone/quinone couple is another redox active additive that can work at a positive potential window and offer high capaci tance in H_2SO_4 electrolyte [258]. The CNTs//$Ti_3C_2T_x$ hybrid superca pacitor with hydroquinone in H_2SO_4 electrolyte showed a 1.6 V working voltage range and a high energy density of 62 Wh kg^{-1} at 281 W kg^{-1} based on the mass of active materials (Fig. 14f). Although interesting performances were achieved by using redox active additives dissolved in the electrolyte, the self discharge is one key concern for these sys tems, as the redox soluble once reduced (oxidized) species can diffuse and/or migrate to be oxidized (reduced) at the counter electrode. Mak ing strong physical or chemical adsorption of the redox active additives on the electrode is then needed to alleviate this problem.

The hybrid supercapacitors with MXene based electrodes in alka line electrolytes were also reported [152,259]. As an example, a hybrid supercapacitor was fabricated with Ti_3C_2/CuS composite cathode and Ti_3C_2 MXene anode, which delivered an energy density of 15.4 Wh kg^{-1} at a power density of 750.2 W kg^{-1} in 1 M KOH electrolyte based on the total mass of the active materials [259].

Neutral aqueous electrolytes with free metal ions (e.g. Li ion and Na ion) can be compatible with both capacitive and battery type elec trodes. $LiMn_2O_4$//$Ti_3C_2T_x$ and MnO_2//$Ti_3C_2T_x$ hybrid capacitors were explored in Li_2SO_4 and Na_2SO_4 electrolytes with voltage range of 2.3 V and 2.4 V, respectively, and exhibited acceptable cycling performances [260]. Similar to the battery field, highly concentrated aqueous elec trolytes were also proposed for supercapacitors, in which free H_2O molecules are nearly nonexistent and almost all the H_2O molecules are intimately bound in the solvation sheath of cations. Compared with free H_2O, the bound H_2O has much higher kinetic barriers during the H_2O desolvation and is more difficult to decompose [261], so the highly con centrated aqueous electrolytes usually show widened electrochemical stability windows. A saturated aqueous solution of LiCl (14 M) as elec

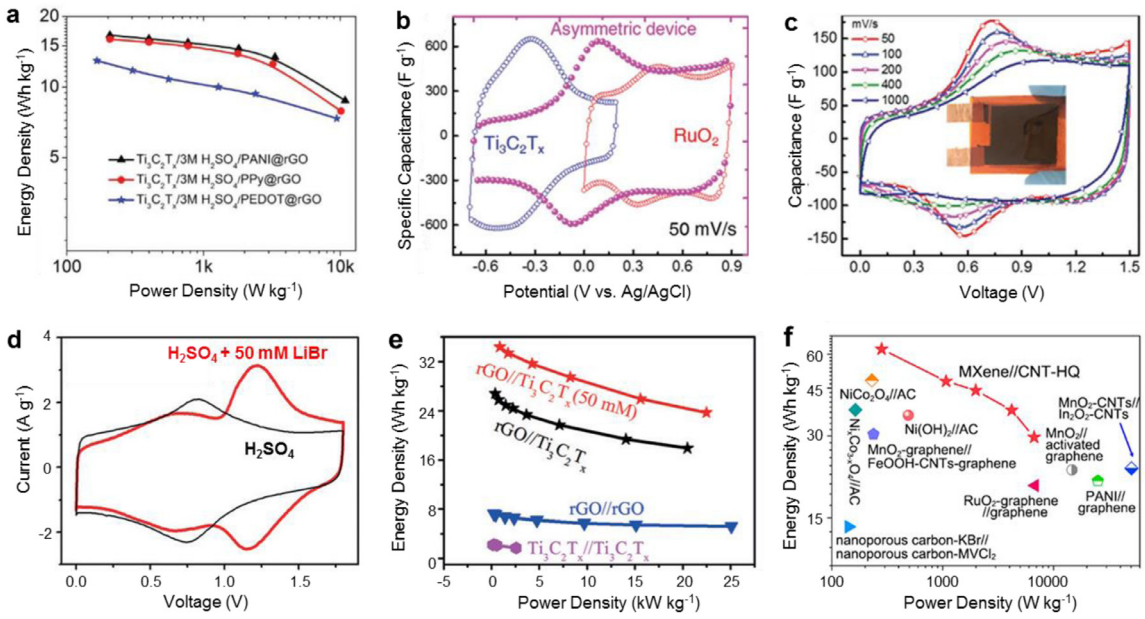

Fig. 14. MXenes in hybrid supercapacitors with acidic electrolytes. (a) Ragone plots of PANI@rGO//$Ti_3C_2T_x$, PPy@rGO//$Ti_3C_2T_x$ and PEDOT@rGO//$Ti_3C_2T_x$ devices. Reproduced from Ref. [254] with copyright permission from Wiley-VCH. (b) CVs of RuO_2, $Ti_3C_2T_x$, and the hybrid device at 50 mV s^{-1}. (c) CVs of RuO_2//$Ti_3C_2T_x$ hybrid device at different scan rates with photo. Reproduced from Ref. [256] with copyright permission from Wiley-VCH. (d and e) CV curves and Ragone plots of the rGO//$Ti_3C_2T_x$ device at 20 mV s^{-1} in H_2SO_4 electrolyte, with/without the Br^--based redox additive. Reproduced from Ref. [257] with copyright permission from Wiley-VCH. (f) Ragone plots of MXene//CNT-HQ hybrid supercapacitors in comparison to some other hybrid supercapacitors. Reproduced from Ref. [258] with copyright permission from American Chemical Society.

trolyte was used in a hybrid device composed with a Mo_6S_8/Ti_3C_2 anode coupled with a nanoporous carbon cathode [262]. The saturated elec trolyte provided high conductivity and a significantly improved elec trochemical stability window of 2.70 V, much exceeding the maximal pseudo equilibrium voltage (2.05 V) of the carbon//Mo_6S_8/Ti_3C_2 sys tem, thus rendered the system with an energy density of 34.2 Wh kg^{-1} based on the mass of the Mo_6S_8/Ti_3C_2 electrode.

In aqueous electrolytes, operating voltage windows of these hybrid supercapacitors are still hindered by the reaction of electrochemical wa ter splitting, and the mechanism of the improvement on operating volt age by these redox active additives in H_2SO_4 electrolyte needs further investigation.

6.2. *Hybrid supercapacitors operating in non aqueous electrolytes*

Organic electrolytes can increase the cell voltage beyond 3 V, re sulting in improved energy density. In organic electrolytes, most of the hybrid capacitors are prepared by assembling a capacitive type elec trode together with a battery type electrode, as they combine the com plementary advantages of both high energy density and high power density. As the cations (Li^+ or Na^+) in these hybrid supercapacitors have relatively large ionic radius and high atomic mass compared to protons in H_2SO_4 aqueous electrolyte, the structure of the MX ene electrodes has to be adapted to enhance ion accessibility in Li ion/Na ion capacitors, by selecting MXenes with large interlayer spac ing [117,184]. For instance, Nb_2CT_x MXene with CNT spacers can store Li^+ in a potential window of 0~3 V (vs Li/Li^+) in 1 M $LiPF_6$ EC/DEC electrolyte, with which three types of Li ion capacitors were fabri cated, i.e. lithiated Nb_2CT_x CNT//graphite, $LiFePO_4$//Nb_2CT_x CNT and Nb_2CT_x CNT//lithiated Nb_2CT_x CNT [263]. Among them, the lithiated graphite/Nb_2CT_x CNT delivered a maximum energy density of 49 Wh kg^{-1} (based on the mass of two electrodes). Higher performance was achieved with the flexible Li ion capacitor combining a $Ti_3C_2T_x$/CNT film anode to a AC cathode in 1 M $LiPF_6$ EC/DEC/DMC electrolyte, which exhibited an energy density of 67 Wh kg^{-1} at a power density of 258 W kg^{-1} (based on the mass of two electrodes) [264]. MXenes can also be applied in decorating battery type active materials to make composite electrodes. The interconnected aerogel like $Ti_3C_2T_x$ MXene wrapped Fe_2O_3 nanospheres were employed as the battery type anode for Li ion capacitors [265]. Coupled with a 3D N, S co doped porous car bon as a capacitor type cathode, the lithium ion capacitor demonstrated an energy density of 216 Wh kg^{-1} based on the mass of active materials.

The resource abundance and global availability of Na and K have led to a booming in the development of the Na ion capacitor and K ion capacitor technologies. Nevertheless, compared with the Li ion capac itors, the larger size of Na^+/K^+ in Na/K ion capacitors brings forward higher request on MXene structures for fast ion transport. The first re ported MXene based Na ion capacitor consisted of a Ti_2C anode com bined with a $Na_2Fe_2(SO_4)_3$ cathode, that could operate at a voltage of 2.4 V and deliver an energy density of 260 Wh kg^{-1} at a power density of 1.4 kW kg^{-1} (based on the mass of Ti_2CT_x) in 1 M $NaPF_6$ EC/DEC electrolyte [266]. Afterwards, a hard carbon//V_2CT_x Na ion capacitor with 1 M $NaPF_6$ EC/DMC electrolyte was constructed with a cell voltage of 3.5 V [267]. Modified by Na^+ pillaring to enlarge its interlayer spac ing and improve the kinetics, a Ti_3C_2 MXene anode was coupled with activated carbon cathode, assembling Na ion capacitor with an energy density of 42.4 Wh kg^{-1} at a high power density of about 6.2 kW kg^{-1} (based on the mass of two electrodes) [268]. Additionally, a bi stacked MXene film architecture was prepared by firstly filtrating delaminated $Ti_3C_2T_x$ to a compact layer as current collector, and subsequently fil trating multilayer $Ti_3C_2T_x$ particles to an open structure for fast Na^+ kinetics [269]. The Na ion capacitor with a total mass loading of 6 mg cm^{-2} was assembled with this bi stacked MXene film as anode and an activated carbon electrode as cathode, delivering an energy density of 39 Wh kg^{-1} (based on the mass of two electrodes) at 1C and maintain ing up to 60% at 60 C. Recently, using 3D printed technology, a Na ion capacitor with porous N doped $Ti_3C_2T_x$ anode and AC cathode was constructed with 1 M $NaClO_4$ EC/PC+2% VC electrolyte [270]. As the porous structure and nitrogen doping resulted in fast charge transport and kinetics for the MXene anode, the Na ion capacitor showed an op eration voltage of 4 V with high areal energy density and power density of 1.18 mWh cm^{-2} and 40.15 mW cm^{-2}, respectively. Also, MXene ma

terials have been used to assemble K ion capacitors, in which advanced structure design is needed to promote fast K^+ transport. A K V_2C MX ene was prepared by treating V_2C with KOH, which shows thin MXene sheets with many pores and cracks [271]. A K ion capacitor combining K V_2C anode and K_x $MnFe(CN)_6$ cathode can operate at an average volt age of 3.3 V in KPF_6 EC/DEC electrolyte and achieve an energy density of 145 Wh kg^{-1} at a power density of 112.6 W kg^{-1} (based on the total mass of active materials). Another advanced structure designed for fast K^+ transport is 3D $Ti_3C_2T_x$ hollow spheres/tubes, which was prepared by a spray lyophilization method [272]. A K ion capacitor combining such 3D $Ti_3C_2T_x$ anode together with a hierarchical porous activated carbon cathode displays an energy density of 98.4 Wh kg^{-1} and a power density of 7 kW kg^{-1} (based on the total mass of the anode and cathode) along with cycling stability of 100% after 10,000 cycles in KPF_6 EC/DEC electrolyte.

As presented above, most of the high energy and power densities reported in the literatures are obtained from the sole weight of the elec trodes. However, for practical application, the total cell weight, includ ing the mass of other components such as current collectors, electrolyte, separator and packaging, should be taken into account. It is then impor tant to use the same metrics for a same comparison [273].

Future research directions for MXene in hybrid capacitors are simi lar with those of Section 5.2, that are the understanding of the role of the surface groups on the electrochemical performance in various elec trolytes (salts and solvents), as well as designing optimized electrode architectures that offer high and highly accessible surface area to elec trolytes ions. Moreover, positive cathode materials with high rate ca pability and long cycle life should be coupled with MXene electrodes to achieve the capacitors with high energy density and high power density.

7. MXenes for flexible- and micro- supercapacitors

The recent booming in portable and wearable electronic systems has highlighted the need for advanced miniaturized and flexible supercapac itors. In these applications, supercapacitors, with high energy density and power density, long cycle life as well as fast charge discharge rate, are used as embedded power supply sources. Especially, high volumetric capacitance is critically important. MXenes are considered as promising materials for flexible supercapacitors and micro supercapacitors since they can achieve high volumetric capacitances due to their intercalation pseudocapacitance and large packing density. Besides, their 2D structure and good mechanical properties are also important for manufacturing flexible devices.

7.1. MXenes for flexible supercapacitors

Owing to their 2D layered structure, MXene nanosheets can be sim ply assembled into flexible film electrodes through vacuum filtration [125, 129], together with graphene [149], or loaded on flexible matrix [156, 161, 274]. The filtration processing, firstly described in the first report on MXene for supercapacitors [26], has become the most com monly used method for fabricating flexible binder free MXene films. What follows is the development of the flexible MXene based hybrid films, in which MXenes can play a variety of roles, such as active materials [231, 239], conductive framework [205, 227], flexible sub strate [275] and even a multifunctional binder [276]. For example, as $Ti_3C_2T_x$ contributed to the brilliant conductivity and good flexibility, a $Ti_3C_2T_x$ /MnO_2 electrode was fabricated into a flexible symmetric su percapacitor device with PVA/LiCl soaked cellulose separator, which showed high electrochemical stability with a capacitance retention of 98.38% after 10,000 cycles and a stable performance during repeated mechanical bending of up to 120° for 100 cycles [205].

Remarkably, MXenes can not only be combined with nanomateri als via vacuum filtration, but also act as a multifunctional conductive binder to assemble conventional activated carbon particles in micron size into film electrodes [276]. Carbon electrodes are conventionally fabricated by coating the mixed slurry of porous carbon, conductive agent and polymer binder such as polyvinylidene di fluoride (PVDF) onto aluminum foil current collector, in which the usage of an insu lating polymer binder (5 20% in mass) reduces electrode conductivity, capacitance, and rate performance. Through a filtration of a mixed sus pensions of MXene flakes and AC particles, a freestanding and flexible MXene bonded AC film electrode was fabricated (Fig. 15a). This elec trode fabrication procedure is not only simpler than the conventional coating method with polymer binder, but also simpler than the previ ously reported similar method with rGO as binder [277], since no re duction process is needed. In the flexible electrode, the activated car bon particles were encapsulated between the MXene layers (Fig. 15b), and the $Ti_3C_2T_x$ MXene acted as a flexible matrix, conductive frame work and electrochemically active materials simultaneously. As a re sult, the MXene bonded AC films presented much better rate capability than the conventional polymer PVDF bonded AC electrode. Evaluated in a symmetrical two electrode supercapacitor with 1 M Et_4NBF_4/AN organic electrolyte, it exhibited a capacitance of 126 F g^{-1} at 0.1 A g^{-1} with a retention of 57.9% at 100 A g^{-1} and a good long term cy cling stability with 92.4% capacitance retention after 10,000 cycles at 10 A g^{-1} (Fig. 15c e). This strategy with MXenes as a multifunctional conductive binder can also be used for fabricating flexible electrodes in high performance secondary batteries, indicating its generality and superiority for next generation flexible energy storage [278 280].

Besides the filtration, the additional free standing matrix or substrate such as nickel foam [161], carbon cloth [156 158], and polymer film [274] can help in preparing flexible MXene based film electrodes. In these film electrodes, the MXene loading can be adjusted easily, and the open structure of the matrix can reduce the restacking of MXene nanosheets, increase the accessible active sites and facilitate fast ion transport. As shown in Fig. 16a, an electrospun polycaprolactone (PCL) fiber network was spray coated with $Ti_3C_2T_x$ nanosheets and CNTs layer by layer, fabricating a free standing and flexible film electrode [274]. Tested in the three electrode system in 1 M H_2SO_4 electrolyte, this composite electrode could deliver high areal capacitance from 30 to 50 mF cm^{-2} at 10 mV s^{-1} with capacitance retentions of 14~16% when the scan rate was increased up to 100 V s^{-1}. Furthermore, the flexible film could maintain the structural integrity and high conductivity during 100 times of folding or twisting, demonstrating good tolerance against repeated mechanical deformation. The circuits built from the films after 100 times of deformation could still light up a blue LED (Fig. 16b).

Stretchable supercapacitors bring forward higher requirement for MXene based film electrodes [146,281]. To add stretchability to the film, a MXene/sodium alginate hybrid nanocoating was compressed on a pre stretched elastomer substrates with a thin layer of silver nanowires (AgNWs) as current collector [146]. As the pre stretched elastomer was relaxed, the lateral dimensions of adhered MXene hybrid nanocoatings reduced by the same ratio as those of the elastomer, leading to com plex out of plane microtextures (Fig. 16c). As a result, the prepared MX ene electrodes can sustain large mechanical deformations. A highly de formable hybrid capacitor was build up with a negative stretchable MX ene and a positive AC electrodes in Li_2SO_4 PVA gel electrolyte, which was operated in 1.0 V and maintained efficient capacitive performance while largely bending to 180° and stretching to 100% strain (Fig. 16d f). Another candidate for stretchable supercapacitors is the $Ti_3C_2T_x$/rGO composite electrode, which was also prepared on a pre stretched elas tomer substrate to form a wrinkled/ridged pattern [281]. Combining the superior electrochemical and mechanical properties of MXene and mechanical robustness of rGO, a MXene/rGO composite film showed a capacitance of 49 mF cm^{-2} (~490 F cm^{-3} and ~140 F g^{-1}) and good electrochemical and mechanical stability when subjected to cyclic uni axial (300%) or biaxial (200% × 200%) strains.

Besides the advantages of 2D layered structure, metallic like elec tronic conductivity, hydrophilicity and pseudocapacitive characteris tics, transparent MXene films can also be prepared. A highly transparent and conductive $Ti_3C_2T_x$ film electrode was fabricated via spin casting

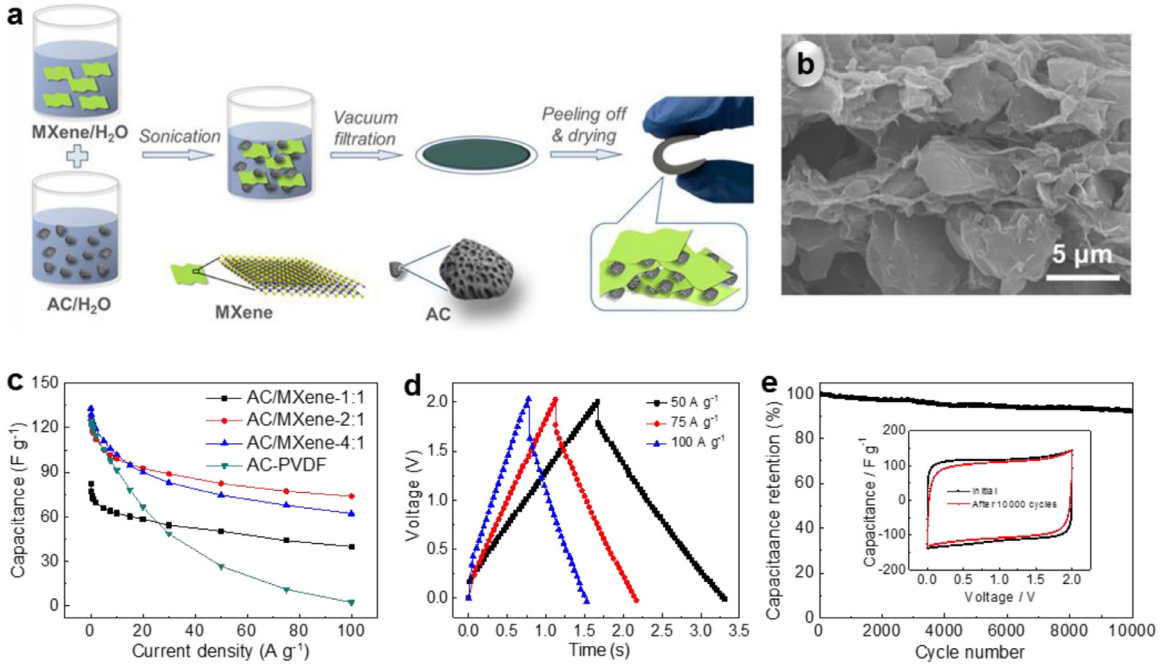

Fig. 15. Flexible AC electrode using MXene as a multifunctional conductive binder. (a) Schematic diagram for the fabrication of MXene-bonded AC films. (b) SEM image of the MXene-bonded AC film. (c) Rate capabilities of the MXene-bonded AC film. (d) V-t curves at enhanced current densities. (e) Cycling performance at 10 A g^{-1} for 10,000 cycles in 1 M Et_4NBF_4/AN organic electrolyte with the CV curves at 20 mV s^{-1} at initial and after 10,000 cycles in the inset. Reproduced from Ref. [276] with copyright permission from American Chemical Society.

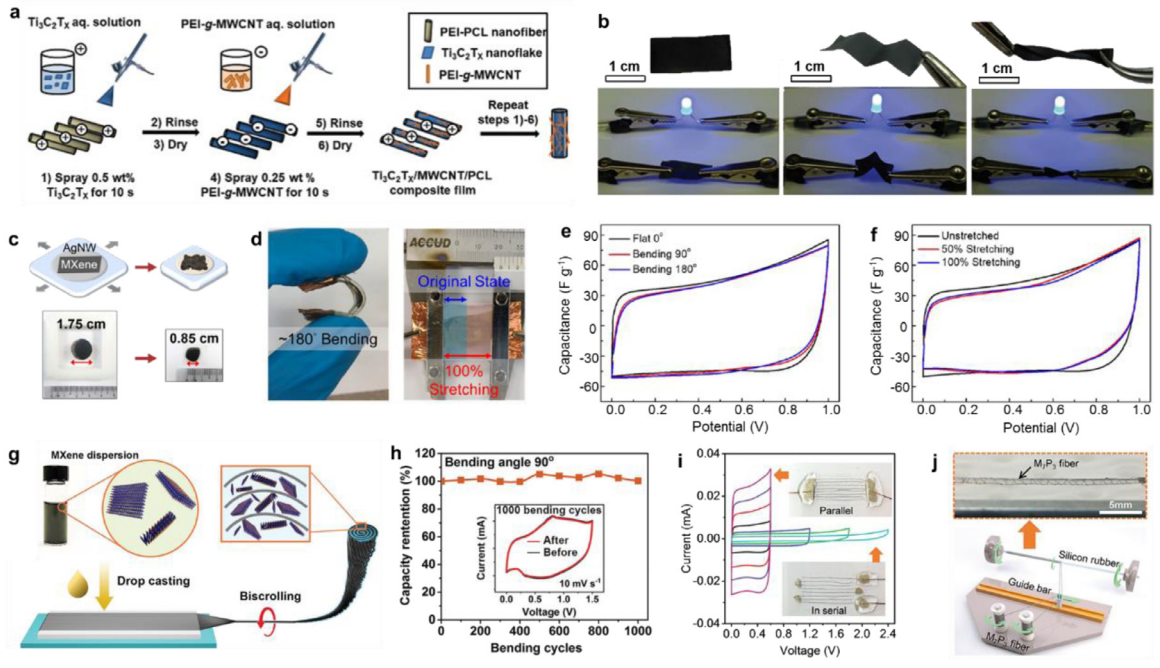

Fig. 16. Film and fiber electrodes based on MXenes for flexible supercapacitors. (a) Fabrication process of hierarchical MWCNT/$Ti_3C_2T_x$ multilayers on the PCL fiber network by layer-by-layer spray coating. (b) Digital images of the deformed (100 times) PCL films with double-layered coatings of $Ti_3C_2T_x$ and MWCNTs, and the corresponding circuits built from them to light up a blue LED. Reproduced from Ref. [274] with copyright permission from Royal Society of Chemistry. (c) Fabrication processes for stretchable MXene/elastomer architectures. (d) Images of the AC//MXene/elastomer hybrid devices under ~180° bending and 100% stretching as well as the CV curves of the devices at different (e) bending angles and (f) stretching states. Reproduced from Ref. [146] with copyright permission from American Chemical Society. (g) Fabrication process of the helical $Ti_3C_2T_x$/CNTs fiber. (h) Capacitance retention of the RuO_2/CNT//$Ti_3C_2T_x$/CNTs fiber supercapactior during 1000 bending cycles at 90° with the CV curves before and after bending. Reproduced from Ref. [286] with copyright permission from Wiley-VCH. (i) CV curves and photos of four symmetric fiber device with MXene/PEDOT:PSS electrodes connected in parallel and in series. (j) Fabrication process of elastic fiber device by wrapping two MXene/PEDOT:PSS fibers on a silicon rubber. Reproduced from Ref. [291] with copyright permission from Royal Society of Chemistry.

followed by vacuum annealing [282]. Such a film electrode exhibited a transmittance of 93% and a volumetric capacitance of 676 F cm^{-3}. Furthermore, it was assembled in a $Ti_3C_2T_x$ //CNTs hybrid capacitor with PVA/H_2SO_4 gel electrolyte, that delivered flexibility, transparent property (72% transmittance) and high energy density (0.05 μWh cm^{-2}), demonstrating the bright prospects for the application in flexible and transparent electronics.

Fiber supercapacitors, as another important kind of flexible supercapacitors, are generally established by parallelizing or twisting two fiber electrodes together. Because of the low lateral sheet size and insufficient interlayer interactions, it is difficult to process MXenes into fiber electrodes directly [283]. To bypass this issue, one method is to coat MXene onto fibers [284, 285]. As an example, MXene coated silver plated nylon fibers were produced by mildly baking the $Ti_3C_2T_x$ suspension loaded on the silver plated nylon fibers [285]. A supercapacitor assembled with two fiber electrodes in parallel in PVA/H_2SO_4 gel electrolyte performed length and areal capacitances of 50 mF cm^{-1} and 328 mF cm^{-2}, respectively, together with capacitance retentions of above 90% on bending or twisting and 82% even when the whole capacitor was knotted.

To further increase the MXene loading and alleviate flaking off of the active materials during deformation, a helical structure by bi scrolling was designed [286, 287]. As shown in Fig. 16g, a MXene/CNTs composite was fabricated by casting MXene nanosheets on well aligned CNT scaffold and subsequently bi scrolled into hybrid fibers [286]. In these MXene/CNTs fibers, the highly delaminated MXene sheets were trapped within helical yarn corridors, and these structures could increase the MXene loading to ~98wt%. When the $Ti_3C_2T_x$ /CNTs fiber electrode with ~98% $Ti_3C_2T_x$ was combined with a bi scrolled RuO_2/CNT fiber cathode into a hybrid fiber device operating in PVA/H_2SO_4 electrolyte, the device reached a maximum energy density of 61.6 mWh cm^{-3} at a power density of 5428 mW cm^{-3}. It maintained a high capacitance retention of nearly 100% during 1000 bending cycles with 90° bending angle (Fig. 16h) [286].

Another efficient approach is to combine MXenes with inherently spinnable materials for processing composite fibers. GO is considered as suitable material to assist building MXene fibers [283]. Furthermore, reducing MXene/GO to MXene/rGO is beneficial for enhancing electronic conductivity of the hybrid fibers [288]. For this point, wet spinned MXene/GO fibers were treated with hydroiodic acid to remove the oxygen containing functional groups on GO [289]. The obtained MXene/rGO hybrid fibers showed well aligned MXene sheets inside with a high ratio of 95 wt%, and achieved high electrical conductivity (2.9×10^4 S m^{-1}) and high electrochemical performance with a volumetric capacitance of 586.4 F cm^{-3} in PVA/H_3PO_4 electrolyte. Such kind of MXene/rGO fibers can also be used as substrate for further loading with active materials. For example, MnO_2 nanosheets were grown on the fiber surface by soaking $Ti_3C_2T_x$ /rGO fibers in $KMnO_4$ solution, forming MnO_2/$Ti_3C_2T_x$ /rGO ternary composite fibers. The symmetric MnO_2/$Ti_3C_2T_x$ /rGO//MnO_2/$Ti_3C_2T_x$ /rGO fiber supercapacitors with PVA LiCl gel electrolyte displayed a volumetric capacitance of 24 F cm^{-3}, which showed no obvious change after bending the device at 90° for 1000 times, indicating outstanding flexibility and mechanical properties [290].

Polymers were also employed to assist spinning of MXene fibers. The polymers can either exist as such in the final fibers [291, 292] or be carbonized into carbon to form MXene/carbon fibers [293]. For instance, using wet spinning with conductive PEDOT:PSS as a binder, fibers containing 70 wt% MXene were prepared [291]. A symmetric MXene/PEDOT:PSS // MXene/PEDOT:PSS device exhibited energy and power densities of ~7.13 Wh cm^{-3} and ~8249 mW cm^{-3}, respectively, in PVA/H_2SO_4 gel electrolyte. When multiple device prototypes were electrically connected in parallel or in series, corresponding increase in current or in voltage output was obtained (Fig. 16i). Furthermore, composite fibers with excellent strength and flexibility could be wrapped on a silicone rubber (Fig. 16j), resulting in an elastic device with 96% capacitance retention after 200 cycles under stretching to 100% strain.

For the latter situation, $Ti_3C_2T_x$/carbon hybrid fibers were fabricated through electrospinning MXenes with polyacrylonitrile (PAN) followed by carbonization. Through this method, the MXene nanosheets were embedded into the *in situ* formed carbon to produce fibers with an areal capacitance of up to 244 mF cm^{-2} tested in a three electrode system with 1 M H_2SO_4 electrolyte [293].

The high volumetric capacitance as well as 2D structure and good mechanical properties make MXenes interesting materials for flexible supercapacitor electrode applications. Actually, lots of reported MXene based electrodes, including the pure MXene electrodes and the hybrid electrodes, in supercapacitors were studied in forms of flexible film. Through using MXenes, more and more high performance flexible supercapacitor systems were built up. However, they have not yet commercially available. In order to meet the needs of commercial applications, the areal energy density should be improved. This could be achieved by developing thick MXene electrodes with good mechanical properties and electrochemical performances. Designing compatible solid electrolyte/MXene interfaces is also needed for developing MXene materials for advanced flexible supercapacitor applications.

7.2. MXenes in micro supercapacitors

The continuous development of microscale electronic devices appeals for increasing demands for micro power sources and energy storage devices. Micro supercapacitors have been regarded as one of the most promising microscale power sources because of their high power density, fast charge discharge rate and long cycle life, like conventional supercapacitors. More specifically, micro supercapacitors are suitable for self powered microscale devices as ideal independent power sources, since they can efficiently harvest energy from various sources, such as from voltage change from the excitation sources like piezoelectric sensors, and then offer power for a long time [294]. Moreover, compared with flexible supercapacitors with sandwich like film electrodes, interdigitated micro supercapacitors have the advantage in alleviating the barrier of ion transport across the separator. However, as most of the electrode materials cannot provide both high packing density and good electronic conductivity simultaneously, micro supercapacitors cannot usually deliver both high areal and volumetric energy density as well as good rate capability. In this context, MXenes can be an alternative to conventional materials since: (1) MXenes possess both large gravimetric capacitances and high packing densities, leading to high volumetric capacitances; (2) MXenes show metallic like electronic conductivity, that help in decreasing the internal resistance and improving the rate performance; (3) MXenes have 2D structure, beneficial for ion transport in interdigital micro supercapacitors.

Micro supercapacitors with interdigitated electrodes can be fabricated by patterning MXene based films via laser cutting [295 300], scratching [301] or automated scalpel engraving [302]. For example, as illustrated in Fig. 17a, after Ti_3C_2 MXene slurries were loaded on a commercial A4 printing paper as substrate over a large area, a scalable direct laser machining was employed to fabricate an interdigitated MXene on paper micro supercapacitor, which achieved competitive power energy densities and excellent flexibility [295]. As the 2D sheets can be self assembled into film easily, MXenes can act as both active material and substrate [297]. An all MXene ($Ti_3C_2T_x$) interdigitated micro supercapacitor was fabricated by spray coating of large size, thin layer MXene sheets as current collector, followed by coating of small size MXene sheets as active material, using photoresist free direct laser cutting treatment (Fig. 17b) [298]. The all MXene micro supercapacitor exhibited areal and volumetric capacitances of 27 mF cm^{-2} and 357 F cm^{-3}, respectively, at a scan rate of 20 mV s^{-1}, as well as 100% capacitance retention after 10,000 cycles at 50 mV s^{-1} in PVA/H_2SO_4 gel electrolyte, indicating the promising prospective of the various combination of MXenes with different flake sizes, structures, chemistries and their heterostructures. The thicker the electrode is, the higher areal capacitance would be realized. Therefore, it is important to increase the thick

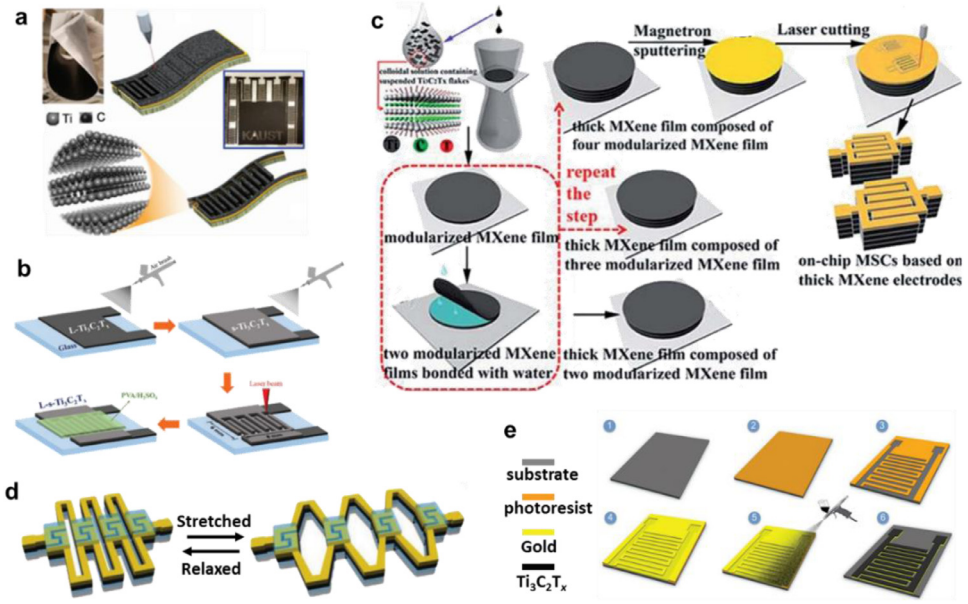

Fig. 17. Schematic illustrations of MXenes for interdigitated micro-supercapacitors. (a) Laser patterning of MXene coated paper to fabricate interdigitated electrodes. Reproduced from Ref. [295] with copyright permission from Wiley-VCH. (b) Fabrication process of the all-MXene micro-supercapacitor by spray-coating MXene sheets with different sizes followed by laser cutting. Reproduced from Ref. [298] with copyright permission from Royal Society of Chemistry. (c) Preparation of a thick MXene electrode via bonding the vacuum-filtrated thin MXene films with water followed by coating Au and patterning. Reproduced from Ref. [299] with copyright permission from Royal Society of Chemistry. (d) The stretched and relaxed kirigami micro-supercapacitor. Reproduced from Ref. [300] with copyright permission from Wiley-VCH. (e) Fabrication process via photolithography including photoresist coating (1–2), UV exposure through the photo mask (2–3), sputtering of Au/Ti (3–4), spray coating of MXene (4–5) and final device after lift-off process in acetone (6). Reproduced from Ref. [303] with copyright permission from Wiley-VCH.

ness of MXene electrodes. An efficient and facile route was developed to increase the MXene electrode thickness, and then the electrode areal capacitance, as displayed in Fig. 17c [299]: first, modularized thin MX ene films were assembled by vacuum filtrating of a MXene nanosheets suspension; then, two modularized thin MXene films were bonded with water into a thicker film; by repeating the bonding process, the thick ness of the MXene films can be increased in a controlled way; after coating Au on the thick MXene film, a laser cutting pattern process was carried out to form the micro supercapacitors with thick MXene based interdigitated electrodes. A micro supercapacitor assembled with these thick electrodes exhibited an areal capacitance of 71.16 mF cm^{-2} in PVA/H_2SO_4 gel electrolyte. In addition, for stretchable application, in order to sustain repeated tensile deformation with negligible sacrifice of energy power densities, a kirigami micro supercapacitor (Fig. 17d) based on the MXene/bacterial cellulose composite was prepared by a laser cutting kirigami patterning process [300]. The micro device de livered bendable, twistable, and stretchable property with mechanical stability and a high areal capacitance of 111.5 mF cm^{-2} in PVA/H_2SO_4 gel electrolyte. Furthermore, a facile, fast and cost effective 'scratch' method was proposed for patterning $Ti_3C_2T_x$ to form planar interdig itated electrodes on various substrates, like SiO_x/Si wafer, PET film and filter paper [301]. All the prepared micro supercapacitors achieved good performances, indicating the availability and effectiveness of this method. Besides, by dip coating and the followed automated scalpel en graving, transparent and semitransparent MXene micro supercapacitors could be fabricated, employing MXene optoelectronic properties [302].

Loading MXenes onto pre patterned interdigital substrates is another effective strategy for fabricating micro supercapacitors [303 305]. Pho tolithography was widely used for patterning high resolution shape on various substrates. Gogotsi and Alshareef et al. designed a micro supercapacitor with interdigitated $Ti_3C_2T_x$ electrodes by using a pho tolithographic lift off process followed by spray coating of the MXene dispersions, as shown in Fig. 17e [303]. The prepared micro device showed great potential for alternating current filtering application. By adjusting the MXene flake size and the electrode thickness to optimize its frequency response, it was found that the device with 100 nm thick electrodes and 10 μm electrode spacing delivered a volumetric capaci tance of 30 F cm^{-3} at 120 Hz and a relaxation time constant of 0.45 ms, indicating the capability of filtering 120 Hz ripples.

Direct printing of functional inks is a feasible technique to build up flexible energy storage systems with desirable architectures, which allows personalized patterning as well as scalable and rapid produc tion. For printable micro supercapacitors, the available ink should have suitable viscosity properties and good energy storage capabilities. With abundant surface terminations, MXene nanosheets can be prepared as negatively charged and hydrophilic, which can form a stable and vis cous colloidal suspension or ink. Together with their superior electro chemical performances, MXene inks are particularly attractive for the printable micro supercapacitors.

Screen printing is a traditional strategy for fabricating the desir able patterns. Interdigital patterns were prepared by loading MXene inks onto an interdigitated mask [207,306]. Using printable ink of RuO_2@MXene Ag nanowires, a micro supercapacitor with micrometer scale resolution was designed [207]. In this RuO_2@MXene Ag ink, the monodispersed RuO_2 nanoparticles were homogeneously anchored on the $Ti_3C_2T_x$ MXene nanosheets by the electrostatic interactions, which ensured fast ion transport by preventing MXene nanosheets restacking and increasing interlayer spacing. Thanks also to the high conductivity and the suitable rheological behavior ensured by the Ag nanowires, the micro supercapacitor based on the RuO_2@MXene Ag nanowires ink de livered remarkable energy (13.5 mWh cm^{-3}) and power density (48.5 W cm^{-3}) in PVA/KOH gel electrolyte together with highly durable and robust mechanical properties. Moreover, printable hybrid inks mix ing small size $Ti_3C_2T_x$ MXene nanosheets and electrochemically exfo liated graphene were developed for fabricating interdigital electrodes via screen printing. In the printed MXene/graphene hybrid electrodes, the MXene between the graphene layers acted as active material and facilitated the electrolyte ion transport, resulting in the preparation of micro supercapacitors with an areal capacitance of 3.26 mF cm^{-2} and a volumetric capacitance of 33 F cm^{-3} at 2 mV s^{-1} in PVA/H_3PO_4 gel electrolyte [307]. Besides, in order to enhance the working voltage of micro supercapacitor, a screen printed interdigital $Ti_3C_2T_x$ MXene elec trodes was immersed into ionic liquid $EMIMBF_4$ for pre intercalation and then used in the $EMIMBF_4$ electrolyte [308]. This non aqueous micro supercapacitor can work at 3 V with high areal and volumetric energy densities of 13.9 mWh cm^{-2} and 43.7 mWh cm^{-3}, respectively. Furthermore, the screen printing route is especially suitable for fabri cating hybrid micro supercapacitors. Using a two step process, cathode and anode can be screen printed in sequence (Fig. 18a) [309,310]. As an example, the rGO//$Ti_3C_2T_x$ hybrid micro supercapacitor with an in terdigitated architecture was assembled via a two step screen printing process [309]. With the advantage in fast ion diffusion, as both of the

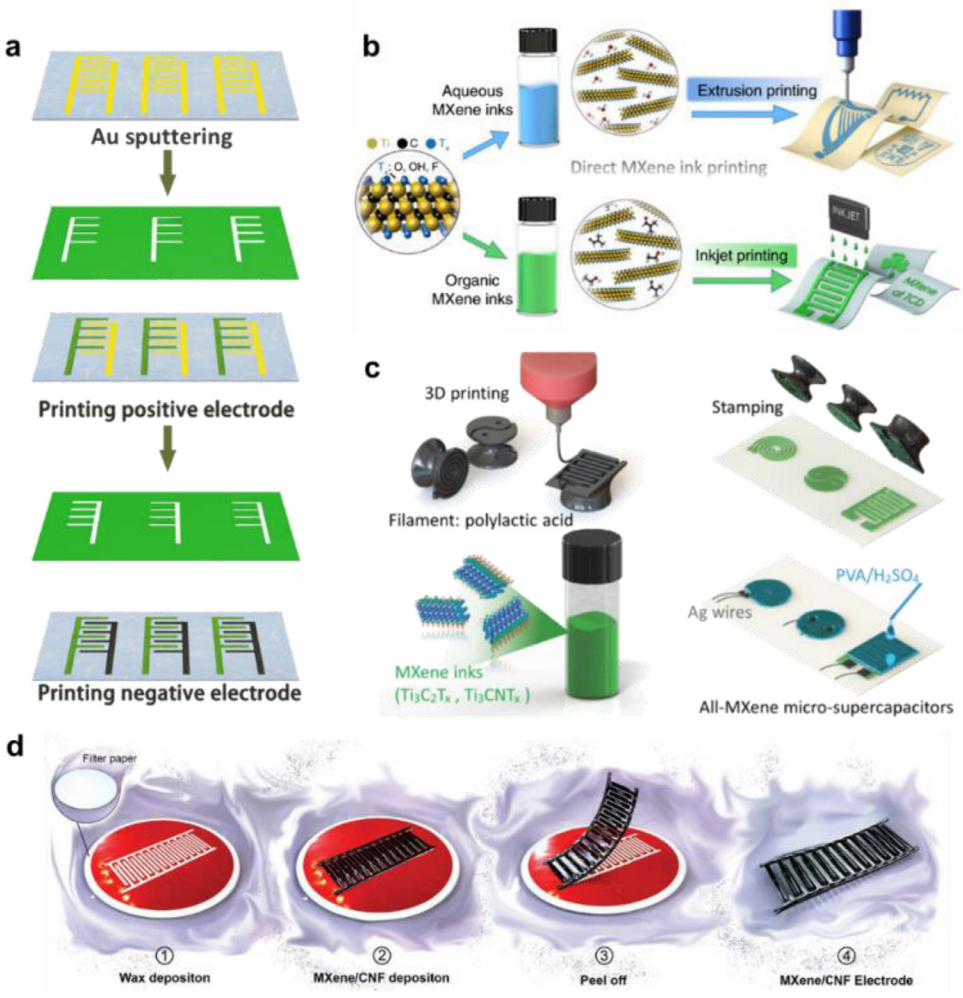

Fig. 18. Schematic illustrations of the micro-supercapacitors based on MXene inks. (a) Fabrication of hybrid micro-supercapacitors by two-step screen-printing process. Reproduced from Ref. [310] with copyright permission from Elsevier. (b) Direct printing of additive-free MXene inks. Reproduced from Ref. [311] with copyright permission from Springer. (c) Stamping of MXene inks for flexible micro-supercapacitors. Reproduced from Ref. [314] with copyright permission from Wiley-VCH. (d) Fabrication steps for $Ti_3C_2T_x$/cellulose nanofibrils-based micro-supercapacitors. Reproduced from Ref. [318] with copyright permission from Wiley-VCH.

two electrodes had 2D layered structure, it showed a voltage window of 1 V, an energy density of 8.6 mW h cm^{-3} at a power density of 0.2 W cm^{-3} in PVA/H_2SO_4 gel electrolyte as well as good flexibility.

Inkjet printing or extrusion printing is also efficient to pattern interdigitated designs. A typical inkjet printing needs inks with suitable viscosity and surface tension, which is usually achieved by adding surfactants and/or polymer stabilizers and then removing by heating. Nevertheless, MXene inks can be used directly without the need for any additive, which avoids these complex and inefficient processes. Zhang et al. reported the additive free $Ti_3C_2T_x$ MXene inks and their direct printing for all MXene micro supercapacitors with good performances and high resolution [311]. As illustrated in Fig. 18b, $Ti_3C_2T_x$ organic inks were used for inkjet printing, while the $Ti_3C_2T_x$ aqueous inks were designed for extrusion printing [311]. The direct MXene ink printing technique is scalable, low cost and efficient, and can be extended to other fields such as sensors and electromagnetic shielding. Furthermore, by increasing the concentration and viscoelasticity of the MXene ink, interdigital MXene electrodes with controllable thickness and loading can be fabricated on flexible polymer films and papers by extrusion printing. For the extrusion based 3D printing process, MXene dispersions were concentrated with superabsorbent polymer beads to reach high concentration (290 mg mL^{-1} and ~28.9 wt %) and suitable rheological properties [312]. The 3D printed micro supercapacitor showed outstanding areal capacitance (1035 mF cm^{-2} at 2 mV s^{-1}) and energy density (51.7 μWh cm^{-2}) that were improved by increasing the electrode thickness. One challenge within the printed electrodes is the dense restacking of MXenes nanosheets, which impedes the ion transport and then limits the performances. To overcome this, crumpled N doped MXene nanosheets were prepared with melamine formaldehyde as template and nitrogen source, in which the crumpled structure enhanced the ion accessibility and the nitrogen doping improved the conductivity and the redox activity [313]. The crumpled N doped MXene inks, after adjusting the viscosity, can be used in either 2D screen printing (70.1 mF cm^{-2} in PVA/H_2SO_4) or 3D extrusion printing (8.2 F cm^{-2}, 0.42 mWh cm^{-2} in PVA/H_2SO_4).

A stamping strategy was also studied for producing flexible coplanar all MXene ($Ti_3C_2T_x$ and Ti_3CNT_x) micro supercapacitors [314]. Pad and cylindrical stamps were constructed by 3D printing, and then the MXene inks were brushed onto the rough, hydrophilic stamp surface and firmly pressed onto substrates to form the interdigitated $Ti_3C_2T_x$ electrodes (Fig. 18c). The obtained micro supercapacitors with PVA/H_2SO_4 electrolyte delivered a high areal capacitance of 61 mF cm^{-2} at 25 μA cm^{-2} and maintained 50 mF cm^{-2} as the current density was increased by 32 fold. Another additive free MXene aqueous inks were prepared from clay like Ti_3C_2 MXene sediments, which can be stamped, printed, painted or written [315]. The inks with controlled particle size, viscosity, surface tension and fluidic parameters can be directly patterned by commercial pens on various substrates such as paper, textile, wood and plastics, and the deposited inks can achieve high conductivity, allowing the fabrication of micro supercapacitors on unconventional substrates without current collector.

Besides the above mentioned strategies, some alternative methods have also been employed for fabricating the micro supercapacitors based on MXenes, such as oxidative etching of the exposed MXene film

in H_2O_2 diluted solution using an interdigital mask [316], vacuum filtrating the MXene solutions through the laser printed paper templates followed by lift off with tetrahydrofuran [317], and vacuum filtrating MXene solutions through a wax printed filter paper [318]. Using fabrication steps shown in Fig. 18d and a freestanding and mechanically robust micro supercapacitor was obtained, in which 1D cellulose nanofibrils were combined with $Ti_3C_2T_x$ MXene nanosheets [318]. With a cellulose nanofibrils loading up to 20%, the hybrid electrode showed a remarkably improved mechanical strength of 341 MPa (pristine MXene film: 29 MPa) without sacrificing the electrochemical performances.

Flexible supercapacitors and micro supercapacitors have huge potential in the field of wearable consumer electronics and become a burgeoning research topic. MXenes, owing to their high volumetric capacitance, tunable surface terminations, 2D structure and metallic like conductivity, have developed rapidly in this field. Their 2D structure allows MXenes to be simply assembled into film electrodes via a facile vacuum filtration. By patterning the MXene based films, interdigitated electrodes for micro supercapacitors can be fabricated. Also, the negatively charged and hydrophilic property enable MXenes to form stable and viscous inks, which can be printed, stamped, painted or even written on various substrates to form micro supercapacitor electrodes. Due to these very appealing results, bright prospects can be foreseen for MXenes in this field.

8. Conclusions and perspectives

Key features of MXene materials such as 2D lamellar structure, metallic like conductivity, high density, variable surface terminations and intercalation pseudocapacitance make them very promising candidates for designing advanced supercapacitors with high energy and power density. This paper summarizes the recent advances on MXene based electrode materials for supercapacitors. Recent efforts devoted to their preparation methods, structure designs, chemical modifications, electrochemical characterizations as well as basic understanding of the charge storage mechanisms in different electrolytes are reviewed. The fabrication strategies and electrochemical performances of MXene based electrodes and devices, such as hybrid supercapacitors, flexible supercapacitors and micro supercapacitors are also discussed.

Since their discovery in 2011, three main synthesis routes have been proposed to prepare MXenes: HF etching with the following delamination by intercalation, etching in moderate F containing solution (like LiF/HCl or NH_4HF_2), and etching in fluoride free electrolytes such as Lewis acidic molten salt. From the point of views of electrochemical performance, safety and environmental friendless, the fluoride free preparation is considered as a promising direction. Most of the work reported in the literature focuses on $Ti_3C_2T_x$, while only few attention was paid to other compositions. The large variety of MXene materials that can be prepared and the possibility to tune their surface chemistry offer great opportunities for many applications, energy storage being one of the most important. Fundamental research efforts will have to be developed to push further basic understanding of the MXene/electrolyte interface as well as to design new strategies to control the surface chemistry. Computational approach will certainly play a significant role to accelerate this research process.

While their 2D lamellar structure improves ion accessibility and then the electrochemical reaction kinetics, it is important to avoid aggregation and restacking of MXene nanosheets. To overcome this problem, various structure and electrode architecture designs have been developed, including the control of flake size and interlayer spacing, designing 3D/porous architectures and fabricating vertical alignments. The rational designs of morphology and structure considerably improve the performances of MXenes, especially regarding the rate capability. It is also remarkable that their volumetric energy density is not compromised thanks to the high density of MXenes. Simple and efficient strategies for designing advanced material and electrode structures needs to be further developed.

Surface chemistry modification is one of the most important strategies for improving the electrochemical performances of MXenes. MXenes can be chemically modified by tuning surface terminations and doping. As the F terminations hinder charge transport and decrease active sites, in addition to developing fluorine free preparation methods, post treatments can be achieved to remove their F termination groups when prepared from F containing etching electrolytes. Besides, nitrogen atoms can be introduced to enlarge the MXene interlayer spacing by annealing MXenes in ammonia or using additional nitrogen source like urea, thus improving the electronic conductivity and providing additional active sites. Studies dedicated to the control of surface terminations groups and heteroatom doping have to be pursued.

MXenes in H_2SO_4 electrolyte can achieve excellent performances, including high capacitance (above 1500 F cm^{-3}), good rate capability and long cycle life, so most of the previous work focused on the H_2SO_4 systems. However, such high capacitance cannot transform into high energy density, as the water splitting reaction limits the operating voltage range of supercapacitors to around 1 V. The challenge for operating MXenes in non aqueous electrolytes lies in the limited capacitance and the relatively low kinetics owing to the size of the intercalated cations (compared to H^+ in aqueous acidic electrolyte); the improvement of MXene electrochemical performance thus relies on mastering the MXene/electrolyte interface and understanding the charge storage mechanism in non aqueous electrolyte. From the view of optimization of chemical compositions, MXenes with a high density of states above the Fermi level are regarded to be able to increase the pseudocapacitance. Tuning the nature and content of the surface termination groups on MXene is another way to affect the charge storage. For example, terminations with lower electronegativity than F (e.g. Cl) are beneficial to enhance the capacity. Electrolyte solvents have great influence on the desolvation process of the intercalated ions, so selecting the solvents in favor of complete desolvation is also essential for increasing the charge storage. Fundamental studies directed toward the understanding of the interaction between the surface groups and the intercalated ions, or the mechanism for ion desolvation in different solvents for instance are needed.

Although the energy storage mechanisms are of critical importance for developing MXenes for supercapacitor applications, their understanding is still at an early stage. In basic and neutral aqueous electrolytes, MXenes can only achieve limited capacitance within a narrow potential window, mainly driven by EDL charge storage mechanism involving hydrated ions in the interlayer spacing. In acidic electrolytes, the presence of confined H_2O molecules in the interlayer allows for fast transport of H^+, resulting in high redox capacitance and good cycle stability.

In non aqueous electrolytes, the solvation shell around the intercalated ions gradually collapse in the MXene interlayer spacing, which causes overlapping of atomic orbitals between the ions and the MXene to form a donor band. The band filling effect results in the reduction of MXene and produces an intercalation pseudocapacitance. Further investigation on charge storage mechanisms, especially in non aqueous electrolytes, are expected for guiding the MXene design.

Though they can work in symmetrical supercapacitors, MXenes are more suitable for application in hybrid supercapacitors as anodes, to avoid the possible oxidation of MXenes at high positive potential. In aqueous systems, the cathode materials with high rate capability and long cycle life, such as graphene and RuO_2, are suggested to pair up with MXene based anodes, but the energy density of the consequent devices is limited by their operating voltage of about 1 V. Moving to non aqueous electrolytes, offering higher voltage should be preferred to increase the energy density, but MXenes performance still need to be improved. In this way, the control of the surface termination groups seems to be a promising approach.

Thanks to their 2D structure, high volumetric capacitances and good mechanical properties, the last few years witnessed the fast growing of MXenes for flexible supercapacitors and micro supercapacitors applica

tions. 2D nanosheets of MXenes can be simply assembled into flexible film, but their layer by layer restacking usually results in the limited ion accessibility and the insufficient utilization of the active surface. The restacking problem is severe especially, when the MXene nanosheets are converted into thick films for high areal capacitance. Therefore, more efforts, such as structural establishment, termination modification or hybridization, are needed to increase the ion transport kinetics and ex pose the whole surface of MXenes. Besides, to enhance the mechanical properties of the MXene based flexible and printable supercapacitors, the reinforced materials can be introduced to MXene matrix without the loss of electrochemical performance.

In the last few years, MXenes have attracted extensive attention of the researchers from more than 40 countries, in the fields of energy stor age, electromagnetic interference shielding, antennas, sensors, cataly sis, medicine, et al. Especially, significant progress of MXenes has been made for capacitive energy storage applications due to their superiority on high gravimetric and volumetric energy and power density. Although many advances and achievements have been obtained, the endless op portunities for preparing new MXenes and tuning their properties imply that the development of MXenes for supercapacitors is still on the initial stage. The future direction lies in the understanding of their capacitive energy storage mechanism, the control of the surface chemistry, and the design of architectures that enable high performance supercapaci tors. The promising potential and the quickly expanding opportunities make MXenes have a bright future for energy storage applications.

Declaration of Competing Interest

The authors declare that they have no known competing financial interests or personal relationships that could have appeared to influence the work reported in this paper.

Acknowledgment

The authors would like to thank Prof. Yury Gogotsi (Drexel Univer sity) for valuable suggestions on the manuscript. This work was finan cially supported by the National Natural Science Foundation of China (Grant No. 51572011 and 51802012), the National Key Research and Development Program of China (Grant No. 2017YFB0102204), and the Agence Nationale de la Recherche, Labex STOREX.

References

[1] J.B. Goodenough, Y. Kim, Chem. Mater. 22 (2010) 587–603.
[2] P.G. Bruce, S.A. Freunberger, L.J. Hardwick, J.-M. Tarascon, Nat. Mater. 11 (2012) 19–29.
[3] H. Yang, H. Li, J. Li, Z. Sunc, K. He, H.-M. Cheng, F. Li, Angew. Chem. Int. Ed. 58 (2019) 11978–11996.
[4] S. Zheng, H. Huang, Y. Dong, S. Wang, F. Zhou, J. Qin, C. Sun, Y. Yu, Z.-S. Wu, X. Bao, Energy Environ. Sci. 13 (2020) 821–829.
[5] Y. Wang, Y. Song, Y. Xia, Chem. Soc. Rev. 45 (2016) 5925–5950.
[6] P. Simon, Y. Gogotsi, Nat. Mater. 19 (2020) 1151–1163.
[7] G. Wang, L. Zhang, J. Zhang, Chem. Soc. Rev. 41 (2012) 797–828.
[8] L.L. Zhang, X.S. Zhao, Chem. Soc. Rev. 38 (2009) 2520–2531.
[9] S. Yu, N. Sun, L. Hu, L. Wang, Q. Zhu, Y. Guan, B. Xu, J. Power Sources 405 (2018) 132–141.
[10] H. Wang, S. Yu, B. Xu, Chem. Commun. 52 (2016) 11512–11515.
[11] V. Augustyn, P. Simon, B. Dunn, Energy Environ. Sci. 7 (2014) 1597–1614.
[12] T. Deng, W. Zhang, O. Arcelus, J.-G. Kim, J. Carrasco, S.J. Yoo, W. Zheng, J. Wang, H. Tian, H. Zhang, X. Cui, T. Rojo, Nat. Commun. 8 (2017) 15194.
[13] Y. Shao, M.F. El-Kady, J. Sun, Y. Li, Q. Zhang, M. Zhu, H. Wang, B. Dunn, B. Kaner, Chem. Rev. 118 (2018) 9233–9280.
[14] H. Tan, X. Lin, J. Huang, J. Huang, M. Shi, X. Du, B. Zhang, Nanoscale 11 (2019) 11445–11450.
[15] Y.-E. Zhu, L. Yang, J. Sheng, Y. Chen, H. Gu, J. Wei, Z. Zhou, Adv. Energy Mater. 7 (2017) 1701222.
[16] T. Lv, M. Liu, D. Zhu, L. Gan, T. Chen, Adv. Mater. 30 (2018) 1705489.
[17] B. Xu, H. Duan, M. Chu, G. Cao, Y. Yang, J. Mater. Chem. A 1 (2013) 4565–4570.
[18] L.-F. Chen, Y. Lu, L. Yu, X.W. Lou, Energy Environ. Sci. 10 (2017) 1777–1783.
[19] S. Yu, H. Wang, C. Hu, Q. Zhu, N. Qiao, B. Xu, J. Mater. Chem. A 4 (2016) 16341–16348.
[20] L. Hu, Q. Zhu, Q. Wu, D. Li, Z. An, B. Xu, ACS Sustain. Chem. Eng. 6 (2018) 13949–13959.
[21] V. Augustyn, J. Come, M.A. Lowe, J.W. Kim, P.-L. Taberna, S.H. Tolbert, H.D. Abruña, P. Simon, B. Dunn, Nat. Mater. 12 (2013) 518–522.
[22] H.-S. Kim, J.B. Cook, H. Lin, J.S. Ko, S.H. Tolbert, V. Ozolins, B. Dunn, Nat. Mater. 16 (2017) 454–460.
[23] Y. Zhu, L. Peng, D. Chen, G. Yu, Nano Lett. 16 (2016) 742–747.
[24] H.D. Yoo, Y. Li, Y. Liang, Y. Lan, F. Wang, Y. Yao, ChemNanoMat 2 (2016) 688–691.
[25] T. Brezesinski, J. Wang, S.H. Tolbert, B. Dunn, Nat. Mater. 9 (2010) 146–151.
[26] M.R. Lukatskaya, O. Mashtalir, C.E. Ren, Y. Dall'Agnese, P. Rozier, P.L. Taberna, M. Naguib, P. Simon, M.W. Barsoum, Y. Gogotsi, Science 341 (2013) 1502–1505.
[27] M. Naguib, M. Kurtoglu, V. Presser, J. Lu, J. Niu, M. Heon, L. Hultman, Y. Gogotsi, M.W. Barsoum, Adv. Mater. 23 (2011) 4248–4253.
[28] M. Naguib, O. Mashtalir, J. Carle, V. Presser, J. Lu, L. Hultman, Y. Gogotsi, M.W. Barsoum, ACS Nano 6 (2012) 1322–1331.
[29] P. Zhang, R.A. Soomro, Z. Guan, N. Sun, B. Xu, Energy Storage Mater. 29 (2020) 163–171.
[30] M. Li, J. Lu, K. Luo, Y. Li, K. Chang, K. Chen, J. Zhou, J. Rosen, L. Hultman, P. Eklund, P.O.Å. Persson, S. Du, Z. Chai, Z. Huang, Q. Huang, J. Am. Chem. Soc. 141 (2019) 4730–4737.
[31] E. Lee, A. VahidMohammadi, B.C. Prorok, Y.S. Yoon, M. Beidaghi, D.-J. Kim, ACS Appl. Mater. Interfaces 9 (2017) 37184–37190.
[32] R.A. Soomro, S. Jawaid, Z. Abbas, B. Xu, Chin. Chem. Lett. 31 (2020) 922–930.
[33] K. Rasool, M. Helal, A. Ali, C.E. Ren, Y. Gogotsi, K.A. Mahmoud, ACS Nano 10 (2016) 3674–3684.
[34] T. Ma, J. Cao, M. Jaroniec, S. Qiao, Angew. Chem. Int. Ed. 55 (2016) 1138–1142.
[35] M. Yu, S. Zhou, Z. Wang, J. Zhao, J. Qiu, Nano Energy 44 (2018) 181–190.
[36] L.M. Azofra, N. Li, D.R. MacFarlane, C.H. Sun, Energy Environ. Sci. 9 (2016) 2545–2549.
[37] H. Yu, Y. Wang, Y. Jing, J. Ma, C.-F. Du, Q. Yan, Small 15 (2019) 1901503.
[38] Y. Liu, P. Zhang, N. Sun, B. Anasori, Q. Zhu, H. Liu, Y. Gogotsi, B. Xu, Adv. Mater. 30 (2018) 1707334.
[39] P. Zhang, D. Wang, Q. Zhu, N. Sun, F. Fu, B. Xu, Nano-Micro Lett. 11 (2019) 81.
[40] Y. Dong, H. Shi, Z.-S. Wu, Adv. Funct. Mater. 30 (2020) 2000706.
[41] P. Das, Z.-S. Wu, J. Phys. Energy 2 (2020) 032004.
[42] H. Shi, Y. Dong, S. Zheng, C. Dong, Z.-S. Wu, Nanoscale Adv. 2 (2020) 4212–4219.
[43] H. Shi, M. Yue, C.J. Zhang, Y. Dong, P. Lu, S. Zheng, H. Huang, J. Chen, P. Wen, Z. Xu, Q. Zheng, X. Li, Y. Yu, Z.-S. Wu, ACS Nano 14 (2020) 8678–8688.
[44] H. Shi, C.J. Zhang, P. Lu, Y. Dong, P. Wen, Z.-S. Wu, ACS Nano 13 (2019) 14308–14318.
[45] J. Zhou, X. Zha, X. Zhou, F. Chen, G. Gao, S. Wang, C. Shen, T. Chen, C. Zhi, P. Eklund, S. Du, J. Xue, W. Shi, Z. Chai, Q. Huang, ACS Nano 11 (2017) 3841–3850.
[46] J. Halim, S. Kota, M.R. Lukatskaya, M. Naguib, M.-Q. Zhao, E.J. Moon, J. Pitock, J. Nanda, S.J. May, Y. Gogotsi, M.W. Barsoum, Adv. Funct. Mater. 26 (2016) 3118–3127.
[47] M. Ghidiu, M. Naguib, C. Shi, O. Mashtalir, L.M. Pan, B. Zhang, J. Yang, Y. Gogotsi, S.J.L. Billinge, M.W. Barsoum, Chem. Commun. 50 (2014) 9517–9520.
[48] P. Urbankowski, B. Anasori, T. Makaryan, D. Er, S. Kota, P.L. Walsh, M. Zhao, V.B. Shenoy, M.W. Barsoum, Y. Gogotsi, Nanoscale 8 (2016) 11385–11391.
[49] Y. Li, H. Shao, Z. Lin, J. Lu, L. Liu, B. Duployer, P.O.Å. Persson, P. Eklund, L. Hultman, M. Li, K. Chen, X.-H. Zha, S. Du, P. Rozier, Z. Chai, E. Raymundo-Piñero, P.-L. Taberna, P. Simon, Q. Huang, Nat. Mater. 19 (2020) 894–899.
[50] Y. Gogotsi, Nat. Mater. 14 (2015) 1079–1080.
[51] C. Xu, L. Wang, Z. Liu, L. Chen, J. Guo, N. Kang, X.-L. Ma, H.-M. Cheng, W. Ren, Nat. Mater. 14 (2015) 1135–1141.
[52] S.-Y. Pang, Y.-T. Wong, S. Yuan, Y. Liu, M.-K. Tsang, Z. Yang, H. Huang, W.-T. Wong, J. Hao, J. Am. Chem. Soc. 141 (2019) 9610–9616.
[53] B. Anasori, M.R. Lukatskaya, Y. Gogotsi, Nat. Rev. Mater. 2 (2017) 16098.
[54] O. Mashtalir, M. Naguib, V.N. Mochalin, Y. Dall'Agnese, M. Heon, M.W. Barsoum, Y. Gogotsi, Nat. Commun. 4 (2013) 1716.
[55] M. Naguib, R.R. Unocic, B.L. Armstrong, J. Nanda, Dalton Trans. 44 (2015) 9353–9358.
[56] M. Ghidiu, M.R. Lukatskaya, M.-Q. Zhao, Y. Gogotsi, M.W. Barsoum, Nature 516 (2014) 78–81.
[57] B. Anasori, Y. Xie, M. Beidaghi, J. Lu, B.C. Hosler, L. Hultman, P.R.C. Kent, Y. Gogotsi, M.W. Barsoum, ACS Nano 9 (2015) 9507–9516.
[58] Y. Lee, S.J. Kim, Y.-J. Kim, Y. Lim, Y. Chae, B.-J. Lee, Y.-T. Kim, H. Han, Y. Gogotsi, C.W. Ahn, J. Mater. Chem. A 8 (2020) 573–581.
[59] Y. Chae, S.J. Kim, S.-Y. Cho, J. Choi, K. Maleski, B.-J. Lee, H.-T. Jung, Y. Gogotsi, Y. Lee, C.W. Ahn, Nanoscale 11 (2019) 8387–8393.
[60] C.-W. Wu, B. Unnikrishnan, I.W.P. Chen, S.G. Harroun, H.-T. Chang, C.-C. Huang, Energy Storage Mater. 25 (2020) 563–571.
[61] V. Natu, J.L. Hart, M. Sokol, H. Chiang, M.L. Taheri, M.W. Barsoum, Angew. Chem. 131 (2019) 12785–12790.
[62] F. Liu, A. Zhou, J. Chen, J. Jia, W. Zhou, L. Wang, Q. Hu, Appl. Surf. Sci. 416 (2017) 781–789.
[63] X. Wang, C. Garnero, G. Rochard, D. Magne, S. Morisset, S. Hurand, P. Chartier, J. Rousseau, T. Cabioc'h, C. Coutanceau, V. Mauchamp, S. Célérier, J. Mater. Chem. A 5 (2017) 22012–22023.
[64] A. Feng, Y. Yu, F. Jiang, Y. Wang, L. Mi, Y. Yu, L. Song, Ceram. Int. 43 (2017) 6322–6328.
[65] J. Halim, M.R. Lukatskaya, K.M. Cook, J. Lu, C.R. Smith, L.-Å. Näslund, S.J. May, L. Hultman, Y. Gogotsi, P. Eklund, M.W. Barsoum, Chem. Mater. 26 (2014) 2374–2381.
[66] L. Wang, H. Zhang, B. Wang, C. Shen, C. Zhang, Q. Hu, A. Zhou, B. Liu, Electron. Mater. Lett. 12 (2016) 702–710.
[67] O. Mashtalir, M.R. Lukatskaya, A.I. Kolesnikov, E. Raymundo-Piñero, M. Naguib, M.W. Barsoum, Y. Gogotsi, Nanoscale 8 (2016) 9128–9133.

[68] T. Li, L. Yao, Q. Liu, J. Gu, R. Luo, J. Li, X. Yan, W. Wang, P. Liu, B. Chen, W. Zhang, W. Abbas, R. Naz, D. Zhang, Angew. Chem. 130 (2018) 6223–6227.
[69] S. Yang, P. Zhang, F. Wang, A.G. Ricciardulli, M.R. Lohe, P.W.M. Blom, X. Feng, Angew. Chem. 130 (2018) 15717–15721.
[70] V. Kamysbayev, A.S. Filatov, H. Hu, X. Rui, F. Lagunas, D. Wang, R.F. Klie, D.V. Talapin, Science 369 (2020) 979–983.
[71] M.R. Lukatskaya, S. Kota, Z. Lin, M.-Q. Zhao, N. Shpigel, M.D. Levi, J. Halim, P.-L. Taberna, M.W. Barsoum, P. Simon, Y. Gogotsi, Nat. Energy 2 (2017) 17105.
[72] Y. Tao, X. Xie, W. Lv, D.-M. Tang, D. Kong, Z. Huang, H. Nishihara, T. Ishii, B. Li, D. Golberg, F. Kang, T. Kyotani, Q.-H. Yang, Sci. Rep. 3 (2013) 2975.
[73] Z. Wang, P. Tammela, M. Strømme, L. Nyholm, Nanoscale 7 (2015) 3418–3423.
[74] X.H. Xia, L. Shi, H.B. Liu, L. Yang, Y.D. He, J. Phys, Chem. Solids 73 (2012) 385–390.
[75] S. Feng, Z. Liu, Q. Yu, Z. Zhuang, Q. Chen, S. Fu, L. Zhou, L. Mai, ACS Appl. Mater. Interfaces 11 (2019) 4011–4016.
[76] B. Xu, D. Zheng, M. Jia, G. Cao, Y. Yang, Electrochim. Acta 98 (2013) 176–182.
[77] K. Huang, Z. Li, J. Lin, G. Han, P. Huang, Chem. Soc. Rev. 47 (2018) 5109–5124.
[78] L. Verger, V. Natu, M. Carey, M.W. Barsoum, Trends Chem. 1 (2019) 656–669.
[79] A.D. Dillon, M.J. Ghidiu, A.L. Krick, J. Griggs, S.J. May, Y. Gogotsi, M.W. Barsoum, A.T. Fafarman, Adv. Funct. Mater. 26 (2016) 4162–4168.
[80] F. Shahzad, M. Alhabeb, C.B. Hatter, B. Abasori, S.M. Hong, C.M. Koo, Y. Gogotsi, Science 353 (2016) 1137–1140.
[81] H. Wang, Y. Wu, J. Zhang, G. Li, H. Huang, X. Zhang, Q. Jiang, Mater. Lett. 160 (2015) 537–540.
[82] J. Zhang, N. Kong, S. Uzun, A. Levitt, S. Seyedin, P.A. Lynch, S. Qin, M. Han, W. Yang, J. Liu, X. Wang, Y. Gogotsi, J.M. Razal, Adv. Mater. 32 (2020) 2001093.
[83] Y. Xie, M. Naguib, V.N. Mochalin, M.W. Barsoum, Y. Gogotsi, X. Yu, K.-W. Nam, X.-Q. Yang, A.I. Kolesnikov, P.R.C. Kent, J. Am. Chem. Soc. 136 (2014) 6385–6394.
[84] K. Maleski, V.N. Mochalin, Y. Gogotsi, Chem. Mater. 29 (2017) 1632–1640.
[85] M. Khazaei, A. Ranjbar, M. Arai, T. Sasaki, S. Yunoki, J. Mater. Chem. C 5 (2017) 2488–2503.
[86] A. Lipatov, H. Lu, M. Alhabeb, B. Anasori, A. Gruverman, Y. Gogotsi, A. Sinitskii, Sci. Adv. 4 (2018) eaat0491.
[87] Z. Ling, C.E. Ren, M.-Q. Zhao, J. Yang, J.M. Giammarco, J. Qiu, M.W. Barsoum, Y. Gogotsi, Proc. Natl. Acad. Sci. 111 (2014) 16676–16681.
[88] K. Hantanasirisakul, M.-Q. Zhao, P. Urbankowski, J. Halim, B. Anasori, S. Kota, C.E. Ren, M.W. Barsoum, Y. Gogotsi, Adv. Electron. Mater. 2 (2016) 1600050.
[89] N. Sun, Z. Guan, Q. Zhu, B. Anasori, Y. Gogotsi, B. Xu, Nano-Micro Lett. 12 (2020) 89.
[90] Y. Gogotsi, B. Anasori, ACS Nano 13 (2019) 8491–8494.
[91] B. Xu, Y. Gogotsi, Chin. Chem. Lett. 31 (2020) 919–921.
[92] K. Zhu, Y. Jin, F. Du, S. Gao, Z. Gao, X. Meng, G. Chen, Y. Wei, Y. Gao, J. Energy Chem. 31 (2019) 11–18.
[93] L. Li, F. Wang, J. Zhu, W. Wu, Dalton Trans. 46 (2017) 14880–14887.
[94] A.V. Mohammadi, M. Mojtabavi, N.M. Caffrey, M. Wanunu, M. Beidaghi, Adv. Mater. 31 (2018) 1806931.
[95] Y. Yoon, M. Lee, S.K. Kim, G. Bae, W. Song, S. Myung, J. Lim, S.S. Lee, T. Zyung, K.-S. An, Adv. Energy Mater. 8 (2018) 1703173.
[96] J. Fu, J. Yun, S. Wu, L. Li, L. Yu, K.H. Kim, ACS Appl. Mater. Interfaces 10 (2018) 34212–34221.
[97] B. Yao, M. Li, J. Zhang, L. Zhang, Y. Song, W. Xiao, A. Cruz, Y. Tong, Y. Li, Nano-Micro Lett. 12 (2020) 3.
[98] A. Djire, A. Bos, J. Liu, H. Zhang, E.M. Miller, N.R. Neale, ACS Appl. Nano Mater. 2 (2019) 2785–2795.
[99] M. Naguib, J. Halim, J. Lu, K.M. Cook, L. Hultman, Y. Gogotsi, M.W. Barsoum, J. Am. Chem. Soc. 135 (2013) 15966–15969.
[100] M.H. Tran, T. Schafer, A. Shahraei, M. Dürrschnabel, L. Molina-Luna, U.I. Kramm, C.S. Birkel, ACS Appl. Energy Mater. 1 (2018) 3908–3914.
[101] Q. Shan, X. Mu, M. Alhabeb, C.E. Shuck, D. Pang, X. Zhao, X.-F. Chu, Y. Wei, F. Du, G. Chen, Y. Gogotsi, Y. Gao, Y. Dall'Agnese, Electrochem. Commun. 96 (2018) 103–107.
[102] M. Naguib, V.N. Mochalin, M.W. Barsoum, Y. Gogotsi, Adv. Mater. 26 (2014) 982–1005.
[103] X. Wang, S. Lin, H. Tong, Y. Huang, P. Tong, B. Zhao, J. Dai, C. Liang, H. Wang, X. Zhu, Y. Sun, S. Dou, Electrochim. Acta 307 (2019) 414–421.
[104] S. Zhao, C. Chen, X. Zhao, X. Chu, F. Du, G. Chen, Y. Gogotsi, Y. Gao, Y. Dall'Agnese, Adv. Funct. Mater. 30 (2020) 2000815.
[105] O. Mashtalir, M.R. Lukatskaya, M.-Q. Zhao, M.W. Barsoum, Y. Gogotsi, Adv. Mater. 27 (2015) 3501–3506.
[106] R. Syamsai, A.N. Grace, J. Alloy Compd. 792 (2019) 1230–1238.
[107] C. Zhan, W. Sun, P.R.C. Kent, M. Naguib, Y. Gogotsi, D. Jiang, J. Phys. Chem. C 123 (2019) 315–321.
[108] Y. Tang, J.F. Zhu, C.H. Yang, F. Wang, J. Electrochem. Soc. 163 (2016) A1975–A1982.
[109] K. Maleski, C.E. Ren, M.-Q. Zhao, B. Anasori, Y. Gogotsi, ACS Appl. Mater. Interfaces 10 (2018) 24491–24498.
[110] E. Kayali, A. VahidMohammadi, J. Orangi, M. Beidaghi, ACS Appl. Mater. Interfaces 10 (2018) 25949–25954.
[111] Q. Zhu, L. Ma, H. Wang, M. Jia, Y. Guan, B. Xu, ChemistrySelect 2 (2017) 4456–4461.
[112] Y. Cheng, S. Lu, H. Zhang, C.V. Varanasi, J. Liu, Nano Lett. 12 (2012) 4206–4211.
[113] W. Wang, S. Guo, M. Penchev, I. Ruiz, K.N. Bozhilov, D. Yan, M. Ozkan, C.S. Ozkan, Nano Energy 2 (2013) 294–303.
[114] S.A. Melchior, K. Raju, I.S. Ike, R.M. Erasmus, G. Kabongo, I. Sigalas, S.E. Iyuke, K.I. Ozoemena, J. Electrochem. Soc. 165 (2018) A501–A511.
[115] C. Zhang, L. Wang, W. Lei, Y. Wu, C. Li, M.A. Khan, Y. Ouyang, X. Jiao, H. Ye, S. Mutahir, Q. Hao, Mater. Lett. 234 (2019) 21–25.
[116] M. Ghidiu, S. Kota, J. Halim, A.W. Sherwood, N. Nedfors, J. Rosen, V.N. Mochalin, M.W. Barsoum, Chem. Mater. 29 (2017) 1099–1106.
[117] J. Luo, W. Zhang, H. Yuan, C. Jin, L. Zhang, H. Huang, C. Liang, Y. Xia, J. Zhang, Y. Gan, X. Tao, ACS Nano 11 (2017) 2459–2469.
[118] P. Yan, R. Zhang, J. Jia, C. Wu, A. Zhou, J. Xu, X. Zhang, J. Power Sources 284 (2015) 38–43.
[119] Y. Dall'Agnese, P. Rozier, P.-L. Taberna, Y. Gogotsi, P. Simon, J. Power Sources 306 (2016) 510–515.
[120] Z. Fan, Y. Wang, Z. Xie, D. Wang, Y. Yuan, H. Kang, B. Su, Z. Cheng, Y. Liu, Adv. Sci. 5 (2018) 1800750.
[121] X. Zhang, Y. Liu, S. Dong, J. Yang, X. Liu, J. Alloy Compd. 790 (2019) 517–523.
[122] C. Chen, M. Boota, P. Urbankowski, B. Anasori, L. Miao, J. Jiang, Y. Gogotsi, J. Mater. Chem. A 6 (2018) 4617–4622.
[123] H. Chen, L. Yu, Z. Lin, Q. Zhu, P. Zhang, N. Qiao, B. Xu, J. Mater. Sci. 55 (2020) 1148–1156.
[124] Y. Xin, Y.-X. Yu, Mater. Des. 130 (2017) 512–520.
[125] M.-Q. Zhao, C.E. Ren, Z. Ling, M.R. Lukatskaya, C. Zhang, K.L.V. Aken, M.W. Barsoum, Y. Gogotsi, Adv. Mater. 27 (2015) 339–345.
[126] A.M. Navarro-Suarez, K.L.V. Aken, T. Mathis, T. Makaryan, J. Yan, J. Carretero–Gonzalez, T. Rojo, Y. Gogotsi, Electrochim. Acta 259 (2018) 752–761.
[127] X. Xie, M.-Q. Zhao, B. Anasori, K. Maleski, C.E. Ren, J. Li, B.W. Byles, E. Pomerantseva, G. Wang, Y. Gogotsi, Nano Energy 26 (2016) 513–523.
[128] Q. Fu, X. Wang, N. Zhang, J. Wen, L. Li, H. Gao, X. Zhang, J. Colloid Interface Sci. 511 (2018) 128–134.
[129] J. Yan, C.E. Ren, K. Maleski, C.B. Hatter, B. Anasori, P. Urbankowski, A. Sarycheva, Y. Gogotsi, Adv. Funct. Mater. 27 (2017) 1701264.
[130] Y. Zhang, Z. Yang, B. Zhang, J. Li, C. Lu, L. Kong, M. Liu, J. Alloy Compd. 835 (2020) 155343.
[131] Y. Li, Y. Deng, J. Zhang, Y. Shen, X. Yang, W. Zhang, J. Alloy Compd. 842 (2020) 155985.
[132] Z. Lin, D. Barbara, P.-L. Taberna, K.L.V. Aken, B. Anasori, Y. Gogotsi, P. Simon, J. Power Sources 326 (2016) 575–579.
[133] L. Shen, X. Zhou, X. Zhang, Y. Zhang, Y. Liu, W. Wang, W. Si, X. Dong, J. Mater. Chem. A 6 (2018) 23513–23520.
[134] L. Yang, W. Zheng, P. Zhang, J. Chen, W.B. Tian, Y.M. Zhang, Z.M. Sun, J. Electroanal. Chem. 830-831 (2018) 1–6.
[135] K. Wang, B. Zheng, M. Mackinder, N. Baule, H. Qiao, H. Jin, T. Schuelke, Q.H. Fan, Energy Storage Mater. 20 (2019) 299–306.
[136] C.E. Ren, M.-Q. Zhao, T. Makaryan, J. Halim, M. Boota, S. Kota, B. Anasori, M.W. Barsoum, Y. Gogotsi, ChemElectroChem 3 (2016) 689–693.
[137] M.-Q. Zhao, X. Xie, C.E. Ren, T. Makaryan, B. Anasori, G. Wang, Y. Gogotsi, Adv. Mater. 29 (2017) 1702410.
[138] X. Xie, K. Kretschmer, B. Anasori, B. Sun, G. Wang, Y. Gogotsi, ACS Appl. Nano Mater. 1 (2018) 505–511.
[139] Q. Zhao, Q. Zhu, J. Miao, P. Zhang, P. Wan, L. He, B. Xu, Small 15 (2019) 1904293.
[140] M. Yao, Y. Chen, Z. Wang, C. Shao, J. Dong, Q. Zhang, L. Zhang, X. Zhao, Chem. Eng. J. 395 (2020) 124057.
[141] J. Liu, H.-B. Zhang, R. Sun, Y. Liu, Z. Liu, A. Zhou, Z.-Z. Yu, Adv. Mater. 29 (2017) 1702367.
[142] P. Collini, S. Kota, A.D. Dillon, M.W. Barsoum, A.T. Fafarman, J. Electrochem. Soc. 164 (2017) D573–D580.
[143] Z. Fan, Y. Wang, Z. Xie, X. Xu, Y. Yuan, Z. Cheng, Y. Liu, Nanoscale 10 (2018) 9642–9652.
[144] P. Zhang, Q. Zhu, R.A. Soomro, S. He, N. Sun, N. Qiao, B. Xu, Adv. Funct. Mater. 30 (2020) 2000922.
[145] L. Shi, S. Lin, L. Li, W. Wu, L. Wu, H. Gao, X. Zhang, Ceram. Int. 44 (2018) 13901–13907.
[146] T.-H. Chang, T. Zhang, H. Yang, K. Li, Y. Tian, J.Y. Lee, P.-Y. Chen, ACS Nano 12 (2018) 8048–8059.
[147] S. Xu, G. Wei, J. Li, W. Han, Y. Gogotsi, J. Mater. Chem. A 5 (2017) 17442–17451.
[148] T. Zhao, J. Zhang, Z. Du, Y. Liu, G. Zhou, J. Wang, Electrochim. Acta 254 (2017) 308–319.
[149] N. Radha, A. Kanakaraj, H.M. Manohar, M.R. Nidhi, D. Mondal, S.K. Nataraj, D. Ghosh, Appl. Surf. Sci. 481 (2019) 892–899.
[150] Y. Yue, N. Liu, Y. Ma, S. Wang, W. Liu, C. Luo, H. Zhang, F. Cheng, J. Rao, X. Hu, J. Su, Y. Gao, ACS Nano 12 (2018) 4224–4232.
[151] T. Shang, Z. Lin, C. Qi, X. Liu, P. Li, Y. Tao, Z. Wu, D. Li, P. Simon, Q.-H. Yang, Adv. Funct. Mater. 29 (2019) 1903960.
[152] L. Li, M. Zhang, X. Zhang, Z. Zhang, J. Power Sources 364 (2017) 234–241.
[153] X. Wang, Q. Fu, J. Wen, X. Ma, C. Zhu, X. Zhang, D. Qi, Nanoscale 10 (2018) 20828–20835.
[154] X. Zhang, X. Liu, S. Dong, J. Yang, Y. Liu, Appl. Mater. Today 16 (2019) 315–321.
[155] Y. Wang, X. Wang, X. Li, Y. Bai, H. Xiao, Y. Liu, R. Liu, G. Yuan, Adv. Funct. Mater. 29 (2019) 1900326.
[156] M. Hu, T. Hu, R. Cheng, J. Yang, C. Cui, C. Zhang, X. Wang, J. Energy Chem. 27 (2018) 161–166.
[157] X. Zhang, Y. Liu, S. Dong, J. Yang, X. Liu, Appl. Surf. Sci. 485 (2019) 1–7.
[158] H. Li, R. Chen, M. Ali, H. Lee, M.J. Ko, Adv. Funct. Mater. 30 (2020) 2002739.
[159] J. Guo, Y. Zhao, A. liu, T. Ma, Electrochim. Acta 305 (2019) 164–174.
[160] Y. Tian, C. Yang, W. Que, Y. He, X. Liu, Y. Luo, X. Yin, L.B. Kong, J. Power Sources 369 (2017) 78–86.
[161] S. Xu, G. Wei, J. Li, Y. Ji, N. Klyui, V. Izotov, W. Han, Chem. Eng. J. 317 (2017) 1026–1036.

[162] M. Hu, Z. Li, H. Zhang, T. Hu, C. Zhang, Z. Wu, X. Wang, Chem. Commun. 51 (2015) 13531–13533.
[163] L. Li, N. Zhang, M. Zhang, L. Wu, X. Zhang, Z. Zhang, ACS Sustain. Chem. Eng. 6 (2018) 7442–7450.
[164] M. Guo, C. Liu, Z. Zhang, J. Zhou, Y. Tang, S. Luo, Adv. Funct. Mater. 28 (2018) 1803196.
[165] Z. Fan, J. Wang, H. Kang, Y. Wang, Z. Xie, Z. Cheng, Y. Liu, ACS Appl. Energy Mater. 3 (2020) 1811–1820.
[166] J. Kong, H. Yang, X. Guo, S. Yang, Z. Huang, X. Lu, Z. Bo, J. Yan, K. Cen, K.K. Ostrikov, ACS Energy Lett. 5 (2020) 2266–2274.
[167] Y. Xia, T.S. Mathis, M.-Q. Zhao, B. Anasori, A. Dang, Z. Zhou, H. Cho, Y. Gogotsi, S. Yang, Nature 557 (2018) 409–412.
[168] M. Lu, W. Han, H. Li, H. Li, B. Zhang, W. Zhang, W. Zheng, Adv. Mater. Interfaces 6 (2019) 1900160.
[169] J. Zhang, Y. Zhao, X. Guo, C. Chen, C.-L. Dong, R.-S. Liu, C.-P. Han, Y. Li, Y. Gogotsi, G. Wang, Nat. Catal. 1 (2018) 985–992.
[170] D.A. Kuznetsov, Z. Chen, P.V. Kumar, A. Tsoukalou, A. Kierzkowska, P.M. Abdala, O.V. Safonova, A. Fedorov, C.R. Müller, J. Am. Chem. Soc. 141 (2019) 17809–17816.
[171] V. Ramalingam, P. Varadhan, H.-C. Fu, H. Kim, D. Zhang, S. Chen, L. Song, D. Ma, Y. Wang, H.N. Alshareef, J.-H. He, Adv. Mater. 31 (2019) 1903841.
[172] C. Ling, L. Shi, Y. Ouyang, Q. Chen, J. Wang, Adv. Sci. 3 (2016) 1600180.
[173] C.-F. Du, X. Sun, H. Yu, Q. Liang, K.N. Dinh, Y. Zheng, Y. Luo, Z. Wang, Q. Yan, Adv. Sci. 6 (2019) 1900116.
[174] X. Sang, Y. Xie, M.-W. Lin, M. Alhabeb, K.L.V. Aken, Y. Gogotsi, P.R.C. Kent, K. Xiao, R.R. Unocic, ACS Nano 10 (2016) 9193–9200.
[175] J.L. Hart, K. Hantanasirisakul, A.C. Lang, B. Anasori, D. Pinto, Y. Pivak, T.v.J. Omme, S.J. May, Y. Gogotsi, M.L. Taheri, Nat. Commun. 10 (2019) 522.
[176] X. Zhang, Y. Liu, S. Dong, J. Yang, X. Liu, Electrochim. Acta 294 (2019) 233–239.
[177] M. Hu, T. Hu, Z. Li, Y. Yang, R. Cheng, J. Yang, C. Cui, X. Wang, ACS Nano 12 (2018) 3578–3586.
[178] Q. Tang, Z. Zhou, P. Shen, J. Am. Chem. Soc. 134 (2012) 16909–16916.
[179] M.R. Lukatskaya, S.-M. Bak, X. Yu, X.-Q. Yang, M.W. Barsoum, Y. Gogotsi, Adv. Energy Mater. 5 (2015) 1500589.
[180] R.B. Rakhi, B. Ahmed, M.N. Hedhili, D.H. Anjum, H.N. Alshareef, Chem. Mater. 27 (2015) 5314–5323.
[181] Y. Dall'Agnese, M.R. Lukatskaya, K.M. Cook, P.-L. Taberna, Y. Gogotsi, P. Simon, Electrochem. Commun. 48 (2014) 118–122.
[182] J. Li, X. Yuan, C. Lin, Y. Yang, L. Xu, X. Du, J. Xie, J. Lin, J. Sun, Adv. Energy Mater. 7 (2017) 1602725.
[183] X. Chen, Y. Zhu, M. Zhang, J. Sui, W. Peng, Y. Li, G.L. Zhang, F. Zhang, X. Fan, ACS Nano 13 (2019) 9449–9456.
[184] S. Kajiyama, L. Szabova, H. Iinuma, A. Sugahara, K. Gotoh, K. Sodeyama, Y. Tateyama, M. Okubo, A. Yamada, Adv. Energy Mater. 7 (2017) 1601873.
[185] M. Okubo, A. Sugahara, S. Kajiyama, A. Yamada, Acc. Chem. Res. 51 (2018) 591–599.
[186] H. Wang, J. Zhang, Y. Wu, H. Huang, Q. Jiang, J. Phys, Chem. Solids 115 (2018) 172–179.
[187] Y. Wen, T.E. Rufford, X. Chen, N. Li, M. Lyu, L. Dai, L. Wang, Nano Energy 38 (2017) 368–376.
[188] H. Li, X. Wang, H. Li, S. Lin, B. Zhao, J. Dai, W. Song, X. Zhu, Y. Sun, J. Alloy Compd. 784 (2019) 923–930.
[189] Y. Tang, J. Zhu, W. Wu, C. Yang, W. Lv, F. Wang, J. Electrochem. Soc. 164 (2017) A923–A929.
[190] L. Yang, W. Zheng, P. Zhang, J. Chen, W. Zhang, W.B. Tian, Z.M. Sun, Electrochim. Acta 300 (2019) 349–356.
[191] C. Yang, Y. Tang, Y. Tian, Y. Luo, M.F.U. Din, X. Yin, W. Que, Adv. Energy Mater. 8 (2018) 1802087.
[192] C. Yang, W. Que, X. Yin, Y. Tian, Y. Yang, M. Que, Electrochim. Acta 225 (2017) 416–424.
[193] T. Qiu, G. Li, Y. Shao, K. Jiang, F. Zhao, F. Geng, Carbon Energy (2020), doi:10.1002/cey2.51.
[194] C. Yang, W. Que, Y. Tang, Y. Tian, X. Yin, J. Electrochem. Soc. 164 (2017) A1939–A1945.
[195] P. Chakraborty, T. Das, D. Nafday, L. Boeri, T. Saha-Dasgupta, Phys. Rev. B. 95 (2017) 184106.
[196] Z.-W. Gao, W. Zheng, L.Y.S. Lee, Small 15 (2019) 1902649.
[197] M. Fatima, J. Fatheema, N.B. Monir, A.H. Siddique, B. Khan, A. Islam, D. Akinwande, S. Rizwan, Front. Chem. 8 (2020) 168.
[198] Y. Tang, J. Zhu, C. Yang, F. Wang, J. Alloy Compd. 685 (2016) 194–201.
[199] W. Yuan, L. Cheng, B. Zhang, H. Wu, Ceram. Int. 44 (2018) 17539–17543.
[200] Q. Wang, Z. Zhang, Z. Zhang, X. Zhou, G. Ma, J. Solid State Electrochem. 23 (2019) 361–365.
[201] R.B. Rakhi, B. Ahmed, D. Anjum, H.N. Alshareef, ACS Appl. Mater. Interfaces 8 (2016) 18806–18814.
[202] H. Jiang, Z. Wang, Q. Yang, M. Hanif, Z. Wang, L. Dong, M. Dong, Electrochim. Acta 290 (2018) 695–703.
[203] Y. Tian, C. Yang, W. Que, X. Liu, X. Yin, L.B. Kong, J. Power Sources 359 (2017) 332–339.
[204] S. Chen, Y. Xiang, W. Xu, C. Peng, Inorg. Chem. Front. 6 (2019) 199–208.
[205] J. Zhou, J. Yu, L. Shi, Z. Wang, H. Liu, B. Yang, C. Li, C. Zhu, J. Xu, Small 14 (2018) 1803786.
[206] J. Zhu, X. Lu, L. Wang, RSC Adv. 6 (2016) 98506–98513.
[207] F. Wang, M. Cao, Y. Qin, J. Zhu, L. Wang, Y. Tang, RSC Adv. 6 (2016) 88934–88942.
[208] W. Zheng, P. Zhang, W. Tian, Y. Wang, Y. Zhang, J. Chen, Z.M. Sun, Mater. Lett. 209 (2017) 122–125.
[209] J. Zhu, Y. Tang, C. Yang, F. Wang, M. Cao, J. Electrochem. Soc. 163 (2016) A785–A791.
[210] M. Cao, F. Wang, L. Wang, W. Wu, W. Lv, J. Zhu, J. Electrochem. Soc. 164 (2017) A3933–A3942.
[211] K. Zhang, G. Ying, L. Liu, F. Ma, L. Su, C. Zhang, D. Wu, X. Wang, Y. Zhou, Materials 12 (2019) 188.
[212] S.B. Ambade, R.B. Ambade, W. Eom, S.H. Noh, S.H. Kim, T.H. Han, Adv. Mater. Interfaces 5 (2018) 1801361.
[213] H. Li, X. Li, J. Liang, Y. Chen, Adv. Energy Mater. 9 (2019) 1803987.
[214] C. Zhang, M. Beidaghi, M. Naguib, M.R. Lukatskaya, M.-Q. Zhao, B. Dyatkin, K.M. Cook, S. J.Kim, B. Eng, X. Xiao, D. Long, W. Qiao, B. Dunn, Y. Gogotsi, Chem. Mater. 28 (2016) 3937–3943.
[215] H. Liu, X. Zhang, Y. Zhu, B. Cao, Q. Zhu, P. Zhang, B. Xu, F. Wu, R. Chen, Nano-Micro Lett. 11 (2019) 65.
[216] R. Liu, A. Zhang, J. Tang, J. Tian, W. Huang, J. Cai, C. Barrow, W. Yang, J. Liu, Chem. Eur. J. 25 (2019) 5547–5554.
[217] H. Liu, R. Hu, J. Qi, Y. Sui, Y. He, Q. Meng, F. Wei, Y. Ren, Y. Zhao, W. Wei, Adv. Mater. Interfaces 7 (2020) 1901659.
[218] Y. Luo, C. Yang, Y. Tian, Y. Tang, X. Yin, W. Que, J. Power Sources 450 (2020) 227694.
[219] H. Liu, R. Hu, J. Qi, Y. Sui, Y. He, Q. Meng, F. Wei, Y. Ren, Y. Zhao, Electrochim. Acta 353 (2020) 136526.
[220] W. Wu, D. Niu, J. Zhua, Y. Gao, D. Wei, C. Zhao, C. Wang, F. Wang, L. Wang, L. Yang, Ceram. Int. 45 (2019) 16261–16269.
[221] Y. Li, P. Kamdem, X.-J. Jin, Dalton Trans. 49 (2020) 7807–7819.
[222] X. He, T. Bi, X. Zheng, W. Zhu, J. Jiang, Electrochim. Acta 332 (2020) 135514.
[223] H. Lia, X. Chen, E. Zalnezhadc, K.N. Huid, K.S. Huie, M.J. Ko, J. Ind. Eng. Chem. 82 (2020) 309–316.
[224] M. Chandran, A. Thomas, A. Raveendran, M. Vinoba, M. Bhagiyalakshmi, J. Energy Storage 30 (2020) 101446.
[225] M.H. Yang, B.G. Choi, S.C. Jung, Y. Han, Y.S. Huh, S.B. Lee, Adv. Funct. Mater. 24 (2014) 7301–7309.
[226] S. Chen, Y. Xiang, M.K. Banks, C. Peng, W. Xu, R. Wu, Nanoscale 10 (2018) 20043–20052.
[227] W. Zhao, J. Peng, W. Wang, B. Jin, T. Chen, S. Liu, Q. Zhao, W. Huang, Small 15 (2019) 1901351.
[228] A. VahidMohammadi, J. Moncada, H. Chen, E. Kayali, J. Orangi, C.A. Carrero, M. Beidaghi, J. Mater. Chem. A 6 (2018) 22123–22133.
[229] L. Qin, Q. Tao, A.E. Ghazaly, J. Fernandez-Rodriguez, P.O.Å. Persson, J. Rosen, F. Zhang, Adv. Funct. Mater. 28 (2018) 1703808.
[230] Z. Chen, Y. Han, T. Li, X. Zhang, T. Wang, Z. Zhang, Mater. Lett. 220 (2018) 305–308.
[231] W. Wu, D. Wei, J. Zhu, D. Niu, F. Wang, L. Wang, L. Yang, P. Yang, C. Wang, Ceram. Int. 45 (2019) 7328–7337.
[232] H. Wang, L. Li, C. Zhu, S. Lin, J. Wen, Q. Jin, X. Zhang, J. Alloy Compd. 778 (2019) 858–865.
[233] M. Boota, M. Pasini, F. Galeotti, W. Porzio, M.-Q. Zhao, J. Halim, Y. Gogotsi, Chem. Mater. 29 (2017) 2731–2738.
[234] X. Lu, J. Zhu, W. Wu, B. Zhang, Electrochim. Acta 228 (2017) 282–289.
[235] Y. Ren, J. Zhu, L. Wang, H. Liu, Y. Liu, W. Wu, F. Wang, Mater. Lett. 214 (2018) 84–87.
[236] J. Li, A. Levitt, N. Kurra, K. Juan, N. Noriega, X. Xiao, X. Wang, H. Wang, H.N. Alshareef, Y. Gogotsi, Energy Storage Mater. 20 (2019) 455–461.
[237] G.S. Gund, J.H. Park, R. Harpalsinh, M. Kota, J.H. Shin, T. Kim, Y. Gogotsi, H.S. Park, Joule 3 (2019) 164–176.
[238] J. Yan, Y. Ma, C. Zhang, X. Li, W. Liu, X. Yao, S. Yao, S. Luo, RSC Adv. 8 (2018) 39742–39748.
[239] M. Boota, B. Anasori, C. Voigt, M.-Q. Zhao, M.W. Barsoum, Y. Gogotsi, Adv. Mater. 28 (2016) 1517–1522.
[240] M. Zhu, Y. Huang, Q. Deng, J. Zhou, Z. Pei, Q. Xue, Y. Huang, Z. Wang, H. Li, Q. Huang, C. Zhi, Adv. Energy Mater. 6 (2016) 1600969.
[241] T.A. Le, N.Q. Tran, Y. Hong, H. Lee, Chem. Eur. J. 25 (2019) 1037–1043.
[242] C. Choi, D.S. Ashby, D.M. Butts, R.H. DeBlock, Q. Wei, J. Lau, B. Dunn, Nat. Rev. Mater. 5 (2020) 5–17.
[243] B.E. Conway, Electrochemical Supercapacitors: Scientific Fundamentals, Technological Applications, Kluwer Academic Plenum Publisher, New York, 1999.
[244] M.D. Levi, M.R. Lukatskaya, S. Sigalov, M. Beidaghi, N. Shpigel, L. Daikhin, D. Aurbach, M.W. Barsoum, Y. Gogotsi, Adv. Energy Mater. 5 (2015) 1400815.
[245] Y. Ando, M. Okubo, A. Yamada, M. Otani, Adv. Funct. Mater. 30 (2020) 2000820.
[246] M. Hu, Z. Li, T. Hu, S. Zhu, C. Zhang, X. Wang, ACS Nano 10 (2016) 11344–11350.
[247] C. Zhan, M. Naguib, M. Lukatskaya, P.R.C. Kent, Y. Gogotsi, D. Jiang, J. Phys. Chem. Lett. 9 (2018) 1223–1228.
[248] X. Mu, D. Wang, F. Du, G. Chen, C. Wang, Y. Wei, Y. Gogotsi, Y. Gao, Y. Dall'Agnese, Adv. Funct. Mater. 29 (2019) 1902953.
[249] H. Shao, K. Xu, Y.-C. Wu, A. Iadecola, L. Liu, H. Ma, L. Qu, E. Raymundo-Piñero, J. Zhu, Z. Lin, P.-L. Taberna, P. Simon, ACS Energy Lett. 5 (2020) 2873–2880.
[250] P. Simon, Y. Gogotsi, Nat. Mater. 7 (2008) 845–853.
[251] X. Wang, T.S. Mathis, K. Li, Z. Lin, L. Vlcek, T. Torita, N.C. Osti, C. Hatter, P. Urbankowski, A. Sarycheva, M. Tyagi, E. Mamontov, P. Simon, Y. Gogotsi, Nat. Energy 4 (2019) 241–248.
[252] Z. Lin, P. Rozier, B. Duployer, P.-L. Taberna, B. Anasori, Y. Gogotsi, P. Simon, Electrochem. Commun. 72 (2016) 50–53.
[253] K. Xu, Z. Lin, C. Merlet, P.-L. Taberna, L. Miao, J. Jiang, P. Simon, ChemSusChem 11 (2018) 1892–1899.
[254] M. Boota, Y. Gogotsi, Adv. Energy Mater. 9 (2019) 1802917.
[255] M. Boota, M. Becuwe, Y. Gogotsi, ACS Appl. Energy Mater. 3 (2020) 3144–3149.

[256] Q. Jiang, N. Kurra, M. Alhabeb, Y. Gogotsi, H.N. Alshareef, Adv. Energy Mater. 8 (2018) 1703043.
[257] S. Wang, X. Zhao, X. Yan, Z. Xiao, C. Liu, Y. Zhang, X. Yang, Angew. Chem. Int. Ed. 58 (2019) 205–210.
[258] M. Hu, C. Cui, C. Shi, Z.-S. Wu, J. Yang, R. Cheng, T. Guang, H. Wang, H. Lu, X. Wang, ACS Nano 13 (2019) 6899–6905.
[259] Z. Pan, F. Cao, X. Hua, X. Ji, J. Mater. Chem. A 7 (2019) 8984–8992.
[260] K. Zhu, H. Zhang, K. Ye, W. Zhao, J. Yan, K. Cheng, G. Wang, B. Yang, D. Cao, ChemElectroChem 4 (2017) 3018–3025.
[261] J. Zheng, G. Tan, P. Shan, T. Liu, J. Hu, Y. Feng, L. Yang, M. Zhang, Z. Chen, Y. Lin, J. Lu, J.C. Neuefeind, Y. Ren, K. Amine, L.-W. Wang, K. Xu, F. Pan, Chem. 4 (2018) 2872–2882.
[262] F. Malchik, N. Shpigel, M.D. Levi, T.S. Mathis, A. Mor, Y. Gogotsi, D. Aurbach, J. Mater. Chem. A 7 (2019) 19761–19773.
[263] A. Byeon, A.M. Glushenkov, B. Anasori, P. Urbankowski, J. Li, B.W. Byles, B. Blake, K.L.V. Aken, S. Kota, E. Pomerantseva, J.W. Lee, Y. Chen, Y. Gogotsi, J. Power Sources 326 (2016) 686–694.
[264] P. Yu, G. Cao, S. Yi, X. Zhang, C. Li, X. Sun, K. Wang, Y. Ma, Nanoscale 10 (2018) 5906–5913.
[265] X. Tang, H. Liu, X. Guo, S. Wang, W. Wu, A.K. Mondal, C. Wang, G. Wang, Mater. Chem. Front. 2 (2018) 1811–1821.
[266] X. Wang, S. Kajiyama, H. Iinuma, E. Hosono, S. Oro, I. Moriguchi, M. Okubo, A. Yamada, Nat. Commun. 6 (2015) 6544.
[267] Y. Dall'Agnese, P.-L. Taberna, Y. Gogotsi, P. Simon, J. Phys. Chem. Lett. 6 (2015) 2305–2309.
[268] J. Luo, C. Fang, C. Jin, H. Yuan, O. Sheng, R. Fang, W. Zhang, H. Huang, Y. Gan, Y. Xia, C. Liang, J. Zhang, W. Li, X. Tao, J. Mater. Chem. A 6 (2018) 7794–7806.
[269] N. Kurra, M. Alhabeb, K. Maleski, C.-H. Wang, H.N. Alshareef, Y. Gogotsi, ACS Energy Lett. 3 (2018) 2094–2100.
[270] Z. Fan, C. Wei, L. Yu, Z. Xia, J. Cai, Z. Tian, G. Zou, S.X. Dou, J. Sun, ACS Nano 14 (2020) 867–876.
[271] F. Ming, H. Liang, W. Zhang, J. Ming, Y. Lei, A.-H. Emwas, H.N. Alshareef, Nano Energy 62 (2019) 853–860.
[272] Y.-Z. Fang, R. Hu, K. Zhu, K. Ye, J. Yan, G. Wang, D. Cao, Adv. Funct. Mater. (2020), doi:10.1002/adfm. 202005663.
[273] T.S. Mathis, N. Kurra, X. Wang, D. Pinto, P. Simon, Y. Gogotsi, Adv. Energy Mater. 9 (2019) 1902007.
[274] Z. Zhou, W. Panatdasirisuk, T.S. Mathis, B. Anasori, C. Lu, X. Zhang, Z. Liao, Y. Gogotsi, S. Yang, Nanoscale 10 (2018) 6005–6013.
[275] L. Tong, C. Jiang, K. Cai, P. Wei, J. Power Sources 465 (2020) 228267.
[276] L. Yu, L. Hu, B. Anasori, Y.-T. Liu, Q. Zhu, P. Zhang, Y. Gogotsi, B. Xu, ACS Energy Lett. 3 (2018) 1597–1603.
[277] B. Xu, H. Wang, Q. Zhu, N. Sun, B. Anasori, L. Hu, F. Wang, Y. Guan, Y. Gogotsi, Energy Storage Mater. 12 (2018) 128–136.
[278] N. Sun, Q. Zhu, B. Anasori, P. Zhang, H. Liu, Y. Gogotsi, B. Xu, Adv. Funct. Mater. 29 (2019) 1906282.
[279] P. Zhang, Q. Zhu, Z. Guan, Q. Zhao, N. Sun, B. Xu, ChemSusChem 13 (2020) 1621–1628.
[280] Q. Zhao, Q. Zhu, J. Miao, P. Zhang, B. Xu, Nanoscale 11 (2019) 8442–8448.
[281] Y. Zhou, K. Maleski, B. Anasori, J.O. Thostenson, Y. Pang, Y. Feng, C.B. Parker, S. Zauscher, Y. Gogosti, J.T. Glass, C. Cao, ACS Nano 14 (2020) 3576–3586.
[282] C. Zhang, B. Anasori, A. Seral-Ascaso, S.-H. Park, N. McEvoy, A. Shmeliov, G.S. Duesberg, J.N. Coleman, Y. Gogotsi, V. Nicolosi, Adv. Mater. 29 (2017) 1702678.
[283] S. Seyedin, E.R.S. Yanza, J.M. Razal, J. Mater. Chem. A 5 (2017) 24076–24082.
[284] J. Zhang, S. Seyedin, Z. Gu, W. Yang, X. Wang, J.M. Razal, Nanoscale 9 (2017) 18604–18608.
[285] M. Hu, Z. Li, G. Li, T. Hu, C. Zhang, X. Wang, Adv. Mater. Technol. 2 (2017) 1700143.
[286] Z. Wang, S. Qin, S. Seyedin, J. Zhang, J. Wang, A. Levitt, N. Li, C. Haines, R. Ovalle-Robles, W. Lei, Y. Gogotsi, R.H. Baughman, J.M. Razal, Small 14 (2018) 1802225.
[287] C. Yu, Y. Gong, R. Chen, M. Zhang, J. Zhou, J. An, F. Lv, S. Guo, G. Sun, Small 14 (2018) 1801203.
[288] N. He, S. Patil, J. Qu, J. Liao, F. Zhao, W. Gao, ACS Appl. Energy Mater. 3 (2020) 2949–2958.
[289] Q. Yang, Z. Xu, B. Fang, T. Huang, S. Cai, H. Chen, Y. Liu, K. Gopalsamy, W. Gao, C. Gao, J. Mater. Chem. A 5 (2017) 22113–22119.
[290] M. Lu, Z. Zhang, L. Kang, X. He, Q. Li, J. Sun, R. Jiang, H. Xu, F. Shi, Z. Lei, Z.-H. Liu, J. Mater. Chem. A 7 (2019) 12582–12592.
[291] J. Zhang, S. Seyedin, S. Qin, Z. Wang, S. Moradi, F. Yang, P.A. Lynch, W. Yang, J. Liu, X. Wang, J.M. Razal, Small 15 (2019) 1804732.
[292] W. Shao, M. Tebyetekerwa, I. Marriam, W. Li, Y. Wu, S. Peng, S. Ramakrishna, S. Yang, M. Zhu, J. Power Sources 396 (2018) 683–690.
[293] A.S. Levitt, M. Alhabeb, C.B. Hatter, A. Sarycheva, G. Dion, Y. Gogotsi, J. Mater. Chem. A 7 (2019) 269–277.
[294] Q. Jiang, C. Wub, Z. Wang, A.C. Wang, J.-H. He, Z.L. Wang, H.N. Alshareef, Nano Energy 45 (2018) 266–272.
[295] N. Kurra, B. Ahmed, Y. Gogotsi, H.N. Alshareef, Adv. Energy Mater. 6 (2016) 1601372.
[296] N. Wang, J. Liu, Y. Zhao, M. Hu, R. Qin, G. Shan, ChemNanoMat 5 (2019) 658–665.
[297] H. Huang, H. Su, H. Zhang, L. Xu, X. Chu, C. Hu, H. Liu, N. Chen, F. Liu, W. Deng, B. Gu, H. Zhang, W. Yang, Adv. Electron. Mater. 4 (2018) 1800179.
[298] Y.-Y. Peng, B. Akuzum, N. Kurra, M.-Q. Zhao, M. Alhabeb, B. Anasori, E.C. Kumbur, H.N. Alshareef, M.-D. Gerc, Y. Gogotsi, Energy Environ. Sci. 9 (2016) 2847–2854.
[299] H. Hu, Z. Bai, B. Niu, M. Wu, T. Hua, J. Mater. Chem. A 6 (2018) 14876–14884.
[300] S. Jiao, A. Zhou, M. Wu, H. Hu, Adv. Sci. 6 (2019) 1900529.
[301] P. Li, W. Shi, W. Liu, Y. Chen, X. Xu, S. Ye, R. Yin, L. Zhang, L. Xu, X. Cao, Nanotechnology 29 (2018) 445401.
[302] P. Salles, E. Quain, N. Kurra, A. Sarycheva, Y. Gogotsi, Small 14 (2018) 1802864.
[303] Q. Jiang, N. Kurra, K. Maleski, Y. Lei, H. Liang, Y. Zhang, Y. Gogotsi, H.N. Alshareef, Adv. Energy Mater. 9 (2019) 1901061.
[304] L. Qin, Q. Tao, X. Liu, M. Fahlman, J. Halim, P.O.Å. Persson, J. Rosen, F. Zhang, Nano Energy 60 (2019) 734–742.
[305] S. Xu, W. Liu, X. Liu, X. Kuang, X. Wang, 19th International Conference on Solid-State Sensors, Actuators and Microsystems (Transducers) (2017) 706–709.
[306] S. Zheng, C. Zhang, F. Zhou, Y. Dong, X. Shi, V. Nicolosi, Z.S. Wu, X. Bao, J. Mater. Chem. A 7 (2019) 9478–9485.
[307] H. Li, Y. Hou, F. Wang, M.R. Lohe, X. Zhuang, L. Niu, X. Feng, Adv. Energy Mater. 7 (2017) 1601847.
[308] S. Zheng, C. Zhang, F. Zhou, Y. Dong, X. Shi, V. Nicolosi, Z.-S. Wu, X. Bao, J. Mater. Chem. A 7 (2019) 9478–9485.
[309] C. Couly, M. Alhabeb, K.L.V. Aken, N. Kurra, L. Gomes, A.M. Navarro-Suárez, B. Anasori, H.N. Alshareef, Y. Gogotsi, Adv. Electron. Mater. 4 (2018) 1700339.
[310] S. Xu, Y. Dall'Agnese, G. Wei, C. Zhang, Y. Gogotsi, W. Han, Nano Energy 50 (2018) 479–488.
[311] C. Zhang, L. McKeon, M.P. Kremer, S.-H. Park, O. Ronan, A. Seral-Ascaso, S. Barwich, C.Ó. Coileáin, N. McEvoy, H.C. Nerl, B. Anasori, J.N. Coleman, Y. Gogotsi, V. Nicolosi, Nat. Commun. 10 (2019) 1795.
[312] J. Orangi, F. Hamade, V.A. Davis, M. Beidaghi, ACS Nano 14 (2020) 640–650.
[313] L. Yu, Z. Fan, Y. Shao, Z. Tian, J. Sun, Z. Liu, Adv. Energy Mater. 9 (2019) 1901839.
[314] C. Zhang, M.P. Kremer, A. Seral-Ascaso, S.-H. Park, N. McEvoy, B. Anasori, Y. Gogotsi, V. Nicolosi, Adv. Funct. Mater. 28 (2018) 1705506.
[315] E. Quain, T.S. Mathis, N. Kurra, K. Maleski, K.L.V. Aken, M. Alhabeb, H.N. Alshareef, Y. Gogotsi, Adv. Mater. Technol. 4 (2019) 1800256.
[316] B.S. Shen, H. Wang, L.J. Wu, R.S. Guo, Q. Huang, X.B. Yan, Chin. Chem. Lett. 27 (2016) 1586–1591.
[317] H. Hu, T. Hua, J. Mater. Chem. A 5 (2017) 19639–19648.
[318] W. Tian, A. VahidMohammadi, M.S. Reid, Z. Wang, L. Ouyang, J. Erlandsson, T. Pettersson, L. Wågberg, M. Beidaghi, M.M. Hamedi, Adv. Mater. 31 (2019) 1902977.